AN INVESTIGATION ON THE PREPARATION AND PROPERTIES OF REACTIVELY EVAPORATED SnSe AND Bi_2Se_3 THIN FILMS AND BISMUTH SELENIDE CRYSTALS

THESIS SUBMITTED BY

K. JACOB JOHN

IN PARTIAL FULFILMENT OF THE REQUIREMENTS FOR THE DEGREE OF

DOCTOR OF PHILOSOPHY

SOLID STATE PHYSICS LABORATORY
DEPARTMENT OF PHYSICS
COCHIN UNIVERSITY OF SCIENCE AND TECHNOLOGY
KOCHI-682 022

1996

CERTIFICATE

Certified that the research work presented in this thesis is based on the original work done by Mr. K. Jacob John under my guidance in the Department of Physics, Cochin University of Science and Technology, and has not been included in any other thesis submitted previously for the award of any degree.

Kochi 682 022

28 February 1996.

Dr. Elizabeth Mathai

Supervising Teacher

CONTENTS

		INTRODUCTION	1
PART A			
Chapter	1	SEMICONDUCTOR PRINCIPLES	
	1.1	Band Structure	8
	1.2	Instrinsic and extrinsic semiconductors	13
	1.3	Hall effect	15
	1.4	Thermoelectric effect	18
	1.5	Optical properties of semiconductors	20
		References	26
Chapter	2	THIN FILM PREPARATION METHODS	
	2.1	Introduction	27
	2.2	Chemical methods	27
	2.3	Physical methods	31
		2.3.1 Sputtering	31
		2.3.2 Ionized cluster beam	33
		2.3.3 Vacuum evaportion	33
		2.3.4 Reactive evaporation	36
		References	45
Chapter	3	EXPERIMENTAL TECHNIQUES	
	3.1	Preparation of compound thin films by reactive evaporation	46
	3.2	X-ray diffraction studies	50
	3.3	Measurement of film thickness	51
	3.4	Measurement of electrical conductivity	55
	3.5	Measurement of Hall voltage	59
	3.6	Measurement of thermoelectric power	62
	3.7	Determination of optical constants of thin films	64
		References	72

Chapter 4 TIN SELENIDE THIN FILMS PREPARED BY REACTIVE EVAPORATION

4.1 Introduction 73
4.2 Experimental 75
4.3 Structural studies 77
4.4 Optical studies 84
4.5 Critical optimization 92
4.6 Conclusion 96
References 97

Chapter 5 ELECTRICAL PROPERTIES OF POLYCRYSTALLINE SnSe THIN FILMS

5.1 Introduction 101
5.2 Electrical measurements on typical polycrystalline films 102
5.3 Variation of electrical properties with substrate temperature 110
5.4 Conclusion 118
References 119

Chapter 6 REACTIVELY EVAPORATED THIN FILMS OF BISMUTH SELENIDE

6.1 Introduction 121
6.2 Experimental 122
6.3 Structural characterization 123
6.4 Electrical properties 126
6.5 Conclusion 135
References 136

PART B

Chapter 7 CRYSTAL GROWTH

7.1 Introduction 139
7.2 Theories of crystal growth 140
7.3 Techniques of crystal growth 144
7.4 Morphology of crystals 152
7.5 Defects in crystals 155
References 160

Chapter 8 EXPERIMENTAL TECHNIQUES
8.1 Growth techniques 162
8.2 Optical microscopy 165
8.3 Etching studies 165
References 168

Chapter 9 DISLOCATION STUDIES IN MELT-GROWTH Bi_2Se_3 CRYSTALS
9.1 Introduction 169
9.2 Experimental 171
9.3 XRD Studies 172
9.4 Dislocation studies 175
9.5 Conclusion 188
References 190

Chapter 10 GROWTH AND MORPHOLOGY OF VAPOUR-GROWTH Bi_2Se_3 CRYSTALS
10.1 Introduction 192
10.2 Experimental 193
10.3 X-ray diffraction studies 194
10.4 Morphology and growth mechanism 197
10.5 Chemical etching studies 202
10.6 Conclusion 204
References 206

ACKNOWLEDGEMENTS

INTRODUCTION

Any object in solid or liquid form with one of its dimensions very much less than that of the other two may be called a "thin film". Basic properties of thin films are still the subject of considerable interest and investigation, because many features of their behaviour may differ from those of materials in bulk form.

A dramatic increase in the industrial usage of thin films, with applications ranging from decorative and protective coatings to high technology requirements for electronic components has occurred during the past two decades. Because of its applications in many diverse areas and the need for new and improved optical and electronic devices, thin film technology has become extremely important in recent years.

The properties of thin films can be influenced greatly by their method of preparation, rate of deposition, substrate temperature and material, and the back ground pressure. Specific applications in modern technology demand such film properties as high optical reflection/transmission, hardness, adhesion, non porosity, high mobility of charge carriers/insulating properties, chemical inertness toward corrosive environments, and stability with respect to temperature, stoichiometry and orientation in single crystal films. Control

and knowledge of preparation conditions are not only necessary for the production of high quality films for specific applications, but are a prerequisite for their characterization also.

There are different methods for the deposition of thin films of various materials. They can be broadly classified as either physical or chemical. Under physical methods, vacuum evaporation is very simple and convenient, and is the most widely used technique. Deposition of compound films by direct evaporation is rather difficult in many cases due to the deviation in the composition of the condensate from that of the source material; consequence of the dissociation of the compound upon heating under vacuum. Gunther's "Three Temperature Method" is able to overcome these difficulties and can effectively be used to produce compound films of definite composition.

Among topics of current interest in material science, the layered chalcogenide compounds occupy a prominent place. The versatility of these compounds is demonstrated by the remarkable range of properties they exhibit. In recent years studies on IV - VI and V - VI family of compounds have been very much in progress due to their device applications in many fields like IR detectors, photo conductors, thin film transistors, thermoelectric coolers etc. The IV - VI compounds formed with Ge, Sn and Pb as cations and S, Se and Te as anions can be grouped in to three according to the crystal structure. The lead chalcogenides (PbS, PbSe and PbTe) crystallize in a cubic structure, while GeTe & SnTe have a rhombohedral structure at low temperatures, converting to cubic at $T = 273$ K for SnTe and at $T = 673$ K for GeTe. The other compounds (GeS, GeSe, SnS and SnSe) have an orthorhombic crystal structure. Of these, the

semiconductor tin selenide, with a band gap of about 1 eV possesses some of the essential qualities for solar materials. It forms solid solutions with lead chalcogenides and is an important material for optoelectronic devices. Due to their application as memory switching devices, thin films of tin selenide have great potentialities.

The semiconducting V_2VI_3 compounds Bi_2Te_3, Bi_2Se_3 and Sb_2Te_3 and their alloys have found many technological applications in thermoelectric power conversion and in fabrication of galvanomagnetic devices. These compounds crystallize in layer structures of rhombohedral symmetry with the space group D^5_{3d} ($R\bar{3}m$). The application of these materials have been extended to fabricate ideal Hall effect magnetometers, hyperfrequency power sensors, thermopiles and wide band radiation detectors.

This thesis contains a study of the preparation and characterization of reactively evaporated tin selenide and bismuth selenide thin films and bismuth selenide crystals grown from its vapour and melt. The three temperature method had been used for the preparation of these semiconductor thin films. In this preparation technique the individual elements were evaporated from separate sources and the compound films were deposited on the substrate kept at an elevated temperature. It has been found that a so called 'stoichiometric interval' exists with a limited degree of freedom in selecting the individual component flux and substrate temperature for the reactive deposition of a stoichiometric compound.

A variety of physical and chemical deposition techniques have been developed for the deposition of thin films of tin selenide and bismuth selenide. However, nobody has yet reported (to the best of our knowledge) the preparation of SnSe and Bi_2Se_3 thin films by reactive evaporation technique. The structure of the thin films, which strongly influences the electronic properties, is highly dependent upon the deposition conditions and the preparation technique employed. In view of this, we have undertaken the study of the structural, electrical and optical properties of reactively evaporated SnSe and Bi_2Se_3 thin films. The first part of the thesis with six chapters, presents these studies.

A brief description of the basic principles of crystalline semiconductor physics relevant to the work reported here is given in the first chapter. The second chapter presents the different techniques used for thin film preparation and describes the reactive evaporation method (a variant of 'three temperature method') in particular, since only this method is of direct interest in the present work. The details of the experimental technique employed in the preparation and characterization of SnSe and Bi_2Se_3 thin films are given in the third chapter.

The fourth and fifth chapters are devoted to the thin films of tin selenide. Polycrystalline stoichiometric thin films of SnSe had been prepared at substrate temperatures ranging from 473-600 K. X-ray diffraction studies of these films indicated that the crystallines of the films prepared at substrate temperatures below 530 K are randomly oriented, while they have a strong preferred orientation on the substrate surface at higher substrate temperatures. Optical absorption studies indicate that the fundamental absorption starts at 1.21 eV

and it is due to an allowed direct transition. The temperature dependences of the electrical conductivity, the Hall coefficient, Hall mobility and thermoelectric power of these films were studied in the temperature range from liquid nitrogen to higher temperatures. The deposition conditions, and micro-structural analysis and the optical characterization of these films are discussed in chapter four and the results obtained from the investigations on the electrical transport properties are included in chapter five.

Chapter six deals with the preparation and characterization of Bi_2Se_3 thin films. X-ray diffraction studies on the reactively evaporated Bi_2Se_3 thin films showed that these films had no particular orientation on the substrate surface. Electrical measurements were made and d.c. conductivity, Hall mobility, carrier concentration and thermoelectric power were studied in the temperature range from liquid nitrogen to 420 K. Hall effect measurements showed that these films had a carrier concentration of $\approx 1.02 \times 10^{19}\ cm^{-3}$ at room temperature with n-type conductivity. These films showed an increase in thermoelectric power with increase in temperature.

The second part of the thesis presents a study on the preparation and microstructure of Bi_2Se_3 single crystals.

Considering the applicability of the semiconductors in modern scientific and industrial fields, semiconducting single crystal chips have an equally important role as that of their thin films. In fact, it is well known that semi-conductor applications are governed by the electrical properties which in turn are strongly influenced by the defects and impurities incorporated to the

crystals during their growth. Unlike point defects, dislocations get introduced into growing crystals as thermodynamically non-equilibrium crystal defects during preparation. Since the number and distribution of dislocations in a crystal have a sensitive effect on many of its physical properties, an upper limit for the dislocation density is now inevitably specified as an essential quality control prerequisite, in numerous modern high tech applications where semi-conducting crystal chips are used in a variety of forms. Therefore, the knowledge of the nature and distribution of defects in crystals is important not only for better understanding of the solid-state phenomena but also for the improved reliability and performance of electronic devices.

A wide range of techniques have been used to study the distribution, arrangement and density of dislocations and to determine their properties. Of the various methods, etching is a simple, yet powerful technique for the detection and characterization of different crystal defects.

Dislocation studies on the as grown and cleavage planes of the crystals of Bi_2Te_3 and other members of the V - VI family have been carried out by various groups. Even though a large number of investigations were carried out on the various properties of Bi_3Se_3 crystals by different groups, dislocation studies on these crystals have not been closely conducted. It is therefore of interest to carry out a study on the etching characteristics of Bi_2Se_3 crystals.

The Physical Vapour Deposition (PVD) method and the melt growth technique; namely - the horizontal zone levelling method were used for growing the Bi_2Se_3 crystals. Topographical and etching studies on the as grown

vapour crystals and on the cleavage planes of the melt- grown crystals had been conducted. A new etchant capable of revealing the dislocations of Bi_2Se_3 crystals had been developed. The detailed descriptions of the experimental techniques adopted in this work and the results obtained from these investigations are presented in the second part of the thesis.

Part of the work reported in this thesis has been published/ communicated in the form of following research papers:

1. "Polycrystalline bismuth selenide (Bi_2Se_3) thin films prepared by reactive evaporation". Solid State Communications, **83**, (1992), 501.
2. "Electrical properties of bismuth selenide (Bi_2Se_3) thin films prepared by reactive evaporation". Solid State Communications, **85** (1993), 879.
3. "Tin selenide (SnSe) thin films prepared by reactive evaporation". Journal of Materials Science, **29** (1994), 1581.
4. "Electrical properties of tin selenide (SnSe) thin films prepared by reactive evaporation". (Communicated)
5. "Optimization of growth conditions of SnSe thin films". (Communicated)
6. "Dislocation studies in Bi_2Se_3 by Etch-Pit Technique." (Communicated)
7. "Growth and morphology of Bi_2Se_3 crystals by physical vapour deposition method." (Communicated)

CHAPTER 1

SEMICONDUCTOR PRINCIPLES

1.1 BAND STRUCTURE

The understanding of the behaviour of electrons in solids is most important to understand the various properties of materials. During the past hundred years, three approaches, which differ considerably in their philosophy and their level of sophistication, have been developed to explain the electronic properties of materials. The "continum theory", developed in the last century, was considered only the macroscopic quantities and the interrelated experimental data. No assumptions were made about the structure of matter when the equations were formulated. At the turn of this century, Paul Drude proposed the 'classical electron theory', by introducing atomistic principles into the description of matter. This theory postulated that free electrons in metals drift as a response to an external force and interact with certain lattice atoms. The values of most parameters derived from this version was in serious disagreement with experiment. An outstanding difficulty was the prediction of a large specific heat and magnetic susceptibility for metals, contrary to observation. A further refinement in understanding the properties of materials was accomplished at the beginning of this century by quantum theory. The first application of quantum mechanics to the motion of electrons in solids was the treatment of conduction of electricity in metals by A Sommerfeld [1].

According to Sommerfeld's quantum free electron theory, the valence electrons of the constituent atoms of the metals are free to move throughout the entire volume of the specimen (Fig.1.1a). The potential energy due to the field of all nuclei and all other electrons is assumed to be a constant every where inside the metal except at the boundary of the solid.

The energy of the free electron as a function of the wave vector is given by

$$E = \frac{\hbar^2 k^2}{2m} \qquad (1.1)$$

where the wave vector $k = \frac{P}{\hbar} = \frac{2\pi}{\lambda}$. Here λ is the wavelength associated with the electron and P is the momentum.

In this theory, the allowed energy levels for the valence electrons lie very close together and their values extend from nearly the bottom of the potential trough in which the electrons move to indefinitely high values; that is, the energy spectrum is quasi- continuous (Fig. 1.1b).

Although the introduction of quantum theory was an important improvement, the Sommerfeld version still makes quantitative predictions that disagree with experimental results. This theory failed to explain the vast differences in the properties of metals, semiconductors and insulators. Inorder to explain this, the motion of electrons in a periodic potential produced by the periodic array of atoms were considered (Fig.1.2). Electron-electron interaction was neglected in this model. The motion of electrons in such a periodic potential was discussed by F.Bloch [2]. In this theory, it was assumed that the nuclei in

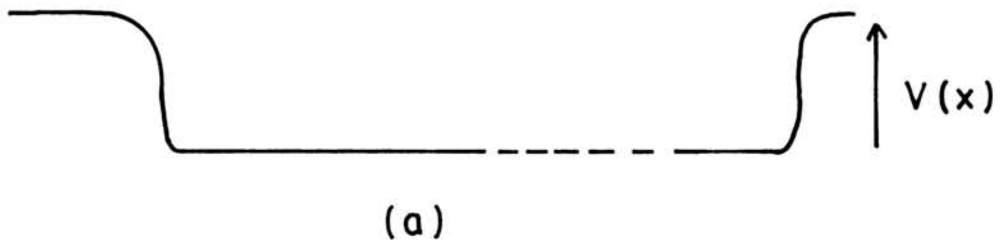

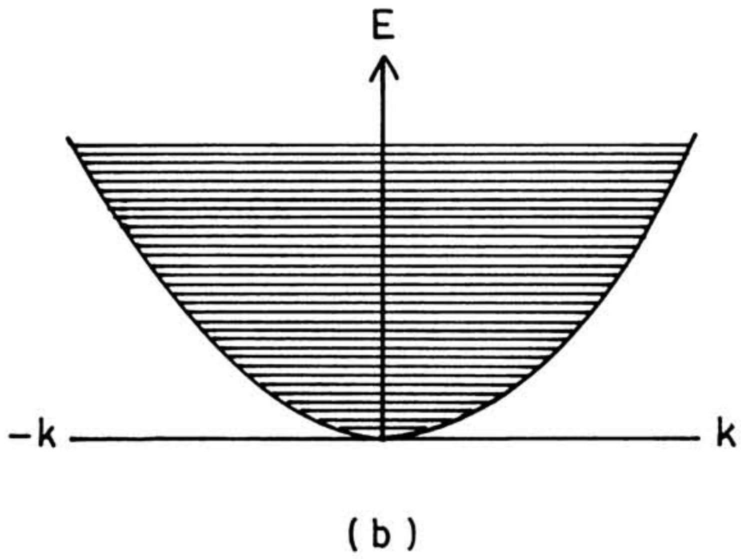

Fig. 1.1a Sommerfeld model for potential energy V(x) of electrons in a crystalline solid

1.1b Energy (E) versus wave vector (k) for a free electron

the crystalline solids are at rest. The total wave function for the system is given by the combination of wave functions, each of which involves the co-ordinate of only one electron. The field seen by a given electron is assumed to be that of the fixed nuclei plus some average field produced by the charge distribution of all other electrons.

If we consider the motion of an electron in a periodic potential we arrive at the following conclusions:

1. The energy spectrum of an electron in a periodic potential consists of a number of allowed energy bands separated by forbidden regions (Fig.1.3).
2. The energy E is a periodic function in wave vector k (Fig.1.3).

The discontinuities in the curve occur for $k = \frac{n\pi}{a}$, where a is the lattice constant and $n = \pm 1, \pm 2, \pm 3, \ldots$. Except for these k values, the electrons in a crystal behave like free electrons. These k values define the boundaries of the first, second etc. Brillouin zones

The concept of band theory put forward the idea of the effective mass of electrons, and is obtained from the dependence of electron energy on wave vector as

$$m^* = \frac{\hbar^2}{d^2E/dk^2} \qquad (1.2)$$

According to the band theory of solids, the presence of a forbidden band or energy gap immediately above the occupied allowed states is the principal difference in the electronic structures of a semiconductor or insulator and a

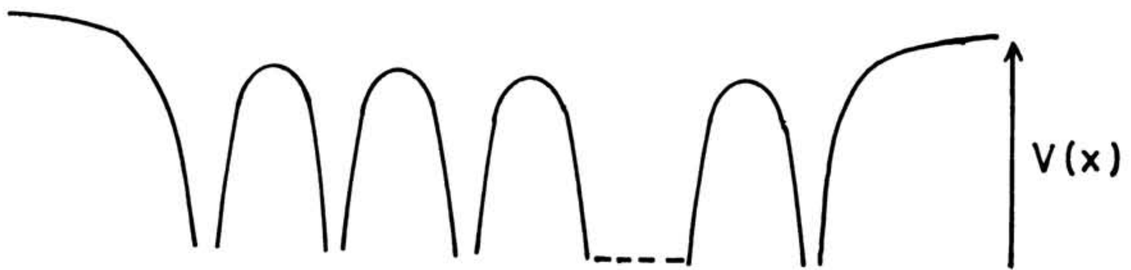

Fig. 1.2 Periodic potential due to the atomic core in a crystalline solid

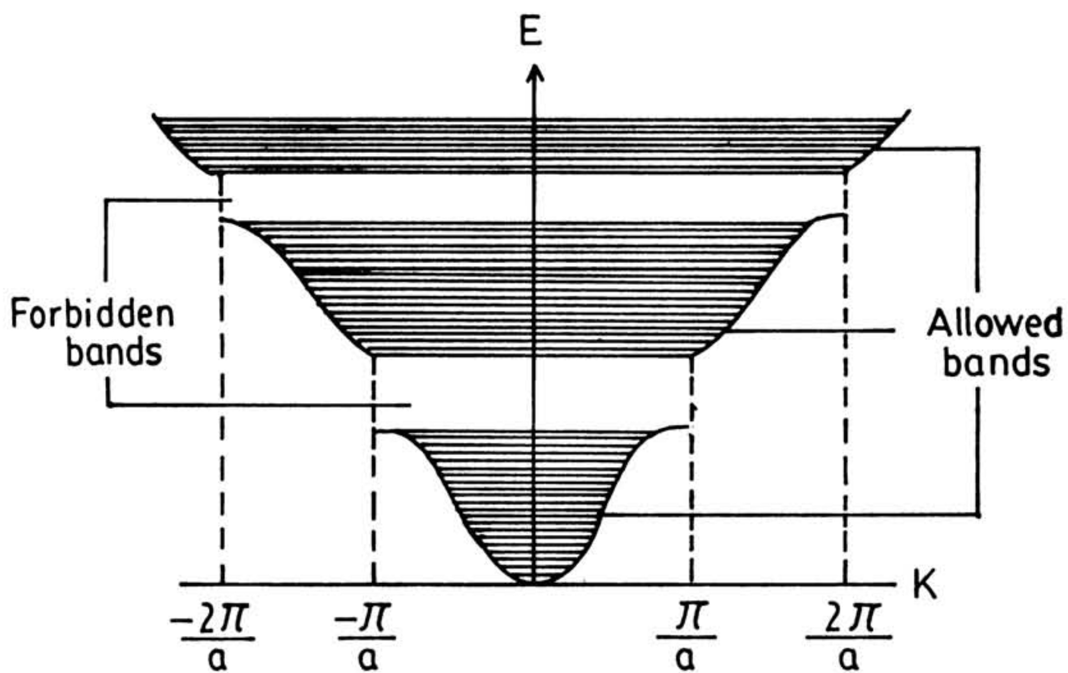

Fig. 1.3 Energy (E) versus wave vector (k) for a periodic lattice of lattice constant, a.

metal. In the first two substances there is a gap between the valence band or normally occupied states and the conduction band, which is normally unoccupied. In a metal there is no gap between occupied and unoccupied states.

The presence of a gap means that the electrons cannot easily be accelerated into higher energy states by an applied electric field. Thus the substance cannot carry a current unless electrons are excited across the gap by thermal or by optical means.

1.2 INTRINSIC AND EXTRINSIC SEMICONDUCTORS

A semiconductor in which the concentration of charge carriers is characteristic of the material itself rather than of the content of impurities and structural defects of the crystal is called an intrinsic semiconductor. At absolute zero temperature, a semiconductor free from impurities is a dielectric – it has neither free electrons nor holes. As the temperature rises, electrons in conduction band and holes in valence band are created by thermal excitation of electrons from the valence to the conduction band. Both of these free electrons and holes are then become carriers of electricity. Since electrons and holes move at random, pair generation is inevitably accompanied by recombination of carrier pairs into neutral atoms. Generation and recombination of electron-hole pairs occur simultaneously, so that there is a limit to the number of electron-hole pairs that can exist at a given temperature. In effect, this is a state of dynamic equilibrium, for as many new pairs are formed as the previous ones recombine. Thus an intrinsic semiconductor has equal concentrations of

electrons and holes; that is, $n = p = n_i$, where n_i is the intrinsic carrier density and is given by

$$n_i = \frac{2}{h^3}(2\pi KT)^{3/2} \left(m_e m_p\right)^{3/4} \exp\left(\frac{-E_g}{2KT}\right) \qquad (1.3)$$

where m_e and m_p are the effective mass of electrons and holes respectively and E_g is the energy gap.

The carrier concentration and hence the conductivity in an intrinsic semiconductor is very sensitive to temperature and depends strongly on the energy gap.

The mobility of the current carriers also contributes its share to the conductivity σ. Taking both electrons and holes into consideration we can write

$$\sigma = n e \mu_e + p e \mu_h \qquad (1.4)$$

where μ_e and μ_h are the mobilities of electrons and holes respectively.

But the temperature dependence of mobility of electrons and holes is less and hence the conductivity, which is proportional to the density of carriers can be expressed as

$$\sigma = \sigma_o \exp(-E_g / 2KT) \qquad (1.5)$$

where σ_o is a constant.

If a semiconductor contains an impurity or impurities, it comes by impurity conduction. The addition of small amount of impurities to the semiconductor material is known as doping. The impurities that can supply a

number of free electrons to the conduction band of a semiconductor are called donors. Since the conduction mechanism in these semiconductors is predominated by negative charge carriers, these materials are called n-type semiconductors. The impurity atoms, which can capture electrons from the valence band, leaving holes in the band are called acceptors. The conduction mechanism in semiconductors with acceptor impurities is predominated by positive carriers, and therefore called p-type semiconductors.

When the carrier concentration is predominantly determined by the impurity content, the conduction of the material is said to be extrinsic. Physical defects in the crystal structure may have similar effects as donor or acceptor impurities. They can also give rise to extrinsic conductivity.

The density of the free electrons in the conduction band due to donor levels is given by the relation,

$$n = (2n_d)^{1/2} \left(\frac{2\pi m_e KT}{h^2} \right)^{3/4} \exp\ (-E_d / 2KT) \qquad (1.6)$$

where n_d is the donor density and E_d, the donor activation energy.

This shows that n is proportional to the square root of donor density. A similar expression holds for the case of acceptors also.

1.3 HALL EFFECT

An effect whereby a conductor carrying an electric current perpendicular to an applied magnetic field develops a voltage gradient which is transverse to

both the current and the magnetic field, is known as Hall effect and the voltage is called the Hall voltage. Analysis of this effect is an important tool, especially in semiconductor research, as it provides a direct estimate of the number and type of charge carriers.

Suppose an electric current J flows in the positive x - direction through an n-type semiconductor and a magnetic field of strength B is applied normal to this electric field in the z-direction. Each electron is then subjected to a Lorentz force $F_L = v B e$, in the y-direction, where v is the velocity of the electrons, and e the electron charge. This force deflects the electrons so that a charge imbalance develops between opposite sides of the conductor. Deflection continues until the electric field E_y resulting from this charge imbalance produces a force $F_y = -e E_y$ which cancels the Lorentz force. Thus, in equilibrium the Hall field is given by

$$E_y = -v_x B_z \qquad (1.7)$$

The current density $J_x = n e v_x$, where n is the carrier density

Therefore

$$E_y = -\frac{1}{ne} J_x B_z \qquad (1.8)$$

The ratio of the transverse electric field strength to the product of the current and the magnetic field strength is defined as the Hall coefficient R_H.

So that $$R_H = -\frac{1}{ne} \qquad (1.9)$$

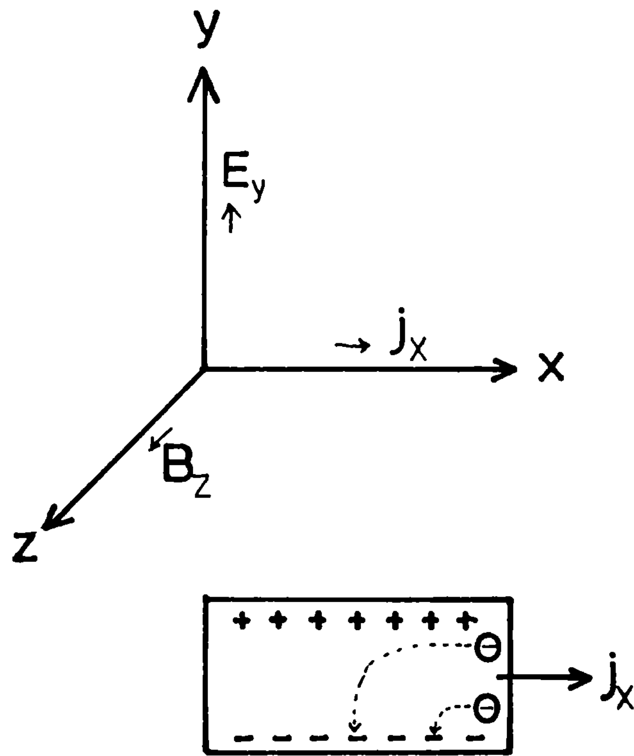

Fig. 1.4 Origin of Hall field and Hall effect

Thus R_H provides a measure of the sign and magnitude of the mobile charge density in a conductor. The above equation holds exactly, only when relaxation time is not a function of the velocity. We generally have to include a numerical factor 'r' which varies between 1 and 2 according to the type of scattering which predominates. Since $\sigma = ne\mu$, by measuring the conductivity of the sample along with the Hall constant, we can determine μ, the mobility of the carriers.

1.4 THERMOELECTRIC EFFECT

In 1821 T.J.Seebeck discovered that when two different conductors A & B are joined in to a loop, and a temperature difference is maintained between the junctions, an emf will be generated. Such a loop is called a thermocouple, and the emf generated is called thermoelectric emf. Experimentally it is established that, for homogeneous conductors A and B the thermoelectric emf depends upon the temperatures of the two junctions and the proportionality constant between these two is known as the thermoelectric power. Thus,

$$Q = \frac{dV}{dT},$$

where Q is the thermoelectric power and dV is the thermo emf developed for the small temperature difference dT between the junctions.

There are two main components contribute to the thermoelectric power of metals and semiconductors : the electron-diffusion component and the phonon-drag component. When a small temperature difference ΔT is established across a conductor, heat is carried from its hot end to its cold end

by the flow of both electrons and phonons. In a metal the conduction electrons are those having energies near the Fermi energy. The energy distribution of these electrons varies with the temperature of the metal. When it is at high temperatures, a metal has more high-energy electrons, and less low-energy electrons, that when it is at low temperatures. This means that if a temperature gradient is established along a sample, the hot end will have more high-energy electrons than the cold end and the cold end will have more low-energy electrons. The high-energy electrons will then diffuse out of the hot end faster than the slower neighbours. This produces a disturbance in the equilibrium distribution of charge carriers and a net electron current will result. This current will cause electrons to pile up at one end of the metal and thereby produce an emf which opposes the further flow of electrons. This is the thermoelectric emf arising from electron diffusion. The same argument can also apply to semi-conductors, except that in this case the carriers (electrons or holes) are those just above (or just below) the band gap.

As the phonons move down the sample, they interact with the electrons and 'drag' them along. This produces an additional contribution to the thermo emf : the phonon-drag component. However, at higher temperatures the phonons begins to scatter more frequently from each other rather than from electrons or impurities. Phonon-phonon scattering eventually becomes dominant, the electrons are no longer dragged along, and the magnitude of the phonon-drag component falls off at higher temperatures.

For a non-degenerate semiconductor, the thermoelectric power is given by the expression [3].

$$Q = -\frac{k}{e}\left\{\frac{\left[\frac{5}{2} - S + \ln\left(\frac{N_c}{n}\right)\right] n\mu_n - \left[\frac{5}{2} - S - \ln\left(\frac{N_v}{p}\right)\right] p\mu_p}{n\mu_n + p\mu_p}\right\} \qquad (1.10)$$

where k is the Boltzmann's constant, e is the charge of the electron or hole, S is a constant depending on the relaxation time of the process and N_c and N_v are the effective density of states in the conduction and valence bands, respectively. This expression indicates that the thermoelectric power is negative for n-type semiconductors and positive for p-type semiconductors, a fact often used to determine the conduction type of a semiconductor. The thermoelectric power can also be used to determine the position of the Fermi level relative to the band edges.

1.5 OPTICAL PROPERTIES OF SEMICONDUCTORS

Optical absorption measurements are now widely used in semiconductor research since they provide the most accurate way to determine the gap energies and the energies of the localized states. The absorption is measured in terms of the absorption coefficient, defined as the rate of attenuation of electromagnetic radiation per unit length, as it passes through a specimen. The absorption spectrum of a semiconductor includes a number of distinct features, known as lattice, intrinsic, extrinsic, or free-carrier, according to the physical process by which energy is extracted from the electromagnetic radiation.

Lattice absorption arises from the excitation of lattice vibrations (phonons) and is responsible for most structure in the absorption spectra of solids at energies below about 0.1 eV. If unbound charges or free carriers such

as conduction electrons and holes are available to carry a current, the electromagnetic field causes motion of the charges directly, with a net energy transfer from the field to the medium as a result of charge-charge and charge-lattice collisions. This process is referred to as free-carrier absorption. The decreasing efficiency of energy dissipation by collision processes at high frequencies causes free-carrier absorption to fall off roughly as $1/E^2$, where E is the energy of the electromagnetic radiation.

Intrinsic semiconductors have a completely filled valence band and an empty conduction band, at low temperatures. Consequently, no intraband transition or low energy absorption is possible at low temperatures. Thus the optical behaviour of an intrinsic semiconductor is similar to that of an insulator, that is, it is transparent in the low energy (far infrared) region. Once the energy of the photon is increased and it eventually reaches the energy gap, then the electrons are excited from the top of the valence band to the bottom of the conduction band. The semiconductor becomes opaque like a metal. The onset of interband transitions, known as the fundamental absorption edge, which marks the boundary between the range of transparency at lower energies and the strong absorption that occurs at higher energies, is thus determined by the forbidden gap of the semiconductor.

Intrinsic absorption spectra are of two types, indirect or direct according to whether or not a phonon participates in the absorption process.

In an absorption process, the total momentum of electrons and photons must remain constant. For optical frequencies, the momentum of a photon and

thus its wave vector **k** is much smaller than that of an electron. Thus k_{phot} is much smaller than the diameter of Brillouin zone. With reference to an energy band diagram, if the maximum of the valence band and the minimum of the conduction and are at the same point in **k**-space as shown in Fig.1.5, vertical transitions are permissible and such transitions are called 'direct transitions'. Conservation of energy must also hold in the transition, so absorption of radiation is possible only if there is an unoccupied state of energy $h\upsilon$ available at the same **k** as the initial state.

The absorption coefficient in such direct allowed transitions is given by [4].

$$\alpha(h\upsilon) \sim (h\upsilon - E_g)^{1/2} \qquad (1.11)$$

where $h\upsilon$ is the photon energy and E_g is the band gap.

In certain cases, quantum selection rules forbid direct transitions at **k**=0, but allow them at $k \neq 0$. The absorption coefficient for such forbidden transitions has the spectral dependence,

$$\alpha(h\upsilon) \sim (h\upsilon - E_g)^{3/2} \qquad (1.12)$$

When a transition requires a change in both energy and momentum, a double transition process is required, because the photon cannot provide a change in momentum. This situation can be overcome with the participation of phonons. Thus, non vertical transitions between the top of the valence band and the bottom of the conduction band as shown in Fig.1.6 are possible with the emission or absorption of phonons and is called the 'indirect transitions'.

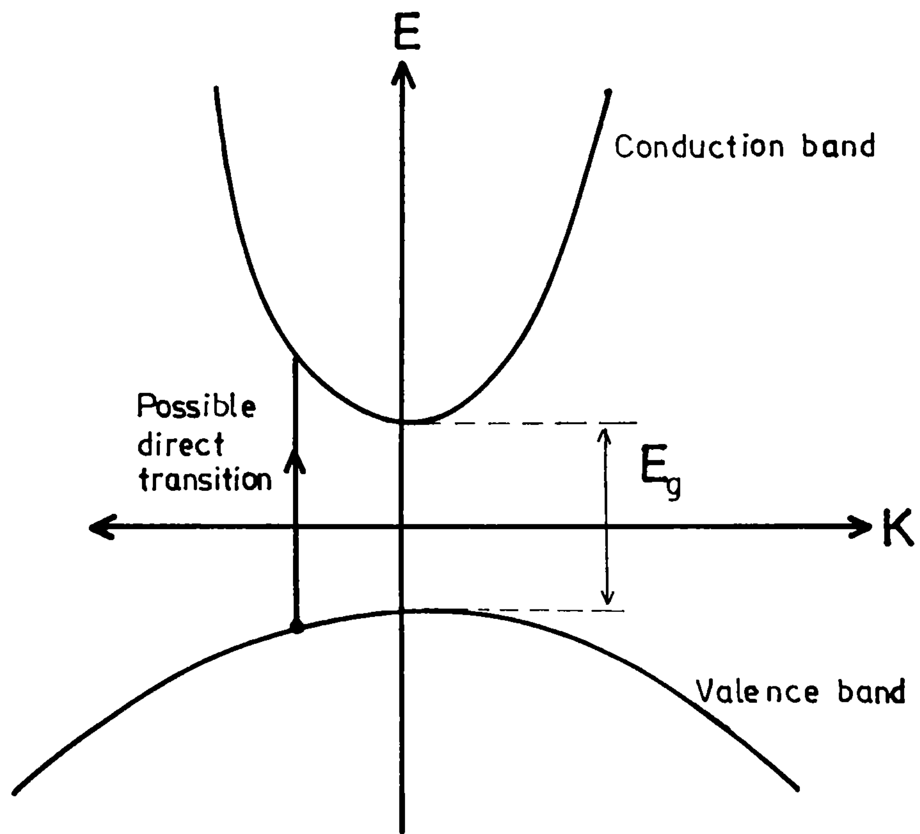

Fig. 1.5 Direct transition from the valence band to the conduction band

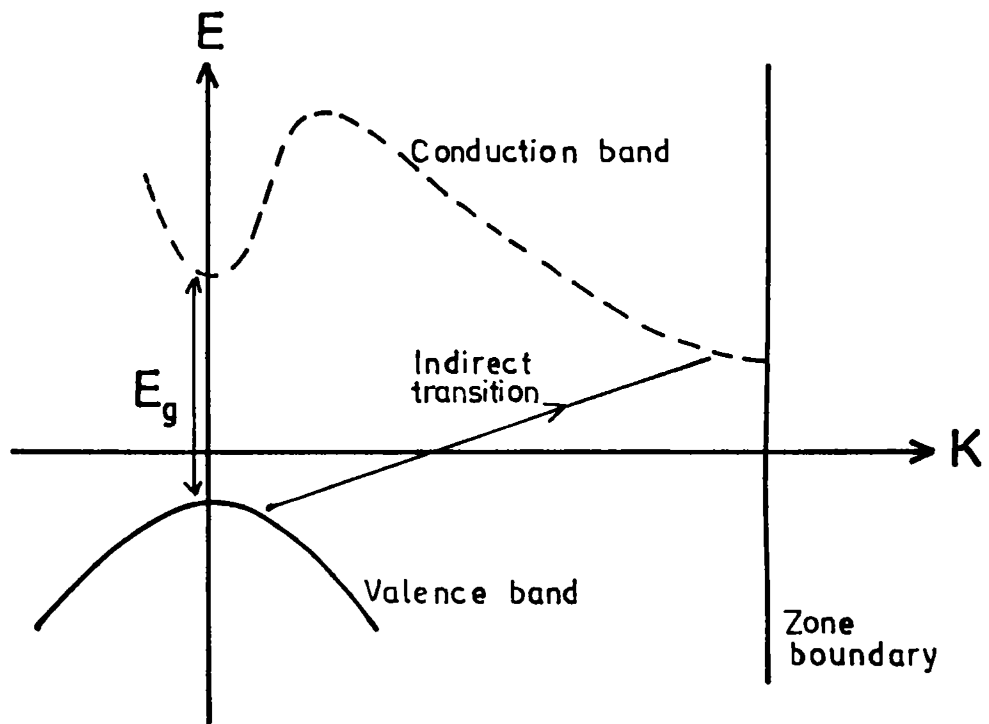

Fig. 1.6 Indirect transitions from the valence band to the conduction band

The energy dependence of the absorption coefficient $\alpha\,(h\upsilon)$ in the indirect inter band transitions is given by [4]

$$\alpha\,(h\upsilon) = \alpha_e\,(h\upsilon) + \alpha_a\,(h\upsilon) \qquad (1.13)$$

where

$$\alpha_e\,(h\upsilon) = \frac{A\,(h\upsilon - E_g - E_p)^2}{[1 - \exp\,(-E_p / KT)]} \qquad (1.14)$$

for $h\upsilon > E_g - E_p$, α_e corresponds to the emission of a phonon of energy E_p inorder to conserve momentum and

$$\alpha_e\,(h\upsilon) = \frac{A\,(h\upsilon - E_g - E_p)^2}{[\,\exp\,(-E_p / KT) - 1]} \qquad (1.15)$$

corresponding to the absorption of a phonon

For either direct or indirect transitions, an excited electron is attracted by the coulomb interaction to the vacancy or hole, that was created in the valence band by its excitation. There is a strong tendency for the electron and hole to bind together to form a hydrogen like state called an exciton. Excitons greatly affect the shape of absorption spectra near the fundamental edge.

Extrinsic absorption processes involve states associated with deviations from crystal perfection, such as vacancies, interstitials, and impurities. Since these states occur in low concentrations relative to the host atoms, extrinsic absorption is weak relative to intrinsic processes.

Thus a careful and systematic study of optical properties can yield a lot of informations regarding the material under investigation.

REFERENCES

1. A Sommerfeld., *Z. Phys*, **47**, 1 (1928).

2. F. Bloch., *Z. Phys*. **52**, 555 (1928).

3. R.A Smith, "Semiconductors", 2nd Edn. Cambridge University Press, (1978).

4. J. Pankove, "Optical Process in semiconductors" Prentice-Hall, New Jersey, (1971).

CHAPTER 2

THIN FILM PREPARATION METHODS

2.1 INTRODUCTION

Thin film deposition techniques have an important role in the fabrication of sophisticate solid state microelectronic devices. Thin film deposition can be broadly classified as either physical or chemical. In physical methods, the particles to be deposited has been transferred to a gaseous state by a physical process, either thermal evaporation or an impact process. Thin film deposition by chemical methods, include thin film formation by chemical processes in the gas or vapor phase as well as from liquid phases. The broad classification of thin film deposition techniques [1-6] is outlined in Fig. 2.1.

2.2 CHEMICAL METHODS

Unlike the physical methods of preparation of thin films involving evaporation or ejection of material from a source, chemical methods depends on a specific chemical reaction. Chemical methods of thin film deposition include the following:

Fig. 2.1

Thin Film Deposition Techniques

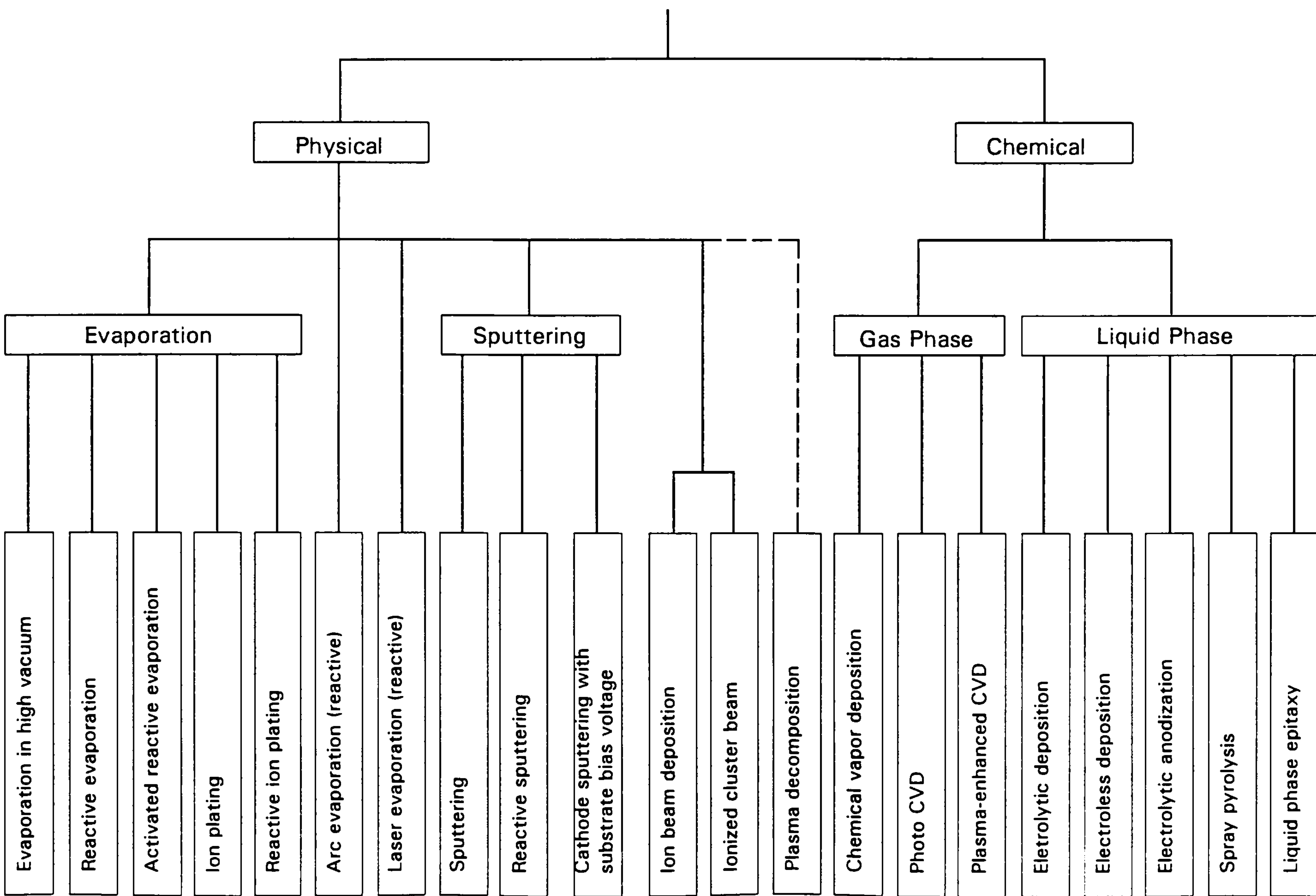

2.2.a Chemical Vapor Deposition (CVD)

It is an important and popular technique for the preparation of thin films of a wide variety of materials, on various substrates. Films of high purity and quality, with required composition and doping levels, can be prepared by this method. In this method, solid films are formed on the substrate, maintained at a suitable temperature, by the reaction of the constituents in their vapor phase. The chemical reaction itself is an important characteristic of all CVD processes. Several type of chemical reactions, such as chemical transfer, thermal decomposition (pyrolysis), reduction, oxidation, nitride and carbide formation etc. are available to carryout the CVD processes.

2.2.b Photochemical Vapor Deposition

Photo CVD is a recently developed, low temperature deposition technique for the preparation of high quality films for many technological applications. In this process, the photochemical deposition takes place when high energy photons selectively excite states in the surface-absorbed or gas phase molecules leading to bond rupture and the production of free chemical species to form the films or to react to form compound films on the adjacent substrate. Ultra violet lamps or lasers are the sources used for the photo-chemical deposition.

2.2.c Plasma-enhanced Chemical Vapor Deposition

A versatile technique for depositing a wide variety of film materials for microelectronic, photovoltaic, and many other applications. In this process, the plasma produced by rf, dc or microwave fields are used to promote the chemical reactions.

2.2.d Electrolytic deposition

This is an electrochemical process in which the anode and cathode are immersed in a suitable electrolyte and the passage of electric current serves to deposit the material on the cathode. By this method, it is possible to deposit only on metallic substrates and the film may be contaminated by the electrolyte.

2.2.e Electroless deposition

Electroless deposition is simple, and is possible for large-area deposition from a solution, in which no electrode potential is applied, unlike electro-deposition. The rate of deposition depends on the temperature of the bath and the chemical reduction in some cases need to be stimulated by a catalyst.

2.2.f Anodization

This is another electrochemical process, used to deposit oxide films over certain metals. Here when the electric current is passed, the anode reacts with negative ions from the electrolyte and forms an oxide coating.

2.2.g Liquid Phase epitaxy

A thermally controlled technique for the preparation of high purity epitaxial films of semiconductor compounds and alloys. A saturated solution of the material at high temperature is prepared and then allowed to cool at a suitable rate and time interval to grow a crystalline phase of the material over the given substrate. The morphology is difficult to control and the quality of the surface is poor compared to that obtained by other expitaxial methods.

2.3 PHYSICAL METHODS

Under physical methods, vacuum evaporation and sputtering are the important techniques for the deposition of thin films. The deposition of the films by these methods occurs mostly at a low gas pressure and hence a vacuum chamber is required.

2.3.1 Sputtering

If ions with high energy, bombard a solid surface, single atoms, molecules or clusters will be ejected and deposited on the surrounding area. This ejection of atoms from the surface due to the bombardment of ions, is commonly known as sputtering. Depending upon the methods used to eject the atoms/molecules, different types of sputtering are there.

2.3.1a Glow discharge sputtering

The simplest sputtering arrangement is the glow discharge sputtering system. In this method an electric field is applied between two electrodes in an inert gas at low pressure. The plate of the material to be deposited is used as the cathode and the substrate is mounted on the anode facing the target. When the electric field is applied, a glow discharge is formed. By the impact of positive gas ions on the target plate, the atoms of the cathode material will be ejected, which eventually condense on the substrate as a thin film.

2.3.1b Bias sputtering

In this case the substrates are biased with a negative potential with respect to anode so that it is subjected to an ion-bombardment throughout the growth. This effectively cleanses the substrate surface, and films with good adhesion to the substrates are formed.

2.3.1c Triode sputtering

In this case extra electrons are injected in the discharge by thermionic emission from an additional hot cathode. The total ionization and the ionization efficiency are increased by accelerating these electrons. This method is often combined with a magnetic field.

2.3.1d Ion-beam sputtering

In this method ions of the inert gas are produced in a discharge and then extracted in a separate vacuum chamber and accelerated on to the target. By this method it is possible to sputter at a pressure even below 10^{-3} torr, and the incorporation of the inert gas atoms into the growing film can be reduced.

2.3.1e R.F Sputtering

This can be used to sputter insulator films directly and also possible to sputter at low pressures. In this case an rf potential is applied to the metal electrode placed behind the dielectric plate target.

2.3.1f Reactive sputtering

Films of oxides, nitrides etc. of metals can be prepared by introducing the reactive gas along with the inert sputtering gas in to the sputtering system. The main advantage of this method is the variation of the composition from the pure metal to the highest reaction product caused only by variation of the pressure of reactive gas.

2.3.2. Ionized Cluster Beam (ICB)

Ionized cluster beam deposition is a recently developed technique that has been widely used for the preparation of high quality films of a wide variety of materials. Clusters are evaporated in a special cell and ionized by electron impact. These ionized clusters will be accelerated against the substrate with a suitable energy. It is assumed that the clusters burst on the substrate and that single atoms with higher mobility diffuse on the substrate surface. The higher energy of the atoms results in an intense mixing of the interface, and hence the adhesion should be improved.

2.3.3. Vacuum Evaporation

Vacuum evaporation is a very simple and convenient technique, and is the most widely used one, for the deposition of thin films, both in the laboratory and in industry.

The following distinguishable steps are involved in the vacuum deposition.

1. Generation of vapor from the condensed phase; solid or liquid.
2. Transfer of the vapor from the source to the substrate.
3. Condensation of the vapor on the substrate surface to form the solid film.

When evaporation is made in vacuum, the evaporation temperature is considerably lowered and the incorporation of the oxides and other impurities is very much reduced. This also ensures a straight line path for the vapor

emitted from the source for the usual working source-to-substrate distance in a vacuum system. The pressure used for normal evaporation is about 10^{-5} torr.

2.3.3a Resistive Heating

Thermal evaporation of the material to be deposited can be achieved by a variety of physical methods. The oldest process is evaporation from a boat or a wire, which consists of a refractory metal (tungsten, tantalum, or molybdenum), heated by an electric current. Vapor sources of different designs are used for evaporation depending on the evaporant material.

2.3.3b Flash Evaporation

This method is useful in the preparation of multicomponent alloys or compounds that tend to fractionate in the evaporation process. In this method, the selected alloy is prepared in powder form with as small a grain size as possible, and is dropped on to a boat that is hot enough to ensure that the material is evaporated instantaneously.

2.3.3c Electron Beam Evaporation

The electrons emitted from a tungsten cathode are accelerated by high voltages are focused on the substance to be evaporated which is put in a water-cooled crucible. The kinetic energy of the electrons is transformed into thermal energy, so that the material in the crucible melts and evaporate into the vacuum.

2.3.3d R.F Heating

Radio frequency can be used to heat the evaporant. By suitable arrangement of rf coils, levitation and evaporation can be achieved, there by eliminating the possibility of contamination of the film by the support crucible.

2.3.3e Laser Evaporation

High power, pulsed laser beams can be used for ejecting particles into the vacuum. The laser source, kept out side the vacuum system, is focused on to the target material, and the ejected material is deposited on the substrate, placed in front of the target material inside the vacuum. An advantage of laser evaporation is that because of its high energy, alloys can be deposited without a change of composition as in flash evaporation techniques.

2.3.3f Arc Evaporation

In this method, an electric arc between the evaporant and an additional electrode is ignited. Sufficiently high temperature can be generated to evaporate the refractory materials, by this method. This process has the advantage that the material to be evaporated need not totally be melted so that no fractionation takes place during evaporation.

2.3.3g Ion Plating

This is a process in which the deposition source is a thermal evaporation source as in ordinary evaporation techniques, and a glow discharge is maintained at a pressure of 10^{-1}–10^{-2} torr between the source crucible or filament as the anode and the substrate as the cathode.

2.3.4 REACTIVE EVAPORATION

Reactive evaporation is a variant of Gunther's three-temperature method [7] and is based on the fact that continuous condensation of a given vapor at a given rate takes place only if the temperature of the substrate drops below a certain critical value. Since these critical values are functions of the interfacial energies, they should differ in magnitude and makes it possible to condense a particular vapor or a combination of vapors (compound) preferentially on the substrate.

The condensation flux N_K of a given vapor on a given substrate exceed zero only if the ratio P/P_e of the actual vapor pressure P and the equilibrium pressure P_e exceeds a critical value of q_c.

i.e. $N_K > 0$ if $(P/P_e) > q_c$ (2.1)

At a given substrate temperature, the condition for progressive condensation can be written as

$N_K = 0$ if $N_+ \leq N_{+c}$ (T)

$N_K > 0$ if $N_+ > N_{+c}$ (T) (2.2)

where N_{+c} is the critical value of incident flux. If the flux exceeds N_{+c}; the condensation flux rises rapidly and approaches its maximum value given by

$N_{K\,max} = \alpha\ (N_+ - N_e)$ (2.3)

where α is the condensation coefficient and N_e is the re-evaporation flux from the substrate. This behaviour is schematically represented in Fig. 2.2. $(P/P_e)_*$ corresponds to the beginning of nucleation due to surface diffusion.

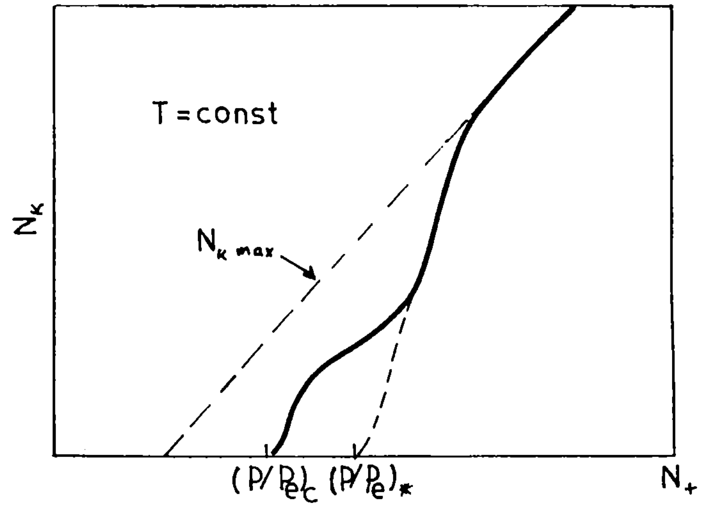

Fig. 2.2 Variation of condensation flux N_k with the incident flux N_+ of the particles

Assuming a constant incident flux N_+ for vapor particles on a substrate, the condition for progressive condensation can be expressed in terms of a critical temperature T_c:

$$N_K = 0 \text{ if } T \geq T_c (N_+)$$

$$N_K > 0 \text{ if } T < T_c (N_+) \qquad (2.4)$$

Thus, by analogy with Fig 2.2, the condensation can be represented schematically as a function of the substrate temperature in the manner of Fig 2.3; i.e., below a critical temperature T_c, the condensation starts spontaneously and quickly approaches a maximum. T^* indicates the beginning of nucleation by surface diffusion.

Let the vapor phase consists of two components A and B and both being incident on the substrate under consideration. As in all cases of high vacuum deposition, if the vapor density is low enough, the collisions between particles of the components A and B in the vapor phase can be neglected. However, interactions can take place between such particles with in the adsorbed stage on the substrate surface. These interactions may lead to the formation of molecules.

where AB stands for all possible compounds $A_n B_m$. A rough estimate of the interaction probability on the surface gives a density

$$n_{AB} = \text{Const. } n_A \, n_B \, . \, \bar{D} \qquad (2.5)$$

where n_A and n_B are the number of adsorbed atoms of A and B, and $\bar{D}$ the mean diffusion coefficient.

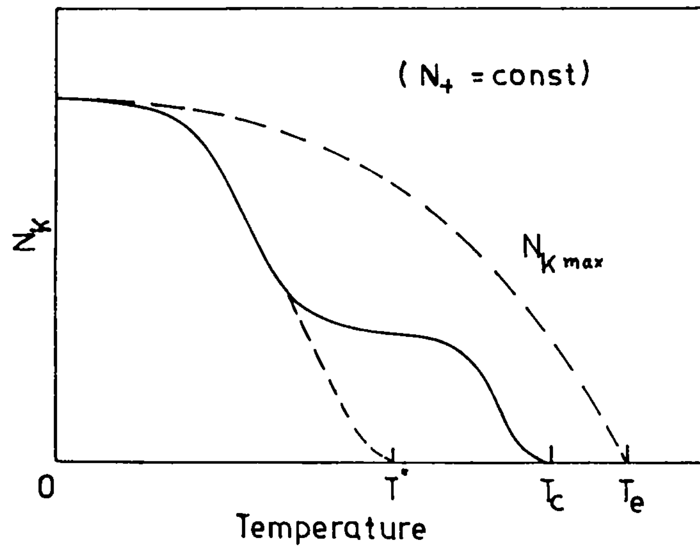

Fig. 2.3 Variation of condensation flux N_K with substrate temperature T.

Since the number of adsorbed atoms is proportional to the actual vapor pressure P, or the incident flux N_+ of the particular vapor, the density n_{AB} should also be proportional to the product of incident fluxes ($N_{+A}\,N_{+B}$) or vapor pressure ($P_A\,P_B$).

Inorder to estimate the critical values which now apply, the equilibrium pressures P_{eA}, P_{eB} of the components and the values P_{eAB} of the compound must be considered. P_{eAB} usually corresponds to the dissociation pressure of the compound, and is equivalent to the pressure of the more volatile component (say A) in equilibrium with the compound. Thus, the critical values of one component A in the presence of the other component B should vary as follows:

$$N_{+CA}\ (B) << N_{+CA}$$

$$T_{CA}\ (B) > T_{CA} \qquad (2.6)$$

This means that at a given substrate temperature, it will be possible to condense A, in combination with B at a lower critical flux. Or in other words, it means that a higher substrate temperature may be used to deposit A in combination with B for a given flux of A.

At a given substrate temperature T and for incident fluxes $N_{+B} < N_{+CB}$, no condensation of any kind is possible while the incident rate N_{+A} is very low. However, at a critical value N_{+CA} (B), sufficient molecules AB are formed on the substrate, and nucleation and progressive condensation of AB starts. This critical value N_{+CA} (B) itself depends on the incident flux of component B. With

further increase of flux N_{+A}, no increase of the condensation flux N_K is possible until, with $N_{+A} > N_{+CA}$, condensation of unreacted A takes place.

Fig. 2.4 shows the condensation diagram for two incident components A and B at a given substrate temperature. It can be seen that well defined areas with layers of different compositions can exist as functions of the incident fluxes. There exists one region in particular where only pure compound layers of the composition AB are obtained, while the unsaturated components are re-emitted in the vapor phase. This region is determined by the straight lines $N_{+A} = N_{+CA}$, $N_{+B} = N_{+CB}$, and by the curve $(N_{+A} N_{+B})$ = constant, as already indicated in equation (2.5). This special region should occur in all cases, where the condition

$$P_e\left(\frac{i}{AB}\right) < P_{ei} \ ; \qquad (i = A, B) \tag{2.7}$$

is satisfied, i.e., a significant increase in adsorption energy due to the reaction A + B ––> AB is necessary. The area of the region is dependent on the substrate temperature T and increases with T, but this is possible only within a limited temperature range.

By applying a method selected on the basis of these considerations, that is, by separate vapor deposition of two components at a suitable substrate temperature (3- temperature method), the deposition of exact stoichiometric compound films should be possible.

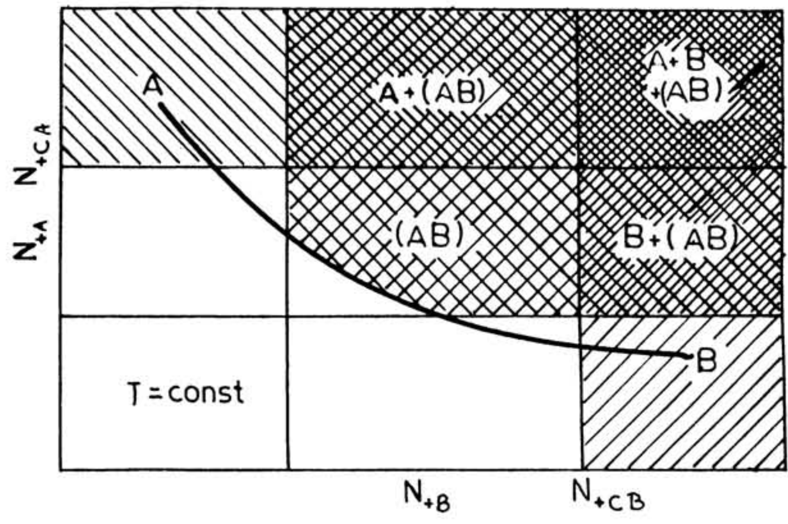

Fig. 2.4 Condensation diagram for two incident components A & B

The advantages of this technique include the following:

1. The need to synthesis the compound from the elements prior to deposition, which is a tedious and sometimes expensive metallurgical process is eliminated.

2. High temperature (>2000°C) are frequently needed to evaporate high melting point carbides, nitrides, and oxides as such and if resistive heating is used, the films will be contaminated as a result of evaporation of the source itself. Reactive evaporation overcomes this difficulty.

3. The decomposition of the compound upon heating in vacuum and the consequent lack of stoichiometry in the films are avoided.

4. High rates of deposition of the compounds are possible.

5. The lowest substrate temperature possible is dictated by condensation temperature of the more volatile component (usually low for O_2, S_2 and Se_2).

6. Dopants can be evaporated simultaneously and a uniform dispersal of the dopants can be easily achieved.

7. Film growth can be started and stopped abruptly and hence abrupt interfaces are possible.

This technique, which has been successfully used for many technologically important compounds, has the following drawbacks:

1. The use of large volatile flux entails the loss of the volatile element.

2. When high deposition rates are required, use of large amounts of volatile flux leads to high volatile partial pressure, which reduces the mean free

path and also scatters the non-volatile beam away from the substrate surface. Also the high pressure in the vacuum system reduces the evaporation rate of the non-volatile component.

3. Because of the high volatile elemental pressure, some unreacted volatile element is likely to be entrapped in the growing film, changing the film properties, especially at low substrate temperatures.

2.3.5 Activated Reactive Evaporation

In this method, a low voltage electrode attracts electrons from the molten pool of the source, which is heated by an electron beam, and these electrons ionize the reactive gas to form a thick plasma. Because of the presence of this plasma, the chemical reaction rate is increased, leading to compound film formation at a higher deposition rate.

REFERENCES

1. L. Holland, *'Vacuum Deposition of Thin Films,'* Champman Hall, London, 1961.

2. R.W.Berry, P.M.Hall and M.T.Harris, *'Thin Film Technology'*, Van Nostrand, New York, 1968.

3. K.L.Chopra, *'Thin Film Phenomena'*, McGraw-Hill, New York, 1969.

4. L.I.Maissel and R.Glang, Eds. *'Handbook of Thin Film Technology'*, McGraw-Hill, New York, 1970.

5. K.Rechielt and X.Jiang, *Thin Solid Films*, **191**, 91 (1990).

6. Joy George, *'Preparation of Thin Films,'* Marcel Dekker, Inc. New York, 1992.

7. K.G.Gunther, in *'The use of Thin Films in Physical Investigation'* (J.C.Anderson, Ed), Academic Press, New York, 1966, P. 213.

CHAPTER 3

EXPERIMENTAL TECHNIQUES

3.1 PREPARATION OF COMPOUND THIN FILMS BY REACTIVE EVAPORATION

Reactive evaporation technique, a variant of Gunther's three-temperature method [1] was used, for the preparation of tin selenide and bismuth selenide thin films, reported in this thesis. The metal (tin or bismuth) was evaporated in an atmosphere of selenium.

The rate of free evaporation of vapour species m_e from a clean surface of unit area in vacuum is given by the Laugmuir expression [2].

$$m_e = 5.83 \times 10^{-2} P_e \left(\frac{M}{T}\right)^{1/2} \text{ g cm}^{-2}\text{s}^{-1} \qquad (3.1)$$

where T is the temperature, M is the molecular weight of the vapour species and P_e ($\approx 10^{-2}$ torr) is the equilibrium vapour pressure. The relationship between the vapour pressure and temperature have been calculated for a wide variety of materials by various authors [3,4].

For purposes of reactive evaporation, the rate at which metal atoms arrive at a substrate is best expressed in terms of the deposition rate as observed

from the same source at the same temperature and substrate-to-source distance, but in the absence of the reactive element flux [5].

$$\frac{dN_m}{A_r dt} = \frac{N_a \rho_m d'}{M_m} \text{ atoms cm}^{-2}\text{s}^{-1} \qquad (3.2)$$

where ρ_m is the density of the metal film (g cm^{-3}), M_m is the molar mass of the metal (g mol^{-1}), d' is the pure metal condensation rate (cm s^{-1}), and A_r is the receiving surface area (cm^2).

The impingement rate of the atoms/molecules on the substrate for a given rate of deposition can be found out using equation (3.2).

3.1a Vacuum system

Thin films of the compounds were prepared in a conventional vacuum system fitted with a 12 inch glass bell-jar. The working chamber was evacuated to low pressure by an oil diffusion pump backed by a double stage rotary pump with a pumping speed 200 litres/min. Pirani and Penning gauges were used to measure the pressure inside the chamber. The evaporation chamber had provisions for two independent resistively heated sources with two high current (100A, 10V) transformers. There were also provisions in the chamber for ion-bombardment cleaning, substrate heating and substrate temperature measurements.

3.1b Substrate cleaning

Optically flat glass slides of the required dimension were used as substrates. These substrates were thoroughly cleaned using liquid Teepol detergent, washed in running water followed by distilled water. Then these

substrates were rinsed thoroughly in an analytical reagent grade acetone and were ultrasonically agitated for fifteen minutes in double distilled water. The cleaned substrates were then dried with a hot-air blower and loaded in the vacuum chamber. The substrates were further cleaned by ion-bombardment in the vacuum system for fifteen minutes prior to the deposition of the film.

3.1c Deposition of the film

The system was initially pumped to the ultimate attainable vacuum, using the oil diffusion pump. The substrates were then heated to the required temperature. The temperature was monitored with chromel-alumel thermocouple placed in contact with the substrate. A 3 ½ digit, 200 mV digital panel meter was used to read the thermocouple voltage. High purity (99.999%) bismuth, tin and selenium were used as the evaporants. A quartz crucible placed in a conical basket of molybdenum wire was used as the selenium source (S_1). The temperature of the source, hence the flux, could easily be controlled by adjusting the current through the molybdenum wire. A boat made of molybdenum sheet (S_2) was used to evaporate the metal (tin or bismuth). The boat was covered with stainless steel heat shields to minimize substrate heating due to radiation from the high temperature source; thus the temperature could be controlled to within $\pm$ 2K. A schematic diagram of the set up is shown in Fig.3.1.

When the substrate had attained the required temperature and stabilized, with a shutter placed over the two sources, the current through S_1 was switched on and adjusted to the pre-calibrated value, for a certain selenium flux. Then the current through the metal source was switched on and increased

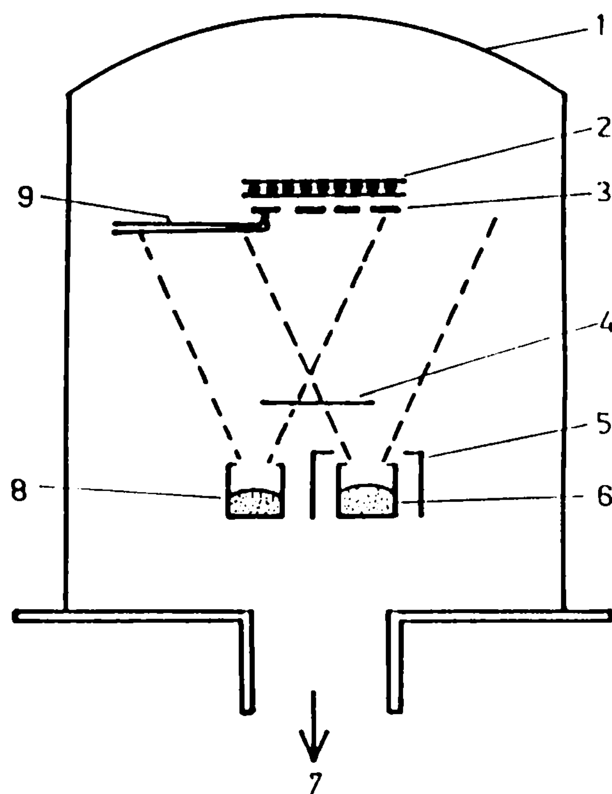

Fig. 3.1 Schematic diagram of the experimental setup:
1, bell jar; 2, substrate heater; 3, substrates; 4, shutter;
5, heat shield; 6, metal source (S_2); 7, to pump;
8, selenium source (S_1); 9, thermocouple

to a pre-set value, which gave the required metal flux for the deposition of the compound film. The shutter was then withdrawn and the deposition of the compound films allowed to take place. The two vapour sources and the substrate were so oriented that the substrate surface was hit by both vapour beams approximately equal angles of incidence. The metal atoms reaching the substrate reacted with those selenium atoms/molecules present on the substrate and the compound film was deposited. Unreacted elemental atoms/molecules will be re-evaporated from the substrate due to the elevated temperature maintained. After completion of deposition, the shutter was put back in position over the sources and the supply to both the sources switched off. The substrate temperature was then slowly reduced.

3.2 X-RAY DIFFRACTION STUDIES

The X-ray diffraction (XRD) method is a non-destructive technique to identify the compound films and to determine the film structures. By use of goniometer and counter, lattice spacings and intensities can be determined with considerably higher accuracy, but greater film thickness are required than for electron diffraction. For obtaining good spectra in the case of strongly texturized films 100-300Å are sufficient, but thicknesses of about 2000Å are needed for the usual polycrystalline films. Electron diffraction is more sensitive and can be used even if the film is very thin; but suffers from the draw back that the film has to be detached from the substrate.

Usually, in x-ray diffractometers the Bragg-Brentano geometry is used. In this, x-ray beam is incident at an angle θ on the film and the detector is at an angle 2θ. The specimen and the detector are rotated at angular velocities ω and

2ω to get the various diffracting planes. In this geometry, when thin films are used, the effective thickness of the films to the incident radiation varies as $t/\sin\theta$, where t is the thickness of the film and θ is the angle of incidence of the X-ray beam. Consequently, scattered intensities will be angle dependent (enhanced by a factor $t/\sin\theta$) and this may not agree with the standard powder diffraction data for comparison of intensities. With proper care, X-ray diffraction can yield good results and any particular compound in the binary or ternary system can be identified without difficulty.

For the present study, monochromatic Cuk_α radiation was used. The accelerating voltage applied was 30 KV and the tube current was 20mA. The X-ray beam was scanned from θ values of 5° to 35°, at a scanning speed of one degree per minute. The intensity of the diffracted radiation versus 2θ was recorded by a chart recorder, running in synchronization with the goniometer.

3.3 MEASUREMENT OF FILM THICKNESS.

The thickness of a thin film can accurately be determine by the multiple beam interferometry method, developed by Tolansky [6]. In this method, Fizeau, fringes of equal thickness are produced by using a monochromatic light source.

The film whose thickness is to be measured is deposited on a glass substrate with sharp step between the surface of the substrate and the surface of the film. An overlayer of highly reflecting opaque film is then deposited on the film and the bare substrate. A semisilvered glass plate is prepared and a

multiple beam interferometer is formed by placing both the film surfaces in contact (Fig.3.2a). This is tightly fixed using a circular jig with three tilt adjustment screws (Fig.3.2b). A typical interferometer arrangement for producing the Fizeau fringes is shown in Fig.3.3a. When the interferometer is illuminated with collimated monochromatic light, fringes with a step at the film boundary, as shown in Fig.3.3b is observed. By adjusting the tilt adjustment screws the fringes can be made to run in straight line perpendicular to the step. The fringe spacing and the fringe displacement across the step are measured and used to calculate the film thickness.

The distance D between successive fringes corresponds to $\lambda / 2$ where λ is the wavelength of the monochromatic radiation used. The abrupt displacement 'd' of the fringe system due to the sharp step on the substrate is a measure of the film thickness t, which is given by

$$t = \frac{d}{D} \cdot \frac{\lambda}{2}$$

For the production of sharp fringes it is necessary to satisfy the following conditions.

1. The overlayer on the film and the bare substrate must be highly reflective.
2. The thickness of the reflecting film must be uniform and the film surface must be as close as possible to the semisilvered surface.
3. The divergence of the incident beam must be less than 3° and should be normal to the plate.

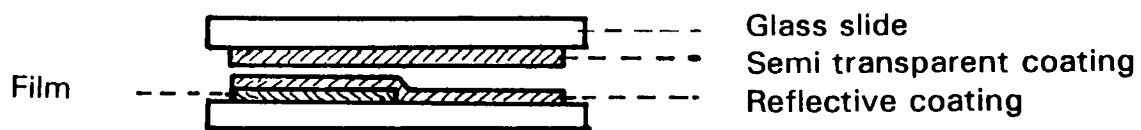

(a)

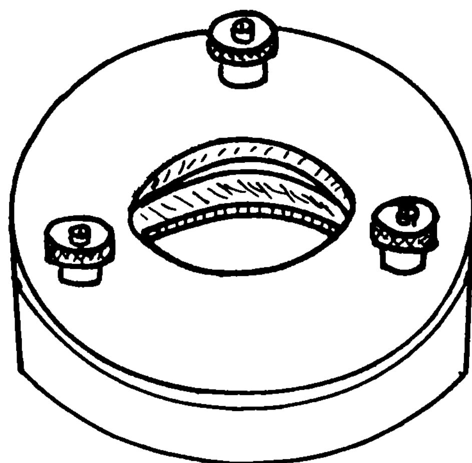

(b)

Fig. 3.2a Cross section of the film arrangement for the multiple beam interferometry

Fig. 3.2b Jig for multiple beam interferometry

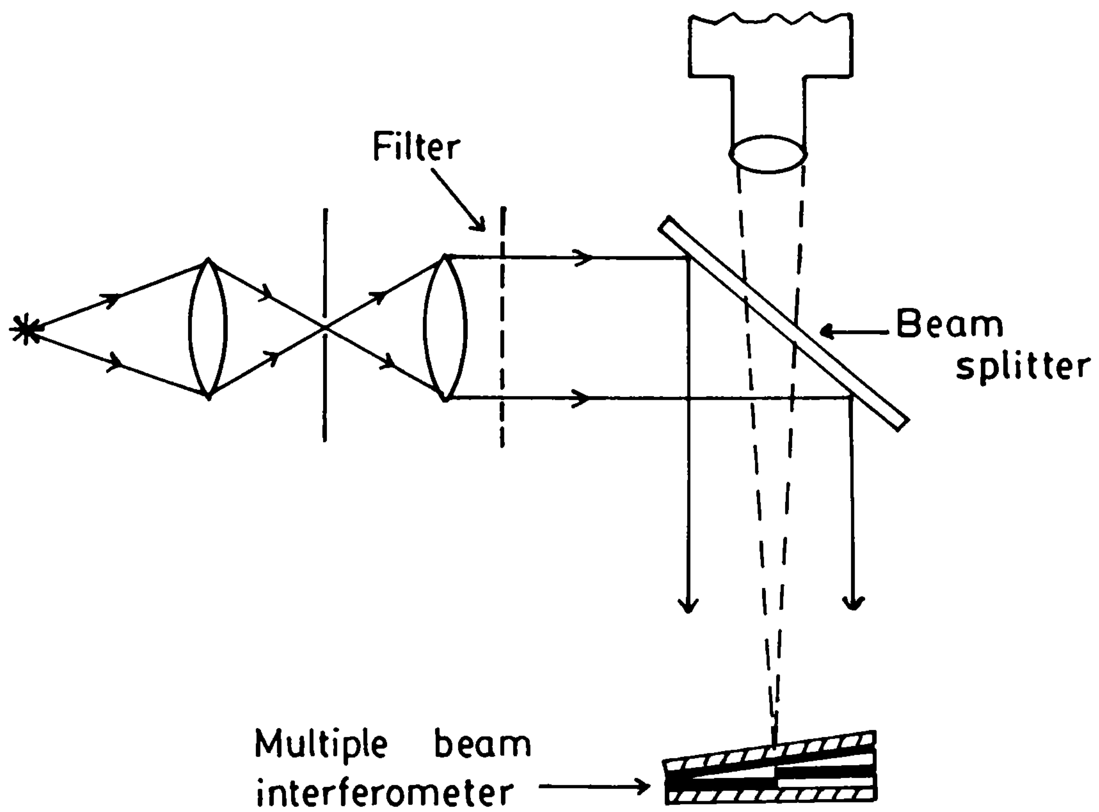

Fig. 3.3a Multiple beam interferometer arrangement

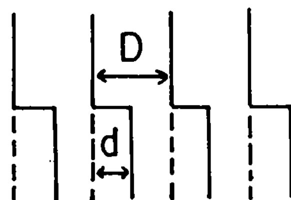

Fig. 3.3b Fringes with steps produced by multiple beam interferometry

3.4 MEASUREMENT OF ELECTRICAL CONDUCTIVITY

Electrical conductivity of semiconductors and its dependence on temperature is of basic interest not only for understanding semiconductor properties but also because they are directly utilized in many device applications. The conductivity of a semiconductor is governed by the mobility and the density of charge carriers available for the conduction. In semiconductors and insulators, there are just enough electrons to fill completely a number of energy bands, leaving the rest of the energy bands empty. At absolute zero temperatures, all semiconductors may be considered as insulators. As the temperature increases from absolute zero, there will be an exponential increase in conductivity of a semiconductor, due to the excitation of the electrons from the closest donor level to the conduction band. Activation energy for the electron transition, in this case is the gap between the donor level and the conduction band. Electrons from the next closest level will be excited with further increase in temperature, and the process continues until all such levels in the forbidden gap are exhausted. In the case of p-type semiconductros, transition will take place between valence band and acceptor levels. At sufficiently high temperatures excitation of electrons from the valence band to conduction band takes place and the intrinsic conduction may start. In this region, the activation energy is the band gap between the valence band and conduction band.

Hence, the study of the variation of conductivity with temperature can give valuable informations regarding the defect levels and the band gap of a semiconductor. The energy gap can be determined from the slope of the

$\ln\sigma$ vs $\frac{1}{T}$ curve, where σ is the conductivity of the material and T is the absolute temperature. Generally, the intrinsic conduction sets in only at a very high temperature.

Electrical conductivity measurements of highly insulating samples are rather difficult, owing to the small value of currents encountered in these measurements. To measure such currents, good quality electrometers at their maximum sensitivity have to be used. This necessitate the heavy shielding of the specimen and the electrometer cable from electrical disturbances. The humidity present in the atmosphere may short circuit the specimen, and this also leads to a false measurement. Hence, the electrical conductivity measurements were done, under a vacuum better than 10^{-2} torr, in an all metal cell. A well smoothed DC was supplied to the heater unit, which maintained the sample at various temperatures. One end of the power supply was earthed to eleminate the ripples, if present, which might induce large current through the specimen, masking the required signal. Inorder to avoid the electrical disturbances, the measuring cell and the heater block were also properly earthed. A fine wire chromel-alumel thermocouple was used to measure the temperature of the sample. The measurement set up and the sample geometry are shown schematically in Fig.3.4.

A well smoothed, regulated power supply was used to apply the specimen current. The voltage across the specimen was measured with a Keithley 195 DMM and the current was measured using a Keithley 616 digital electrometer. The circuit diagram used for the electrical measurements is shown in the Fig.3.5. All the electrical insulations inside the measuring cell were done with teflon.

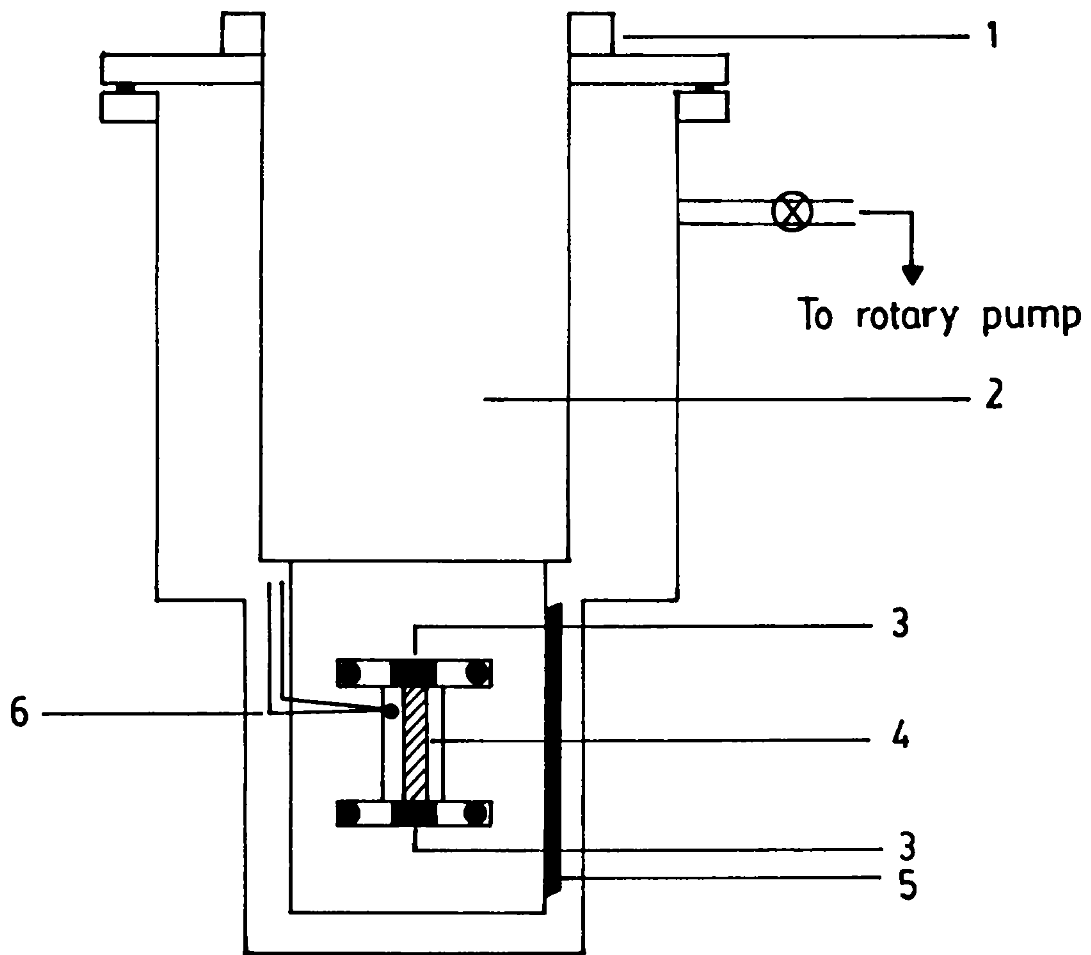

Fig. 3.4 Cross section of conductivity measurement cell

1. Wilson seal 2. Cryogenic fluid 3. Electrodes
4. Specimen 5. Heater 6. Thermocouple

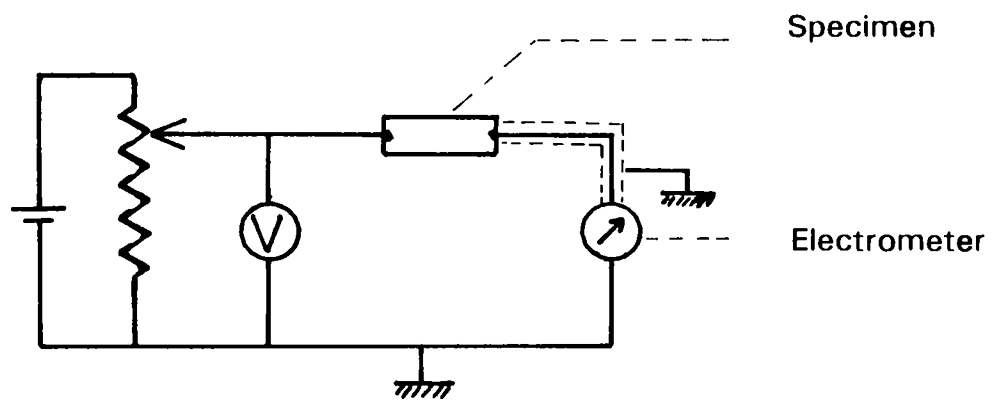

Fig. 3.5 Circuit diagram for the measurement of conductivity

3.5 MEASUREMENT OF HALL VOLTAGE

The number and type of charge carriers (electrons or holes) can be obtained directly from the Hall measurement provided that one type of carrier dominates. Hall effect studies are also a standard tool for studying the mobility of charges in solids. In these experiments one applies a magnetic field perpendicular to the current flow and observes the resulting deflection of the current. The measured quantity is the Hall coefficient R_H. The product of the Hall coefficient and the conductivity is the Hall mobility. Conventional DC method is applicable only if the carrier mobility is greater than few $cm^2v^{-1}s^{-1}$, below which single or double AC method is to be used. This is because of the inverse proportionality between the Hall voltage and carrier concentration. In the case of highly resistive samples, it may be very difficult to send an appreciable amount of current, so as to get a reasonable Hall voltage, without producing Joule heat. In such cases, the measurement of the required signal may become difficult, due to the increased noise.

The circuit diagram used for the Hall effect measurements is shown in Fig.3.6. The Hall voltage developed across the sample was measured using Keithley 181 nanovoltmeter and a Keithley 195 digital multimeter was used to measure the current through the specimen. Magnetic field was applied to the sample, using an electromagnet, generating stabilized field, values ranged between zero and 5 KG; which is fully described in [7]. Measurements were carried out in a vacuum better than 10^{-2} torr, using an all metal cell with provisions for cooling the sample down to liquid nitrogen temperature and heating to higher temperatures. Chromel-alumel thermocouple was placed in contact with the sample and the output was read by a 3½ digit, 200 mV digital panel meter. A schematic diagram of the Hall effect measuring cell is shown in Fig. 3.7.

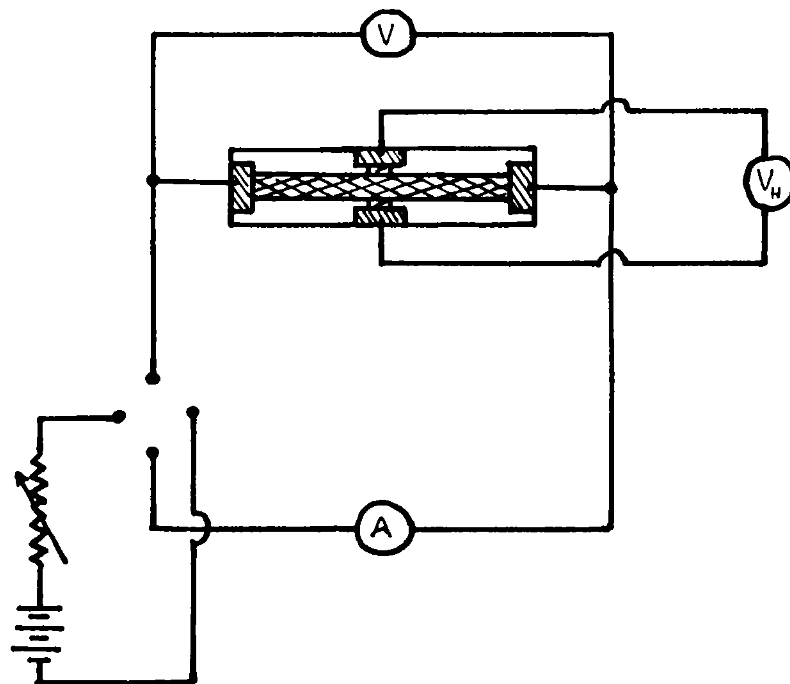

Fig. 3.6 Circuit diagram for the measurement of Hall voltage

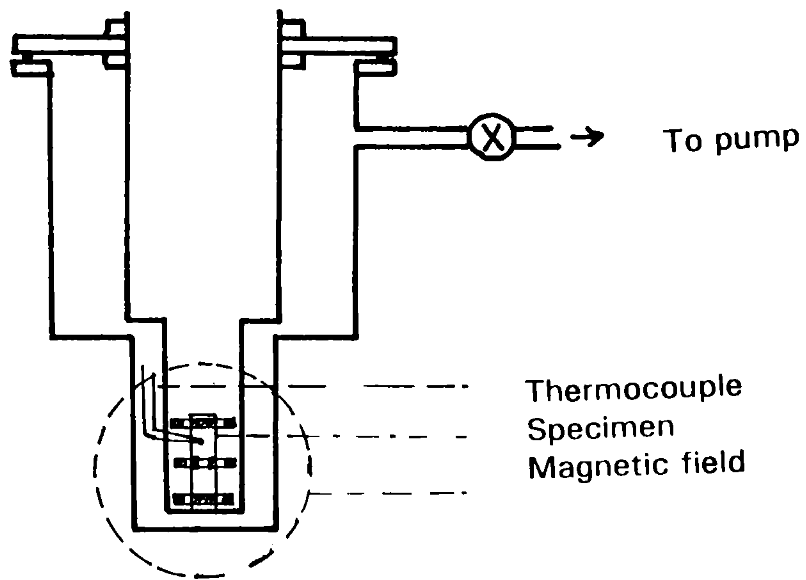

Fig. 3.7 Schematic diagram of the Hall effect measuring cell

3.6 MEASUREMENT OF THERMOELECTRIC POWER

Thermoelectric effects have significant applications in both science and technology. Practical applications of this effect include the measurement of temperature, generation of power, cooling and heating. The thermopower of a semiconductor depends upon the scattering mechanism, carrier density, carrier sign and effective mass, and perhaps the forbidden energy gap, mobility ratio and aspects of the band structure.

Hot probe method; based on thermoelectric properties, is a simple and convenient one to identify the majority carriers in a semiconductor. The hot probe of a multimeter heats the semiconductor immediately under it, with a consequent rise of number of high energy carriers. These then move with higher thermal velocities and will diffuse out of the hot region, and the low-energy carriers will diffuse towards the hot end. However, the diffusion rate is a function of the carrier energy. The net effect is the hot end becoming slightly depleted of majority carriers. Current will therefore flow through the multimeter and the direction of current depends on the sign of the charge. Thus, on an n-type semiconductor, the hot probe is more positive one, while on a p-type it is more negative.

For the measurement of thermoelectric power of the thin film samples, an all metal cell, which can be evacuated to better than 10^{-2} torr, was used. The sectional view of the arrangement is illustrated in Fig.3.8(a,b). The set up is such that one end of the film can be connected to a heater attachment and the other end to a cold finger. With this arrangement one end of the specimen can be cooled down to liquid nitrogen temperature and the other end can be heated.

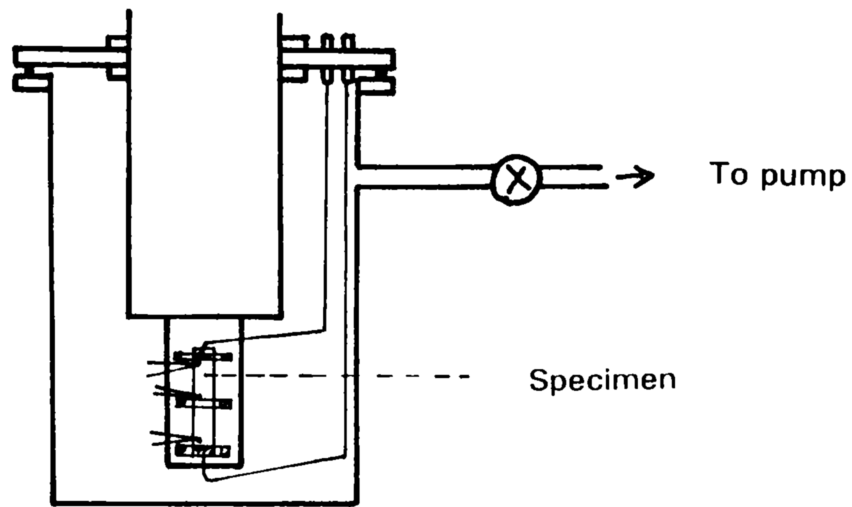

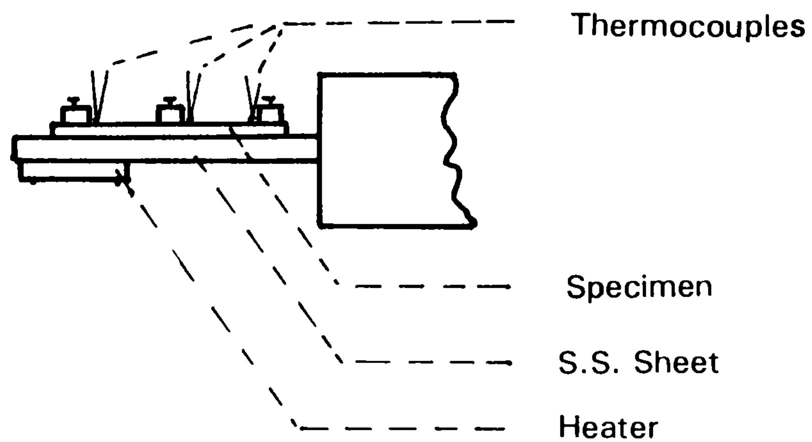

Fig. 3.8a Sectional view of the thermoelectric power measuring cell

Fig. 3.8b Side view of the sample mount

A stainless steel plate is used to mount the specimen, since it has got relatively low thermal conductivity. Fine wire chromel-alumel thermocouples are attached to the ends of the sample using teflon strips to get firm contact. The thermocouple voltages are measured to determine the temperature of each end of the sample and hence the average temperature and the temperature difference ΔT. 3½ digit, 200 mV digital panel meters were used to measure these voltages. The thermo emf developed across the film was measured using a Keithley 195 digital multimeter, through suitable contacts made to the ends of the sample. All electrical insulation inside the cell were done with teflon and a well smoothed DC was supplied to the microheter attachment.

3.7 DETERMINATION OF OPTICAL CONSTANTS OF THIN FILMS

The study of the optical properties of solids has proved to be a powerful tool in our understanding of the electronic and atomic structure of solids. Measurement of the optical constants; the refractive index (n) and the extinction coefficient (k) of solids has crucial importance in view of both basic and applied research. The study of these quantities as a function of wavelength constitutes the most important means of determining the band structures of materials and also to predict the photoelectric bahaviour of a device.

The refractive index and absorption coefficient are usually determined by the spectroscopic ellipsometry and by using both the transmission and reflection spectra. The development of spectroscopic ellipsometry promises more precise determination of optical constants, particularly at photon energies well above the fundamental edge. But this method is applicable only in the region of wavelength where polarizers and analysers are available. Moreover,

elaborate computer iteration procedures are required for its calculations. Simultaneous measurement of transmission and reflection is the most used method for the measurement of n and k. This method is applicable in any region of the spectrum if suitable light sources and detectors are available and also if the material is fairly transparent. In the highly absorbing region of the spectra of a material, reflectivity measurements is the only available method.

A rather straight forward method has been developed by Swanepoel [8] to determine the refractive index (n) and absorption coefficient (α), using transmission spectrum alone. The procedure is very simple and fast, and the accuracy is of the order as for other conventional methods. All formulae in this process are in closed form and can be used on a programmable calculator. Because of its extreme simplicity and availability of commercial scanning spectrophotometer in the UV-Vis-NIR regions of wavelength, this method was used in the studies reported in this thesis.

The practical situation for a thin film on a transparent substrate is as shown in Fig.3.9. The film has thickness d and complex refractive index $\eta = n - ik$, where n is the refractive index and k the extinction coefficient which can be expressed in terms of the absorption coefficient α using the relation

$$k = \frac{\alpha \lambda}{4 \pi} \qquad (3.4)$$

where λ is the wavelength of light. The transparent substrate has a thickness several orders of magnitude larger than d and has index of refraction s and absorption coefficient $\alpha_s = 0$. The system is surrounded by air with refractive index $n_o = 1$. If the substrate and film surfaces are perfectly smooth and the

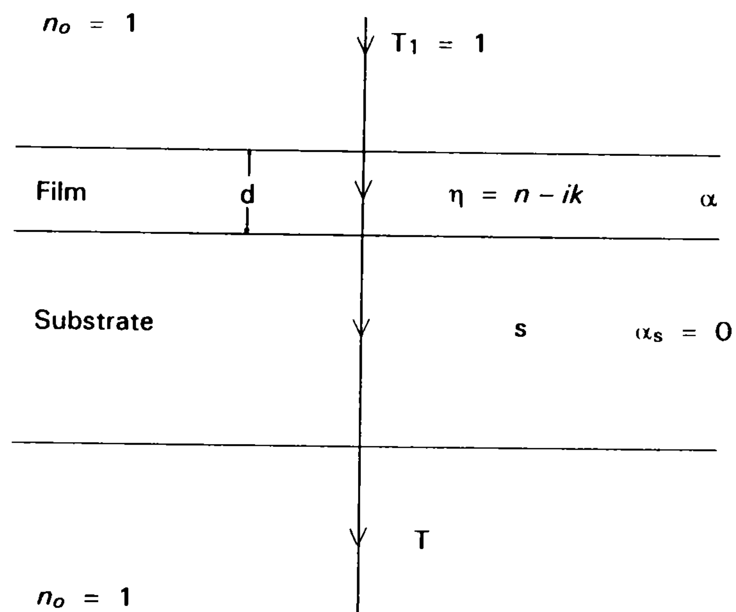

Fig. 3.9. System of an absorbing thin film on a thick finite transparent substrate

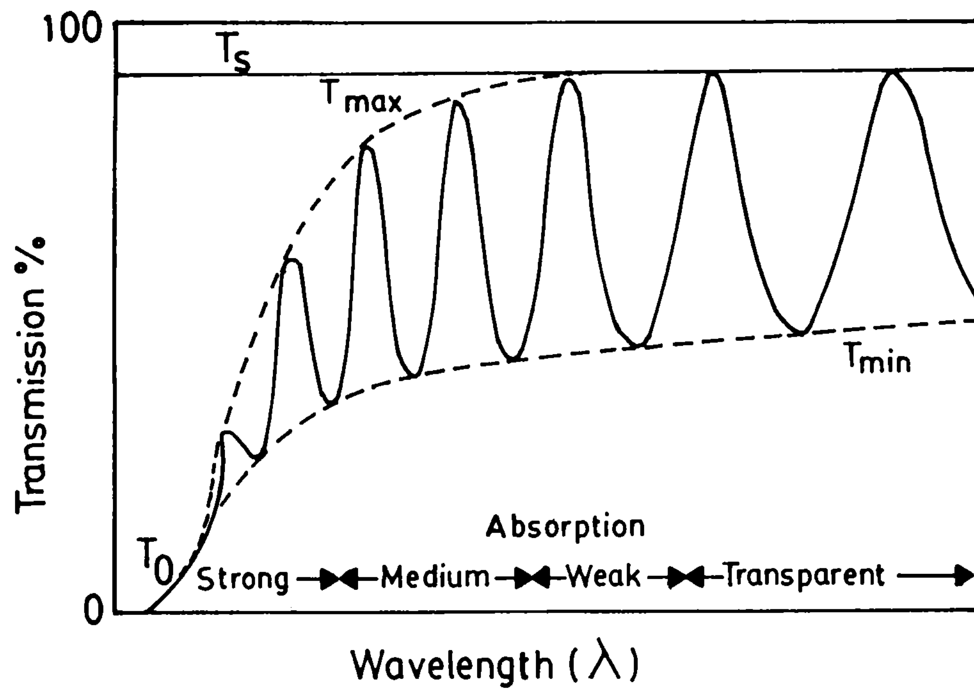

Fig. 3.10. Typical transmission spectrum for a thin film of uniform thickness

film thickness d is uniform, interference effects give rise to a spectrum as shown in Fig.3.10. These fringes of the transmission spectrum of a thin film surrounded by non-absorbing media can be used to calculate the optical constants of the film.

Considering the thick substrate alone in the absence of a film, the interference free transmission is given by the expression

$$T_s = \frac{(1-R)^2}{(1-R^2)}$$

where $R = \left[\frac{(s-1)}{(s+1)}\right]^2$

or $$T_s = \frac{2s}{s^2+1} \tag{3.5}$$

and $$s = \frac{1}{T_s} + \left(\frac{1}{T_s^2} - 1\right)^{1/2} \tag{3.6}$$

The transmission T for the case of Fig.3.10 is a complex function. Taking all the multiple reflections at the three interfaces into account, in the case $k^2 << n^2$ the expression for the transmission T for normal incidence is given by

$$T = \frac{Ax}{B - Cx\cos\phi + Dx^2} \tag{3.7}$$

where

$$A = 16n^2s \tag{3.8a}$$

$$B = (n+1)^3 (n+s^2) \tag{3.8b}$$

$$C = 2(n^2-1)(n^2-s^2) \tag{3.8c}$$

$$D = (n-1)^3 (n^2-s^2) \tag{3.8d}$$

$$\phi = 4\pi nd/\lambda \tag{3.8e}$$

$$x = \exp(-\alpha d) \tag{3.8f}$$

The envelops around the interference maxima T_{max} and minima T_{min} are now considered to be a continuous function of λ, where

$$T_{max} = \frac{Ax}{B - Cx + Dx^2} \tag{3.9}$$

$$T_{min} = \frac{Ax}{B + Cx + Dx^2} \tag{3.10}$$

The spectrum can roughly be divided into four regions. In the transparent region $\alpha = 0$ and the transmission is determined by n and s through multiple reflections. In the region of weak absorption α is small but starts to reduce the transmission. In the region of medium absorption α is large and the transmission decreases mainly due to the effect of α. In the region of strong absorption the transmission decreases drastically due almost exclusively to the influence of α.

In the transparent region $\alpha = 0$ or $x = 1$. Substituting equations (3.8) into (3.9) yields

$$T_{max} = \frac{2S}{S^2 + 1} \tag{3.11}$$

which is identical to equation (3.5). This equation can be used to calculate s in the transparent region. Substituting equations (3.8) in (3.10) for $x = 1$ yields

$$T_{min} = \frac{4n^2 s}{n^4 + n^2(s^2 + 1) + s^2}$$

or $$n = [M + (M^2 - s^2)^{1/2}]^{1/2} \tag{3.12}$$

where $M = \dfrac{2s}{T_{min}} - \dfrac{s^2+1}{2}$

T_{min} is thus a function of both n and s and n can be calculated from T_{min} using equation (3.12). In the region of weak and medium absorption, $\alpha \neq 0$ and $x < 1$. Subtracting reciprocal of equation (3.9) from equation (3.10) yields an expression that is independent of x.

$$\frac{1}{T_{min}} - \frac{1}{T_{max}} = \frac{2C}{A} \qquad (3.13)$$

substituting equation (3.8) into (3.13) and solving for n yields

$$n = [N + (N^2 - s^2)^{1/2}]^{1/2} \qquad (3.14)$$

where $N = 2s \dfrac{T_{max} - T_{min}}{T_{max} T_{min}} + \dfrac{s^2+1}{2}$

From T_{max} and T_{min}, $n(\lambda)$ can be calculated using equation (3.14) and since $n(\lambda)$ is known, x can be calculated in different ways. Solving equation (3.9) gives

$$x = \frac{E_M - [E_M^2 - (n^2-1)^3 (n^2 - s^4)]^{1/2}}{(n-1)^3 (n - s^2)} \qquad (3.15)$$

where $E_M = \dfrac{8n^2 s}{T_{max}} + (n^2 - 1)(n^2 - s^2)$

solving equation (3.10) gives

$$x = \frac{E_m - [E_m^2 - (n^2-1)^3 (n^2 - s^4)]^{1/2}}{(n-1)^3 (n - s^2)} \qquad (3.16)$$

$$\text{where } E_m = \frac{8n^2s}{T_{min}} - (n^2 - 1)(n^2 - s^2) .$$

The reciprocals of equations (3.9) and (3.10) gives

$$x = \frac{F - [F^2 - (n^2 - 1)^3 (n^2 - s^4)]^{1/2}}{(n - 1)^3 (n - s^2)} \tag{3.17}$$

$$\text{where } F = \frac{8n^2s}{T_i}$$

$$\text{and } T_i = \frac{2\, T_{max}\, T_{min}}{T_{max} + T_{min}}$$

T_i represents the interference free transmission.

In the region of strong absorption the interference fringes disappear. Values of n can be estimated by extrapolating the values calculated in the other parts of the spectrum. For very large α the curves $T_{max,}$ T_i and T_{min} converge to a single curve T_o. Then

$$x \approx \frac{(n + 1)^3 (n + s^2)}{16n^2s} T_o \tag{3.18}$$

The refractive index of the substrate can be determined by measuring the interference-free transmission of the clean substrate alone and using equation (3.6) to calculate s.

Since $n(\lambda)$ is calculated, $x(\lambda)$ can be determined from any of the curves T_{max} , T_i or T_{min} using their respective formulae. Measuring the thickness d of the film, $\alpha(\lambda)$ can be calculated from $x(\lambda)$ using the equation $x = \exp(-\alpha d)$.

For the measurements, a Hitachi Model No. U - 3410, UV - Vis - NIR spectrophotometer which can cover the wavelength range from 2600 to 185 nm, was used. This instrument has got fairly high resolution and a spectral band width of 2 nm was used in the instrument.

REFERENCES

1. K.G.Guenther, in *The Use of Thin Films in Physical Ivestigations* (J.C.Anderson, Ed.), Academic Press, New York, 1966, P.213.

2. J.George, in *Preparation of Thin Films*, Marcel Dekker, New York, 1992.

3. S.Dushmen, in *Scientific Foundations of Vacuum Techniques*, John Wiley, New York, 1962.

4. M.A.Nesmeyanov, in *Vapor Pressure of Chemical Elements*, Elsevier, Amsterdam, 1963.

5. R. Glang, in *Handbook of Thin Film Technology* (L.I.Maissel and R.Glang, Eds.), McGraw-Hill, New York, 1970.

6. S.Tolansky, in *Multiple Beam Interferometry of Surface and Films*, Oxford University Press, London. 1948.

7. B.Pradeep, *Ph. D. Thesis*, Cochin University of Science and Technology, 1986.

8. R.Swanepoel, *J. Phys. E: Sci. Instrum.*, **16**, 1214 (1983).

CHAPTER 4

TIN SELENIDE (SnSe) THIN FILMS PREPARED BY REACTIVE EVAPORATION

4.1 INTRODUCTION

Tin monoselenide (SnSe) belongs to the IV - VI compounds, is a semiconductor with layer-type character and has an orthorhombic crystal structure with a space group D_{2h}^{16}. According to Okasaki [1] and Wyckoff [2], the lattice parameters of SnSe are: a = 4.46, b = 4.19 and c = 11.59 Å. Crystals of SnSe are formed by tightly bound double layers of metal and chalcogen atoms stacked along the c-axis. This lattice structure can be described as a strongly distorted NaCl type. The atoms in the planes are held together by strong forces, while the bonding between the planes is weak and thought to be of Van der Waals type. SnSe exhibits a strong anisotropy in its physical properties and has received considerable attention due to its possible technical applications in various fields. It can be used as cathodic materials in lithium intercalation batteries [3] and its solid-solutions with lead chalcogenides is a promissing material for optoelectronic devices [4]. The energy gap of SnSe reported by different authors is in the range of 0.9 to 1.3 eV at room temperature. Because of its application as memory switching devices [5,6] and being an efficient material for solar applications [9,10], thin films of SnSe have great potentialities. The electrical and optical properties of tin monoselenide both in the bulk and

thin film form had been investigated by a number of scientists [11-38]. An anomalous variation of the Hall coefficient of crystalline SnSe was observed by Asanabe [11]. Maier & Daniel [12] studied the electrical properties of single crystals of SnSe grown by sublimation method. J.G.Yu et al. [13] have reported the electrical and optical properties of the crystals grown by the close-tube-vapor-transport technique. X-ray photoemission studies of the valence band of SnSe were performed by Shalvoy [14] and IR and Raman spectra were analysed by Chandra Shekhar et al. [15]. Absorption spectra analysis has been carried out by Mochida [16], Takashashi [17], Guseinova et al. [18], Elkorashy [19, 20] and Garg [21].

A variety of physical and chemical deposition techniques have been employed for the preparation of amorphous and polycrystalline thin films of tin monoselenide [22-38]. They can be generally classified into two, viz; vacuum evaporation and chemical deposition.

Baxter and McLeman [6] have analysed the vacuum deposited amorphous films of SnSe and observed a switching property of it. Engelken et al. [22] have prepared SnSe films by electrodeposition and studied their optical properties and photo conductance. An energy gap of 1.3 eV for annealed polycrystalline films was observed by them. Pramanik and Bhattacharya [23] have deposited amorphous SnSe films with n-type conductivity by a chemical method and conducted its optical absorption studies. Nuriev et al. [25], Mikolaichuk et al. [25a], Chopra [26] and Avilov et al. [27] have been concentrated their studies on the structural aspects of SnSe thin films while Ganesan and Sivaramakrishnan [28] have examined the gas absorption effects

on the electrical properties of these films. The electrical properties and optical absorption of evaporated SnSe films [29] and the films obtained by solid state reactions [30] have been reported by Quan. Structural analysis of these films showed that the crystallites of the films have preferential orientation on the substrate surface. Subba Rao and Chaudhuri [31-35] have investigated the structural, electrical and photoelectronic properties of the thermally evaporated films of SnSe. They have observed the formation of the high temperature phase of SnSe films, when deposited at substrate temperatures of 473 K and above. Photoelectric and optical properties of evaporated poly-crystalline SnSe films have been studied by Bennouna et al. [24]. The electrical and optical absorption of the flash evaporated SnSe films [36] and the films grown by hot wall epitaxy [37] were reported by Singh & Bedi. Hot wall expitaxial films had a preferred orientation with their (111) planes parallel to the substrate plane. Bhatt et al. [38] have also investigated the electro-optic properties of vacuum evaporated SnSe thin films. However, nobody has yet reported the preparation of SnSe thin films by reactive evaporation method.

In the present chapter is reported the preparation of polycrystalline stoichiometric SnSe films by three temperature method. Structural characterisations of these films are done by X-ray spectra. From the transmission spectra, the refractive index absorption coefficient and band gap of the films are determined.

4.2 EXPERIMENTAL

Tin monoselenide films were prepared by reactive evaporation, a variant of the three temperature method, in which the individual elements were

evaporated from separate sources and the compound films were deposited on the substrate, kept at an elevated temperature. It has been found [39,40] that for many binary materials a stoichiometric interval exists with a limited degree of freedom in selecting the individual component flux and the substrate temperature.

Tin and selenium (purities 99.999%) were used as evaporants. Tin was evaporated from a molybdenum boat and selenium from a conical quartz crucible with molybdenum wire windings. The deposition was performed in an oil diffusion pumped low pressure (~10^{-6} torr) chamber as discussed in chapter 3. Glass substrates used for the deposition of the films were fixed on to a specially designed heater whose temperature could be controlled with an accuracy of ± 2 °C. Chromal-alumel thermocouple placed in contact with the substrate was used for measuring its temperature.

When the substrate had attained the required temperature and stabilized, the current through the selenium source was switched on and the selenium was allowed to melt in the crucible with a shutter placed over the tin and selenium sources. The tin source current was then switched on and increased to a pre-set value. After adjusting the flux from the two sources to a predetermined value the shutter was withdrawn and the deposition of the compound films allowed to take place.

When the tin and selenium atoms impinge on the substrate surface, they are adsorbed and begin to react by acquiring sufficient activation energy from it to form the compound. This is an ordering process where by the adsorbed

atoms diffuse across the surface until they fall into potential wells represented by regular lattice sites. The unreacted atoms are unable to stick to the substrate independently at the given elevated temperature and they are desorbed after a finite interval of time.

It has been found that good stoichiometric films of tin selenide are obtained with the following deposition parameters:

tin flux = $3.7 \times 10^{14} - 4.1 \times 10^{14}$ atoms $cm^{-2}s^{-1}$

selenium flux = $4.6 \times 10^{14} - 5.2 \times 10^{14}$ atoms $cm^{-2}s^{-1}$

substrate temperature = 473 - 600 K

The deposition rate of SnSe films was 0.2 - 0.3 nm s^{-1}. Highly reproducible films were obtained under these conditions and these films had a metallic lusture. All the films used in this study were deposited on optically flat glass substrates.

4.3 STRUCTURAL STUDIES

Structural characterizations of the prepared films were carried out by X-ray diffraction using films with a thickness around 325 nm. Diffraction profiles of the film-substrate system prepared at different temperatures were recorded on a chart recorder using monochromatic CuK_{α} radiation.

Fig.4.1 (a-d) show the X-ray diffractograms of typical SnSe thin films prepared at different substrate temperatures. The corresponding substrate temperature and (hkl) planes are also indicated.Table 4.1 compares the d-values calculated from the X-ray diffractograms of Fig. 4.1 (a-d) with the standard d-values of SnSe obtained from the JCPDS Powder Diffraction File [41]. The relative intensities of the peaks are also compared [Table 4.2]. All the diffraction lines are matched well with the standard pattern of SnSe. A very slight change in d-values is obtained for the films prepared at different substrate temperatures and it is due to the different amount of strain present in the films. Because every line in the JCPDS card with moderate intensity could be identified, it must be concluded that the prepared films were polycrystalline stoichiometric SnSe films, maintaining the same structure as that of the bulk SnSe. The grains of the films prepared below 530 K were randomly oriented.

The relative intensities of the peaks obtained for the films prepared at different temperatures are compared in Table 4.2. With the increase of the substrate temperature, the intensity of (400) reflection increased considerably where as that of the other reflections diminished. Comparison of the diffractograms of Fig. 4.1(a-d) reveals the gradual increase in intensity of the (400) reflection with a simultaneous decrease in intensity of (111) peak, with the raise in substrate temperature. The number of peaks were also found to increase with deposition temperature, which is due to the improved crystallinity of the films at higher temperatures. Further increase in substrate temperature gave a preferred orientation to the grains.

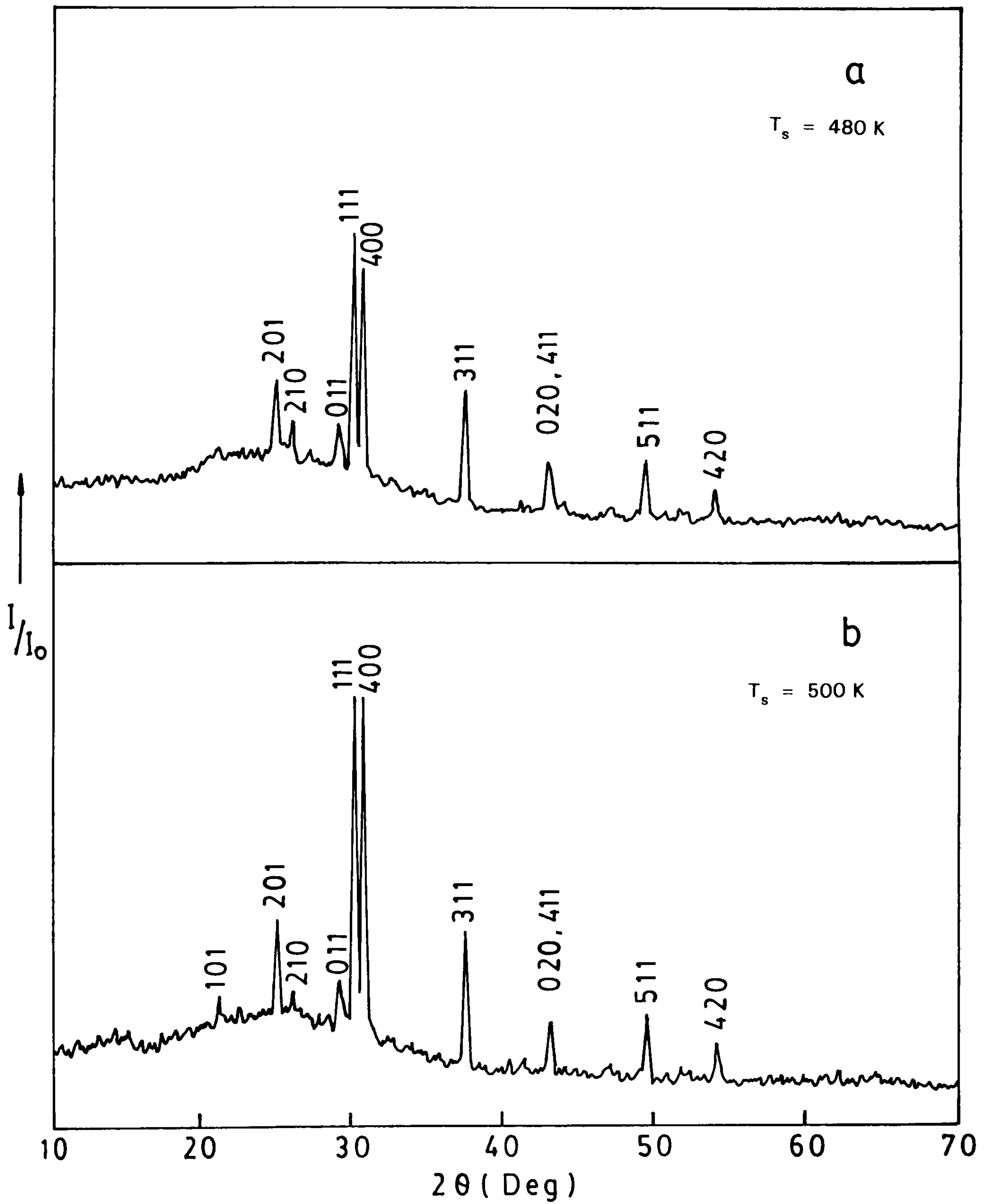

Fig. 4.1(a,b) X-ray diffractograms of SnSe thin films prepared at different substrate temperatures: (a) 480 K and (b) 500 K

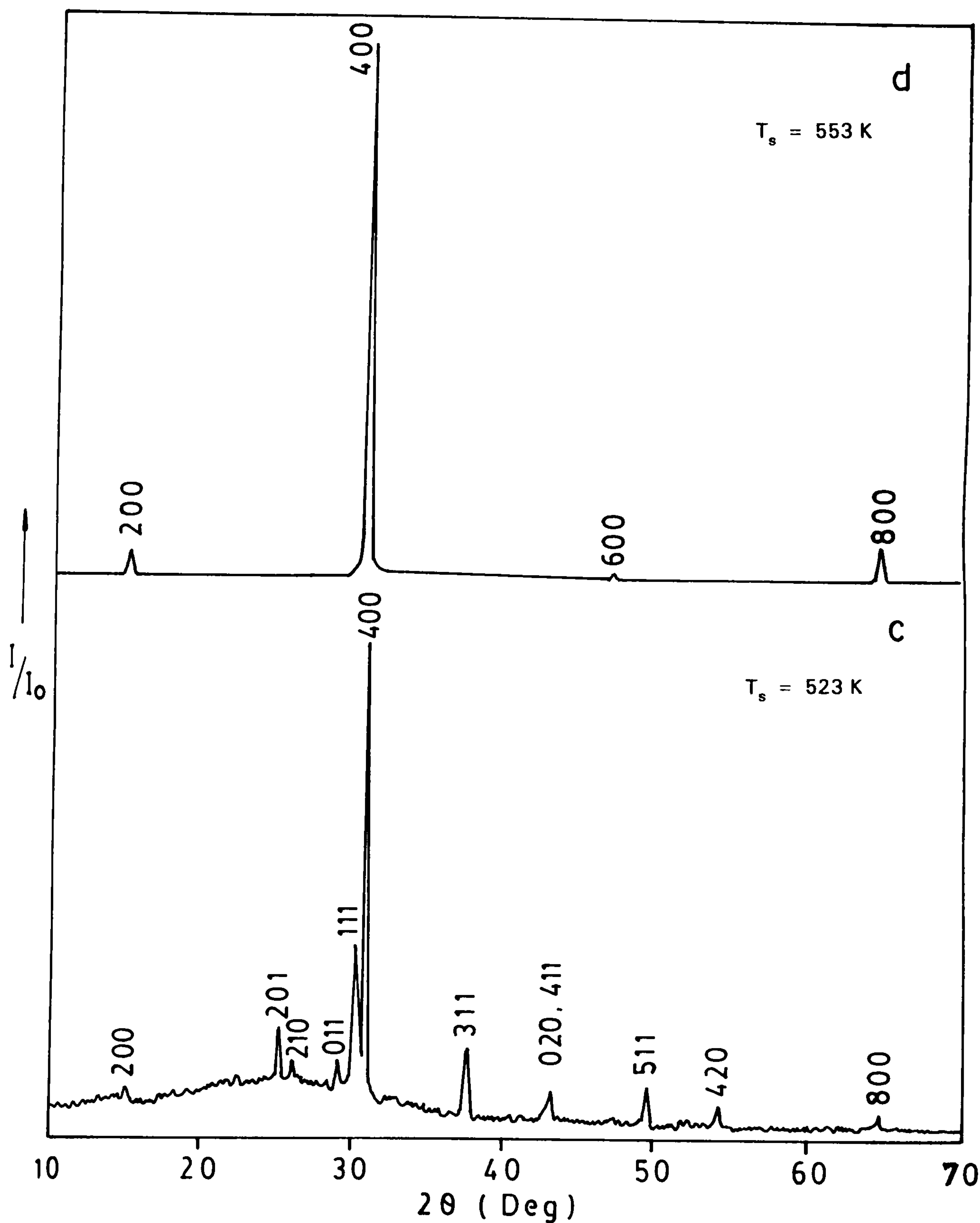

Fig. 4.1(c,d) X-ray diffractograms of SnSe thin films prepared at different substrate temperatures: (c) 523 K and (d) 553 K

TABLE 4.1

X-ray diffraction data of SnSe films prepared at different substrate temperatures

hkl	Standard Pattern d Å	T_s=480 K d Å	T_s=500 K d Å	T_s= 523 K d Å	T_s=553 K d Å
200				5.701	5.70
101	4.11		4.109		
201	3.49	3.491	3.491	3.49	
210	3.35	3.355	3.353	3.348	
011	3.02	3.017	3.017	3.021	
111	2.921	2.919	2.919	2.921	
400	2.862	2.863	2.863	2.864	2.862
311	2.372	2.368	2.369	2.372	
411,020	2.080	2.077	2.075	2.079	
600	1.917				1.911
511	1.829	1.825	1.827	1.830	
420	1.680	1.682	1.682	1.682	
800	1.435			1.435	1.435

TABLE 4.2

Relative intensities of different peaks of SnSe thin films deposited at different substrate temperatures (T_s)

hkl → / T_s [K] ↓	200	101	201	210	011	111	400	311	411,020	600	511	420	800
480			36	19	18	100	86	50	24		28	17	
500		12	33	12	15	100	100	42	17		20	12	
523	3		14	6	7	32	100	17	8		10	7	4
553	5						100			1			7
Standard Pattern		1	6	2	6	95	100	50	20	4	55	25	4

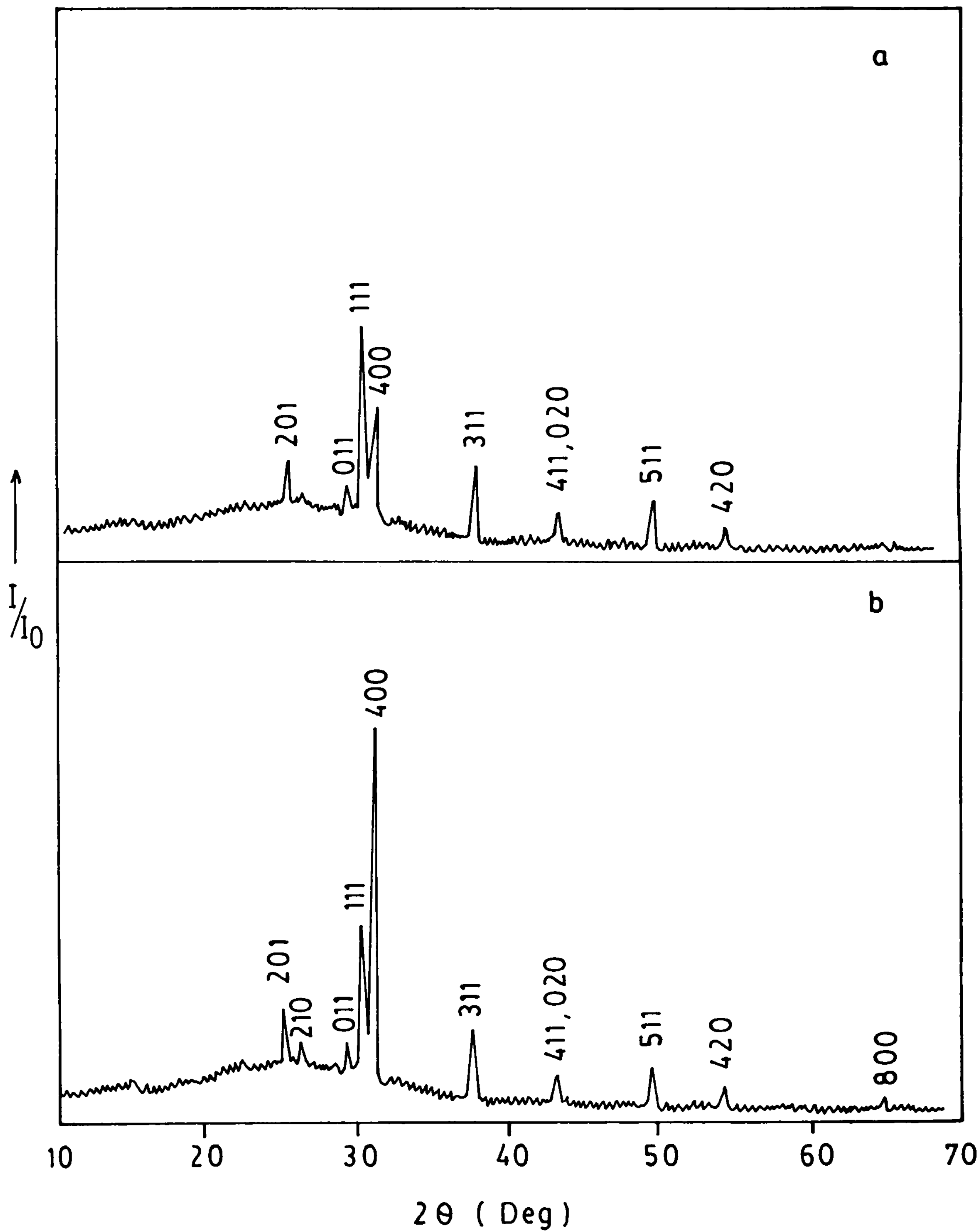

Fig. 4.2(a,b) XRD patterns of SnSe films prepared at 473 K: (a) before annealing and (b) after annealing at ≈ 600 K

In the X-ray diffraction pattern of the films prepared at substrate temperatures 553 K and above, the (400) and its equivalents (200), (600) and (800) reflections alone were observed. This indicates that the SnSe films prepared at these temperatures have a strongly preferred orientation on the substrate surface and their crystallites are perpendicular to the (400) plane. This preferential orientation is similar to the orientation of the SnSe thin films synthesized by solid state reaction [30] and is different from the (111) orientation of the films grown by hot wall epitaxy [37].

Fig. 4. 2 (a& b), respectively show the X-ray diffraction profiles of the as grown film at substrate temperature $\approx$ 475 K and that of the film after annealing at a higher temperature $\approx$ 600 K for three hours. It can be seen that the intensity of (111) reflection is reduced considerably where as that of the (400) reflection is increased simultaneously, with annealing. Any other significant change in profile shape of the film has not occurred due to the post-deposition annealing. Therefore, it may be concluded that the preferential orientation of the grains of SnSe films on the substrate surface solely depends on the substrate temperature at the time of deposition.

4.4 OPTICAL PROPERTIES

Optical measurements of the films were made using Hitachi U-3410, UV-Vis-NIR spectrophotometer. A typical transmission spectrum of the SnSe films of thickness about 325 nm, prepared at a substrate temperature of 553 $\pm$ 2 K is shown in Fig. 4.3. The refractive index of the film has been determined from the interference maxima and minima using Swanepole's

method [42]; described in chapter 3. Knowing the value of the refractive index, the absorption coefficient in the fundamental absorption region was calculated.

The spectral response of the refractive index n is shown in Fig. 4.4. It can be seen that the refractive index is an increasing function of $h\upsilon$. At the lower energy side n remains almost constant while a rapid increase occurs in the vicinity of the absorption edge. Its value is in reasonable agreement with the bulk value reported for single crystals [16, 21, 43].

Fig. 4.5 shows the optical absorption coefficient α, as function of photon energy. The absorption has its minimum value at its low energy and increases with increasing optical energy in a similar manner to the absorption edge of the semiconductor.

The optical absorption data of SnSe films were analysed for evidence of either indirect or direct transitions in accordance with the theory of Bardeen[44] and Smith [45]. The theory predicts that, the fundamental absorption coefficient α due to the direct transitions between the valence and conduction bands is given by

$$(\alpha h \upsilon) = A (h\upsilon - E_g)^x$$

where x takes the value of 1/2 for the allowed direct transition and 3/2 for the forbidden direct transition. On the other hand, for the absorption due to the indirect transition, absorption and emission due to phonon are involved and the expression for α is written as

$$(\alpha h \upsilon) = B (h\upsilon - E_g \pm E_p)^x$$

E_g is the indirect energy gap and E_p the absorbed (+) or emitted (-) phonon energy. In this case $x = 2$ for allowed indirect transitions and $x = 3$ for forbidden indirect transitions.

Fig. 4.6 shows $(\alpha h \upsilon)^2$ as a function of photon energy. Due to the appreciable linearity of the curve, it is confirmed that the absorption near the fundamental edge is caused by a direct allowed transition. Moreover, from the Fig. 4.5 (α vs $h\upsilon$) it is clear that the value of α, which is of the order of 10^4 cm^{-1}, is a characteristic of the allowed direct transition in accordance with Smith [45]. Because the measurements were made at room temperature exciton bands are not likely to be present. Hence, it is reasonable to believe that the absorption in SnSe films is due to band to band transitions. The extrapolation of the linear part of the graph gives a band gap of (1.21 ± 0.01) eV. This is in good agreement with the reported values for SnSe thin films prepared by bulk evaporation [29], solid state reaction [30] and hot wall epitaxy [37]. Investigations on SnSe single crystals by Gueseinova et al. [18] have also been confirmed the direct band gap of about 1.2 eV at room temperature.

Indirect allowed type fundamental absorption in SnSe with energy gaps in the range of 0.9 to 1.3 eV at room temperature has also been reported by different authors. These values of band gaps are given in Table 4.3.

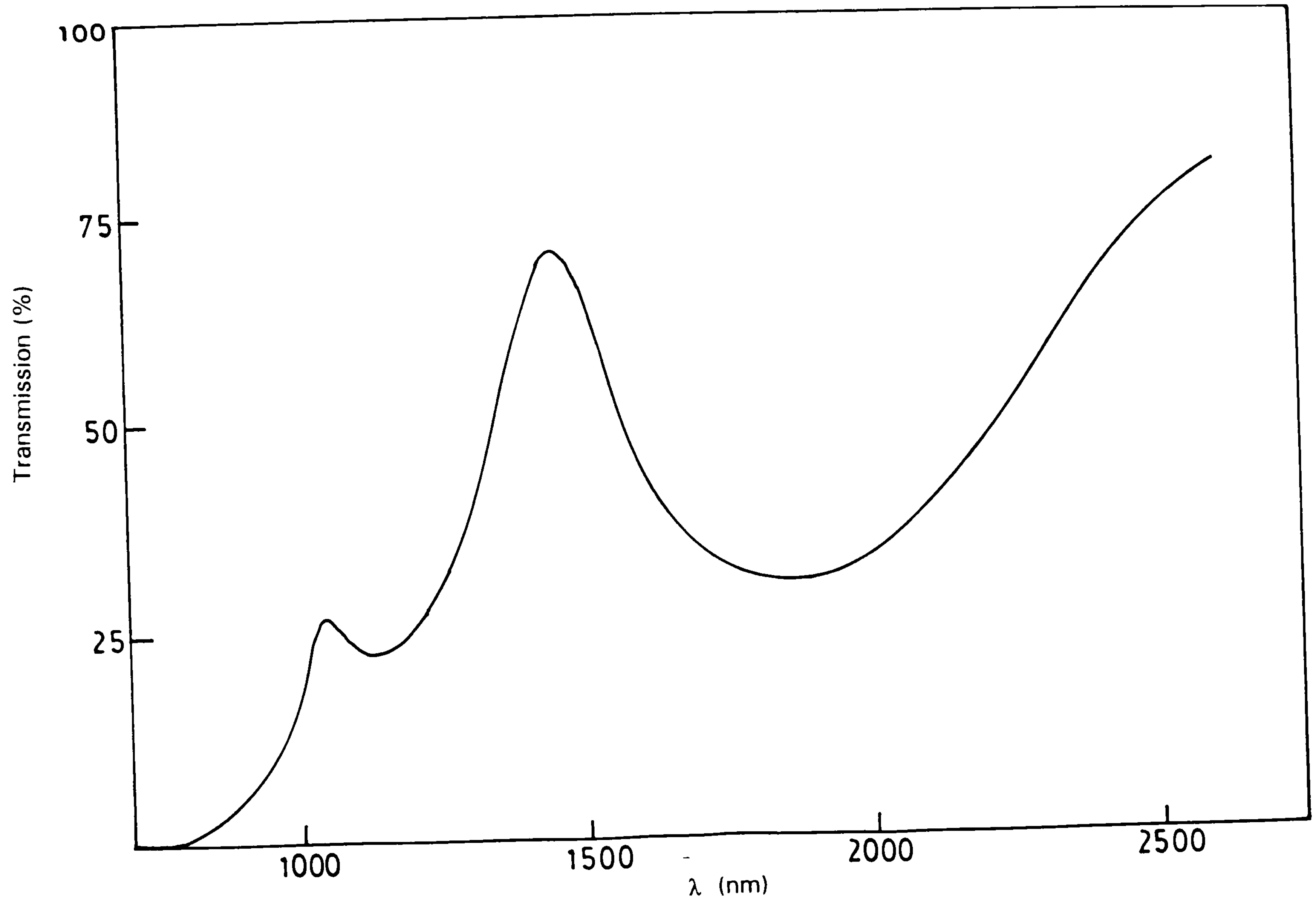

Fig. 4.3 Transmission spectrum of a typical SnSe thin film

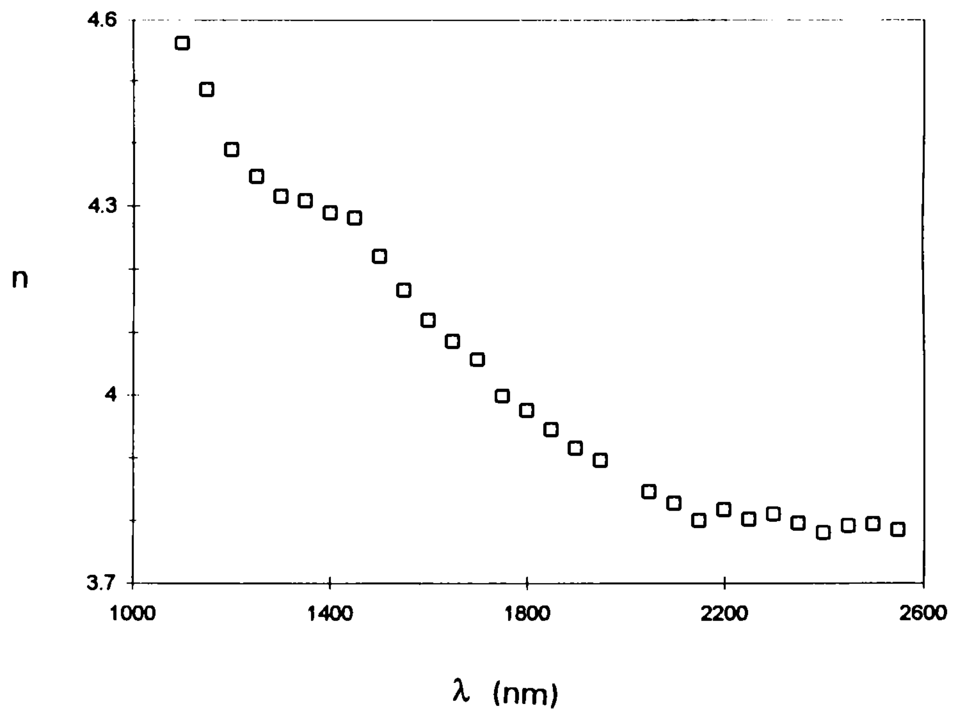

Fig. 4.4 Variation of refractive index, (n), with wavelenth, (λ).

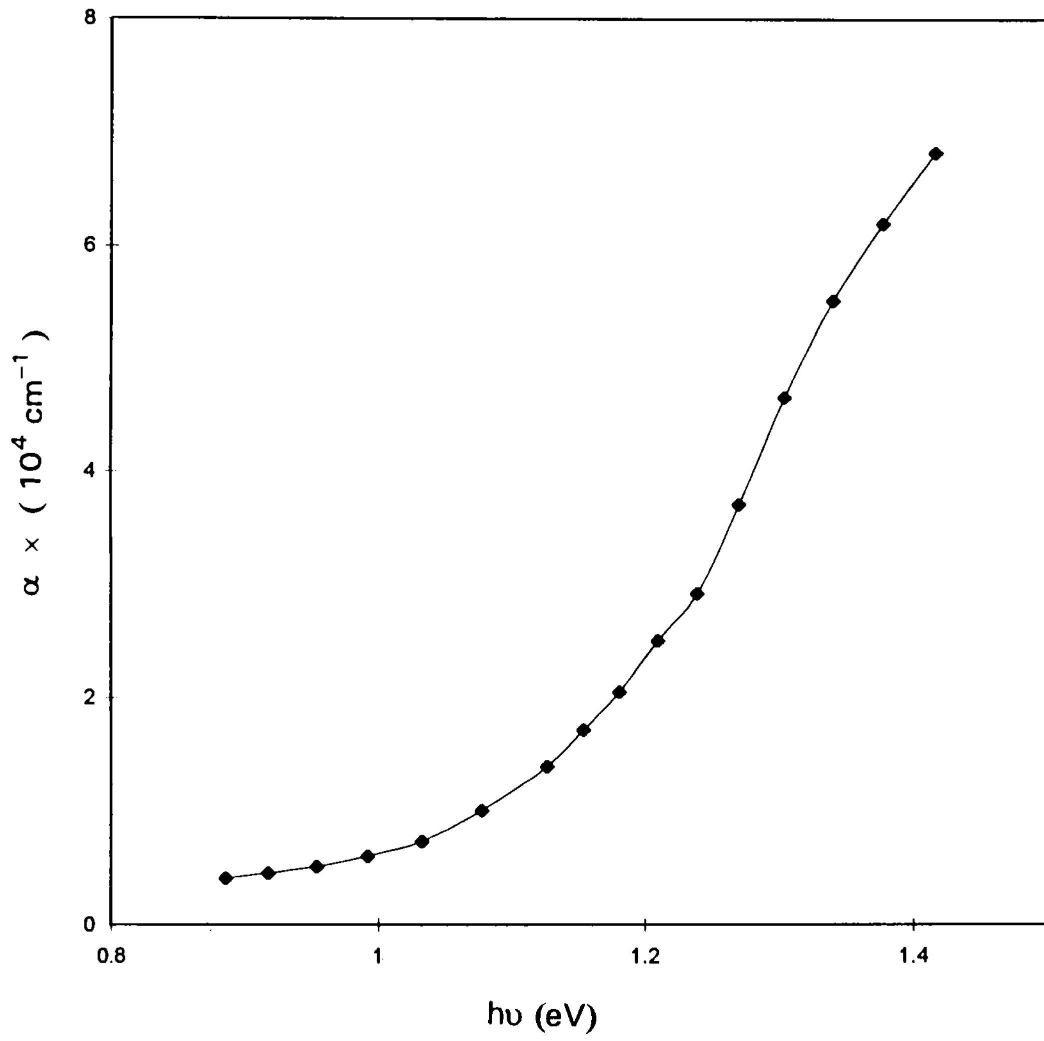

Fig. 4.5 **Variation of absorption coefficient, α, with photon energy, hυ**

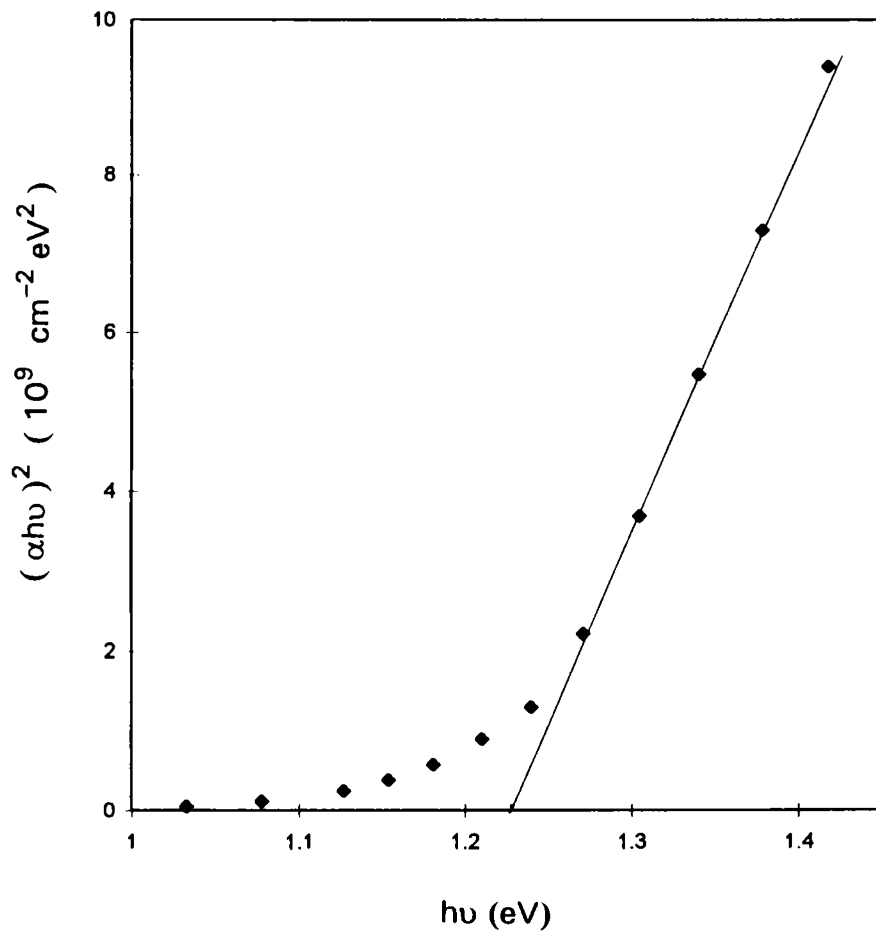

Fig. 4.6 The absorption edge of SnSe film plotted as $(\alpha h\upsilon)^2$ against the photon energy, $h\upsilon$.

TABLE 4.3

Reported values of band gap of tin selenide

Sl. No.	Authors with reference	Type of material	Band gap (eV)		
			Direct allowed	Indirect allowed	Indirect forbidden
1.	J G Yu et al. [13]	Crystalline solid		0.923	
2.	Y Mochida et al. [16]	"		0.932	
3.	K Takahashi et al. [17]	"		0.939	
4.	D A Guseinov et al. [18]	"	1.2		
5.	A M Elkorshy [20]	"			0.948
6.	A K Garg et al. [21]	"		0.94	
7.	C Julien et al. [48]	"		0.90	
8.	V P Bhatt et al. [49]	"		0.936	
9.	D L Mitchell [Ref of 22]	"	1.2		
10.	R D Engelken et al. [22]	Amorphous film		0.95	
11.	-do-	Crystalline film		1.3	
12.	P Pramanik et al. [23]	Amorphous film		0.95	
13.	D T Quan [29]	Crystalline film	1.21		
14.	D T Quan [30]	"	1.195		
15.	J P Singh et al. [37]	"	1.2		
16	V P Bhatt et al. [38]	"		0.935	
17.	Present study [50]	"	1.21		

4.5 CRITICAL OPTIMIZATION

The transmission spectra of SnSe films prepared at various substrate temperatures are shown in Fig. 4.7 The thickness of the films is around 325 nm. It is well known that the 'amplitude' of the interference fringes produced by a film is depending on its surface smoothness and its scattering/absorption ability. Large amplitude interference fringes will be obtained, if the film surface is highly reflecting and there is not much scattering/absorption in the bulk of the film. The amplitude of the interference fringes can therefore be considered as a measure of the film quality. If this is used as a criterion for the quality of the films, it may be seen that films prepared with a substrate temperature around (550 ± 10) K are the best films. When the substrate temperature is lowered the amplitude of the fringes becomes smaller and at 473 K, which is the lowest substrate temperature used, it becomes the smallest. When the substrate temperature is raised to 600 K, transmission decreases. This latter effect is certainly due to absorption by selenium vacancies in the film, because at this substrate temperature re-evaporation of the chalcogen from the growing film will be considerable.

Fig. 4.8 shows the refractive index as a function of wavelength for films prepared at different substrate temperatures. It can be seen that the refractive index attains maximum value for the films prepared at substrate temperature around 550 K.

From the results given above, it is clear that the film properties are optimized at a substrate temperature (550 ± 10) K; ie, the films are smoother, have good transmission and the refractive index approaches the bulk value.

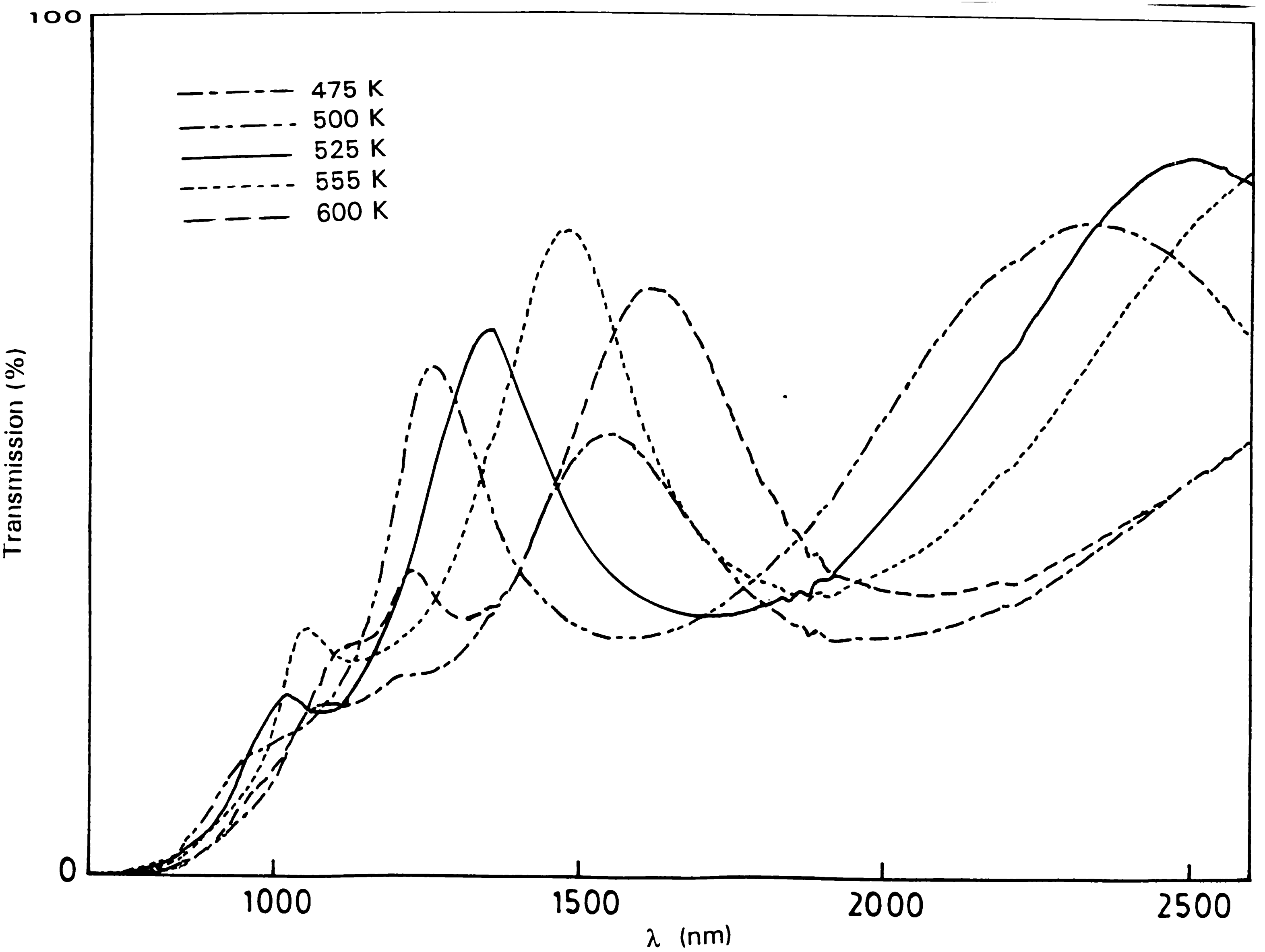

Fig. 4.7 Transmission spectrum of typical SnSe thin films prepared at different substrate temperatures

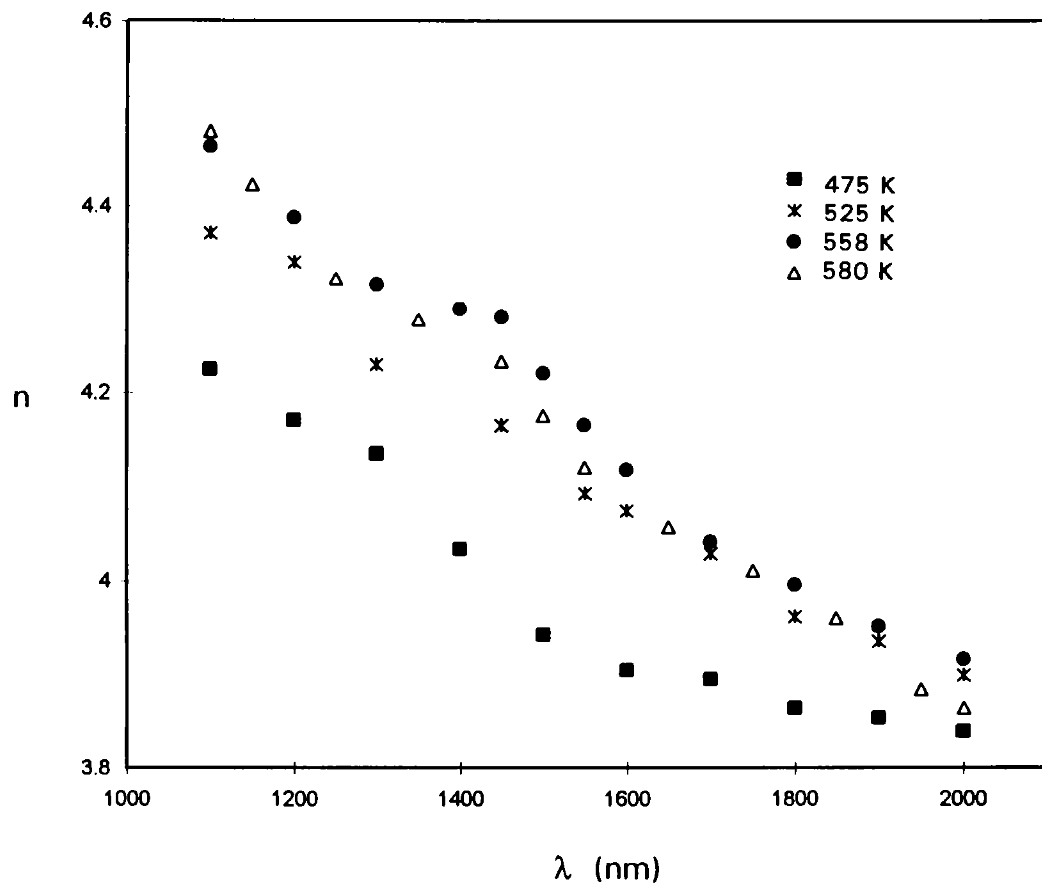

Fig. 4.8 **Variation of refractive index with wavelength for SnSe films prepared at different temperatures**

These results can be qualitatively explained in terms of the concept of critical optimization of Vincett [46]. He has shown that when the substrate temperature is approximately equal to one-third of the boiling point of the material, nucleation of the films with larger crystallites takes place and the film qualities (surface smoothness, optical transmission, carrier mobility, etc.) improve considerably. From thermodynamic considerations he has obtained the above criterion and has experimentally verified this for a large number of compounds. According to Vincett, when the substrate temperature is low, disordered as well as crystalline region condense on the substrate surface. But when one goes to a higher substrate temperature preferential evaporation of disordered regions in the growing film occurs and substantial diffusion and re crystallization takes place. Thus the volume occupied by the disordered region of the film falls and the film quality increases as a increasing function of substrate temperature. As the temperature approaches one-third of the boiling point of the substance, the re-evaporation of the disordered areas of the film becomes equal to the deposition rate and a complete re-evaporation of the original disordered region occurs in this stage [47]. Films prepared at substrate temperature in this range will have a smooth surface and grain boundary will be less. If the substrate temperature is increased further, evaporation of the crystalline areas in the growing films takes place, which results in a film of poor quality.

For SnSe films prepared at different substrate temperatures, Subba Rao et al. [35] have observed an increase in the crystallite size upto a substrate temperature, $T_s \approx 422$ K and a fall in the size value at higher temperatures.

The ratio of the optimum substrate temperature T_s to the boiling temperature T_b of SnSe observed by them is ≈ 0.27, which is lower than that given by the criterion proposed by Vincett et al. [46].

As said earlier, in the present case the transmission spectra of the film prepared in the temperature range (550 ± 10) K, exhibit large amplitude interference fringes, which is a measure of the film quality. The refractive index of the film also goes through a maximum and attains the bulk value in this range. This shows that the film properties are optimized at this range of substrate temperature. This optimum value of substrate temperature is approximately equal to one-third of the boiling point of SnSe. The value $T_s/T_b \approx 0.35$, is very close to that in accordance with Vincett's empirical concept. The highly preferential orientation of the crystallites observed in films prepared at the same range of temperature (which is discussed in the previous section) also supports the concept of critical optimization.

4.6 CONCLUSION

Polycrystalline stoichiometric SnSe thin films are prepared by reactive evaporation at substrate temperatures ranging from 473 - 600 K. The grains of the films prepared at substrate temperatures below 530 K have no preferred orientation, while the crystallites of the films prepared at higher substrate temperatures have a strongly preferred orientation on the substrate surface. Optical absorption studies show that the fundamental absorption starts at (1.21 ± 0.01) eV and the transition leading to this is a direct allowed one.

REFERENCES

1. Okazaki A., and Ueda.I., *J. Phys. Soc. Japan.* **11**, 470 (1956).

2. Wyckoff R.W.G., *Crystal structures*, vol. I. Interscience, New York (1963)

3. J.Yamaki and A.Yamaji., *Physica*, **105B**, 466 (1981)

4. Harman T.C. and Melngailis I., *Applied solid state Science*, Vol. 4, P.1 (Plenum: New York) (1974).

5. Dongwoo Chu R.M., Walser R.W.B. and Courtney T.H., *Appl. Phy. Lett.* **24**, 479 (1974).

6. Baxter C.R and McLeman WD. *J. Vac. Sci. Technol.* **12**, 110 (1975)

7. Loferski J, *J. Appl. Phys.* **27**, 777 (1956).

8. Loferski J, *Proc. IEEE.* **51**, 667 (1963).

9. Rodot M., *Acta Electronica.* **18**, 345 (1975).

10. Rodot M., *Rev. Phys. Appl.* **12**, 411 (1977).

11. Asanabe S., *J. Phys. Soc. Japan.* **14**, 281 (1959)

12. Maier H and Daniel D.R., *J. Elect. Mater.* **6**, 693 (1977).

13. Yu J.G., Yue A.S. and Stafsudd O.M., *J. Cryst. Growth.* **54**, 248 (1981).

14. Shalvoy R.B, Fisher G.B. and Shiles P.J., *Phys. Rev.* **B15**, 2021 (1977)

15. Chandrashekhar H.R, Humphery R.G., Zwick. U and Cardona M., *Phys. Rev.* **B15**, 2177 (1977).

16. Mochida Y., *Sci. Light* **17**, 57 (1968).

17. Takahashi K., Arai T and Kudo K., *Sci. Light* **21**, 131 (1972).

18. Guseinova D.A, Krivaite G.Z. and Marnedov M.M., *Sov. Phys. Semicond.* **19**, 923 (1985).

19. Elkorashy A.M., *J. Phys. Chem. Solids* **47**, 497 (1986).

20. Elkorashy, A.M., *J. Phys. Chem. Solids* **50**, 893 (1989).

21. Garg A.K., Jain A.K. and Agnihotri O.P., *Ind. J. Pure & Appl. Phys.* **21**, 276 (1983).

22. Engelken R.D, Berry A.K., Van Doren T.P., Boone J.L, and Shahnazary A., *J. Electrochem. Soc.*, **133**, 581 (1986).

23. Pramanik.P. and Bhattacharya S. *J. Mater. Sci. Lett.*, **7**, 1305 (1988).

24. Benaouna A, Tessier P.Y, Priol M., Quan D.T and Robin S., *Phys. Stat. sol* (b) **117**, 51 (1983).

25. Nuriev I.R and A.K.Sharifova; *Sov. Phys. Crystallogr.* **34**, 635 (1989).

25a. A.G.Mikolaichuk, Dutchak Ya I and D.M. Freik; *Sov. Phys. Crystallogr.* **13**, 490 (1968).

26. K.L.Chopra., *Appl. Phys. Lett.* **10**, 282 (1967).

27. A.S.Avilov, R.M.Imamov and S.N.Navasardayan., *Sov. Phys. Crystallogr.* **24**, 504 (1979).

28. N.Ganesan and V.Sivaramakrishnan., *Semicond. Sci. Technol.* **2**, 519 (1987).

29. Dang Tran Quan., *Phys. Stat. Sol* (a) **86**, 421 (1984).

30. Dang Tran Quan., *Thin Solid Films*, **149**, 197 (1987).

31. Subba Rao. T, B.K.Samantharay and A.K.Chaudhuri., *J. Mater. Sci. Lett.* **4**, 743 (1985).

32. Subba Rao T and Chaudhuri A.K., *J. Phys. D: Appl. Phys.* **18**, L35 (1985).

33. Subba Rao T and Chaudhuri A.K., *J. Phys. D: Appl. Phys.* **19**, 861 (1986).

34. Subba Rao T, Samantaray B.K. and Chaudhuri A.K., *Z.Kristallogr.*, **175**, 37 (1986).

35. Subba Rao T, Samanataray B.K. and Chaudhuri A.K., *Thin Solid Films*, **165**, 257 (1988).

36. Singh J.P. and Bedi R.K. , *Thin Solid films*, **199**, 9 (1991).

37. Singh J.P. and Bedi R.K., *J. Appl. Phys.* **68**, 2776 (1990).

38. Bhatt V.P., Gireesan K and Desai C.F., *Cryst. Res. Technol.* **24**, 187 (1989).

39. K.G.Gunther, in *The Use of Thin Films in Physical Investigations* (J.C.Anderson, Ed), Academic Press, New York, (1966) P. 213.

40. J. George, in *Preparation of Thin Films* (Marcel Dekker, Inc. New York), (1992), P. 141.

41. JCPDS Card No. 14-159.

42. Swanepoel,R., *J. Phys E. Sci. Instrum.* **16**, 1214 (1983)

43. A.M.Elkorashy., *J. Phys. Chem. solids*, **51**, 289 (1990).

44. J. Bardeen, F.J.Blatt and L.H.Hall, in "*Proceedings of the Photoconductivity Conference*: Atlantic City (Wiley, New York. 1956)

45. R.A.Smith in "*Semiconductors*", 2nd Edn (Cambridge University Press, 1978) P. 314.

46. P.S.Vincett, *Thin Solid Films* **100**, 371 (1982).

47. P.S.Vincett., *J. Vac. Sci. Technol.* **21**, 972 (1982).

48. Julien C. Eddrief M. Samaras. I and Balakanski M., *Mater Sci & Eng*. **B15**, 70 (1992).

49. Bhatt V.P., Gireesan K and Pandya G.R., *J. Cryst. Growth*. **96**, 649 (1989).

50. K.J. John, B.Pradeep and E.Mathai., *J. Mater. Sci.* **29**, 1581 (1994).

CHAPTER 5

ELECTRICAL PROPERTIES OF POLYCRYSTALLINE SnSe THIN FILMS

5.1 INTRODUCTION

Tin monoselenide (SnSe); the semiconductor with applications in optoelectronics, holographic recording systems and electrical switching, has been subjected to various analysis by a good number of investigators [1-21], as mentioned in the previous chapter. While most of the earlier studies have been concentrated on the structural and optical characteristics, the electrical transport studies on SnSe both in the bulk [1-3] and thin film state [15-20] are rather limited. Conductivity studies by Quan [15,16], Subba Rao & Chaudhuri [17] and Singh & Bedi [18,19] has revealed that the grain boundary potential barrier mechanism is predominant in polycrystalline thin films of this semiconductor.

The identification and definition of electronic transport in poly-crystalline semiconductor films has largely been a modeling effort. Even though a large number of theoretical models have been proposed, most of the analysis and modeling techniques correlating the transport properties with the polycrystallinity of thin films are based upon the consideration that the conduction mechanism in it is dominated by the inherent intercrystalline boundaries rather than the intracrystalline characteristics. The 'intercrystalline'

or the 'grain' boundaries have a significant role in controlling the carrier transport. If charge carriers become localized at the grain boundaries, the charged boundaries that arise could then act as potential barriers preventing the flow of free carriers. The charge density at the boundaries and consequently the barrier height should be a function of temperature and carrier density inside the blocks. For barrier heights close to the Fermi-energy the boundaries should scatter strongly the carriers with energies lower than the Fermi value and much less strongly those with energies above the Fermi level and this should reduce the energy in a carrier flux.

Preparation of SnSe thin films by reactive evaporation was done as described in chapter 4. The electrical properties such as conductivity, Hall mobility, thermoelectric power etc. of these films are included in this chapter. The electrical measurements on typical SnSe films prepared at a substrate temperature (553 ± 2) K and the variation of the transport properties with preparation temperature are reported below.

5.2 ELECTRICAL MEASUREMENTS ON TYPICAL POLYCRYSTALLINE FILMS

The films prepared for electrical measurements were of thickness about 325 nm. The thickness of the samples were found out using multiple beam interferometry. The electrical properties such as conductivity, carrier concentration, Hall mobility and thermoelectric power were measured using standard techniques described in chapter 3. Ohmic contacts to the bridge shaped samples were made by evaporating high purity aluminium through masks on to the film. The ohmic nature of the contacts was confirmed by the

linear current-voltage characteristics through out the temperature range studied (100 - 420 K). Hall voltages were determined only at temperatures above 220 K. The length-to-width ratio of the samples used for the Hall measurements was greater than four so that the influence of the film geometry was negligible. Each measurements were repeated many times and were found to be reproducible.

The Hall coefficient (R_H) of the film was calculated using the relation,

$$R_H = \frac{V_H \cdot d}{I \cdot H} \times 10^8 \ cm^3 / coulomb \qquad (5.1)$$

where V_H is the Hall voltage (volts), d thickness of the film (cm), I the current (amperes) and H the applied magnetic field (gauss).

The carrier concentration P of the samples was calculated from the relation

$$P = \frac{r}{e R_H} \qquad (5.2)$$

where r is the Hall factor and e the electric charge.

Hall mobility μ_H was calculated using the relation

$$\mu_H = \sigma R_H \ cm^2 V^{-1} S^{-1} \qquad (5.3)$$

where σ is the conductivity of the samples.

Hall measurements showed that the films obtained were p-type. Studies on SnSe single crystals by Maier & Daniel [2] revealed that an excess chalcogen

atom is responsible for the acceptor (an excess Sn for the donor). Hence, it is obvious that the p-carrier-type of the film is due to the presence of excess selenium, which will not leave any unreacted tin inside the crystallites, during the deposition of the film.

A typical plot of the conductivity σ on a logarithmic scale against the reciprocal temperature for an SnSe sample prepared at 553 K is shown in the Fig. 5.1. It can be seen that there are two distinct regions, each obeying an equation of the form.

$$\sigma = \sigma_o \exp\left(\frac{-E_\sigma}{KT}\right) \qquad (5.4)$$

where E_σ is the conductivity activation energy. A similar behaviour has been observed in SnSe films prepared by other methods also [15, 16, 18, 19].

Figures 5.2 and 5.3 show the variation of carrier density and Hall mobility of the film against reciprocal temperature, respectively. It may be seen that both the mobility and carrier density increases with increasing temperature. This is typical of many polycrystalline films and is due to the existence of potential barriers in the intercrystalline boundaries. The grain boundary potential barrier mechanism with the polycrystallinity of thin films are based upon the consideration that the grain boundaries have an inherent space charge region due to the interface. Band bending occurs, and potential barriers to the charge transport result. Petritz [22] and others [23-25] have shown that the mobility and carrier concentration in such cases are temperature

activated and obeys a law of the form,

$$\mu_H = \mu_o \exp\left(\frac{-E_a}{KT}\right)$$

$$\text{and } P = P_o \exp\left(\frac{-E_p}{KT}\right) \tag{5.5}$$

where E_a is the grain boundary barrier potential and μ_o is the grain boundary limited mobility in the absence of potential barrier and E_p is the carrier activation energy for p-type films.

The relationship among the conductivity, mobility and carrier concentration activation energies predicted by the grain boundary potential barrier model are observed:

$$E_\sigma \ (0.248 \text{ eV}) \approx E_p \ (0.233 \text{ eV}) + E_a \ (0.013 \text{ eV})$$

Fig. 5.4 shows the variation of thermoelectric power of a 323 nm thick film over a temperature range from 250 to 450 K. It is seen that thermoelectric power decreases with the increase in temperature. On account of the various possible dependent factors; - scattering mechanism, carrier density, carrier sign, effective mass etc. Asanabe [1] has reported that the thermoelectric power Q in SnSe crystals obeys the following empirical formula.

$$Q = \left(\frac{k}{e}\right)\left[\ln\left(|R|T^{3/2}\right) - 4.82\right] \tag{5.6}$$

where R is the Hall coefficient. In accordance with this formula, the observed decrease in thermoelectric power is due to the fall in Hall coefficient with the raise in temperature which has already been confirmed from the studies on the

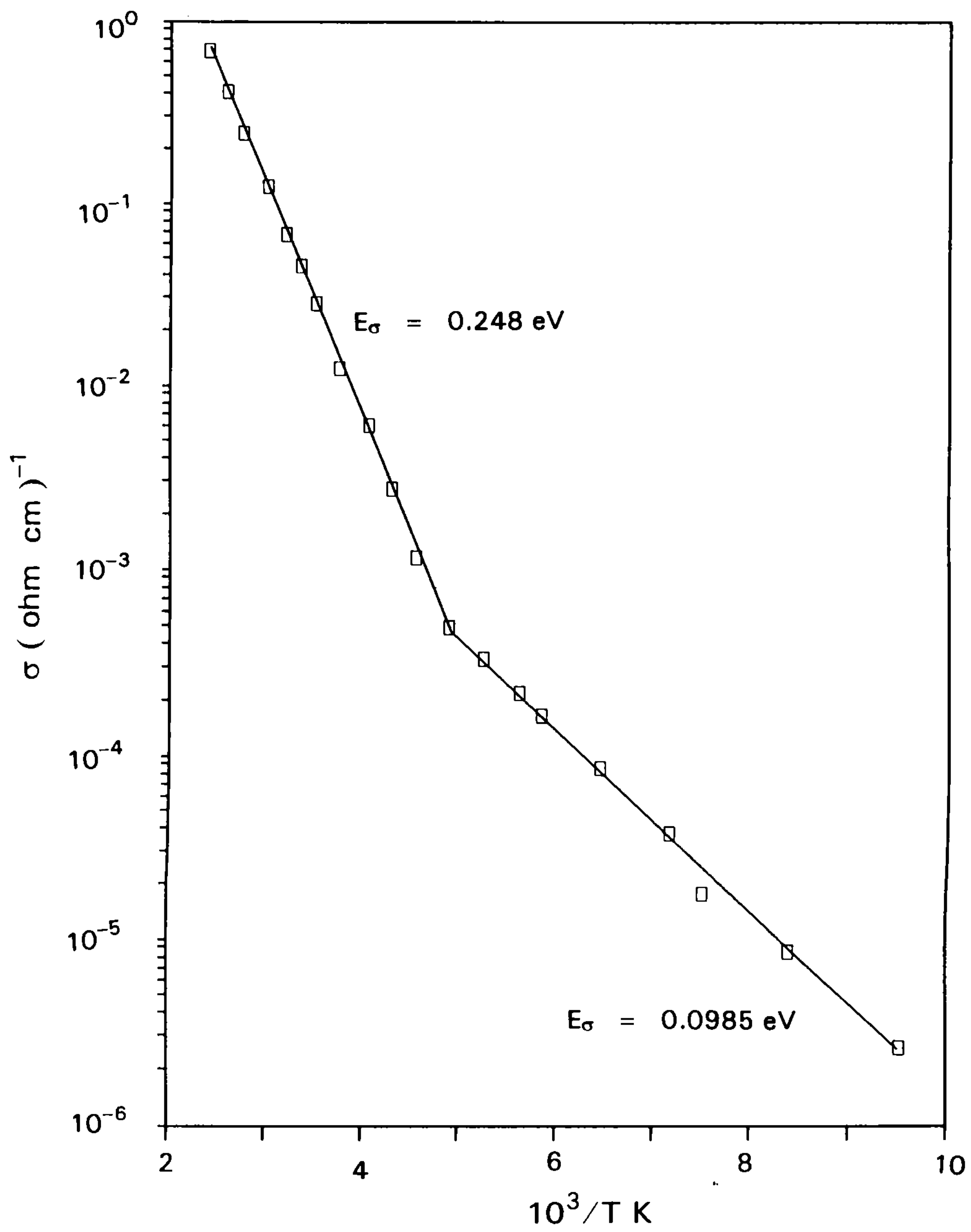

Fig. 5.1 Dependence of conductivity on inverse temperature (log σ vs 1/T)

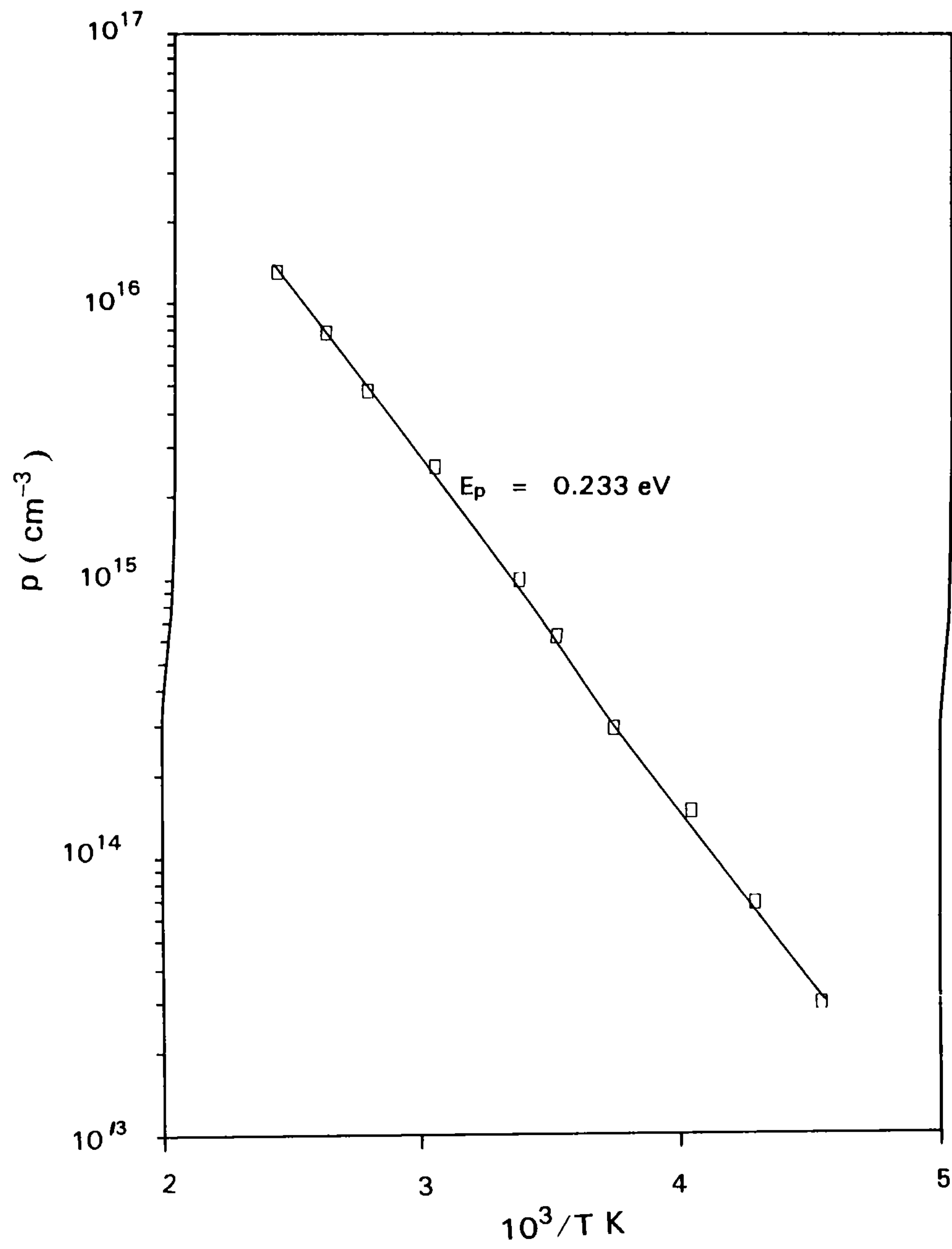

Fig. 5.2 Dependence of carrier concentration on inverse temperature (log p vs 1/T)

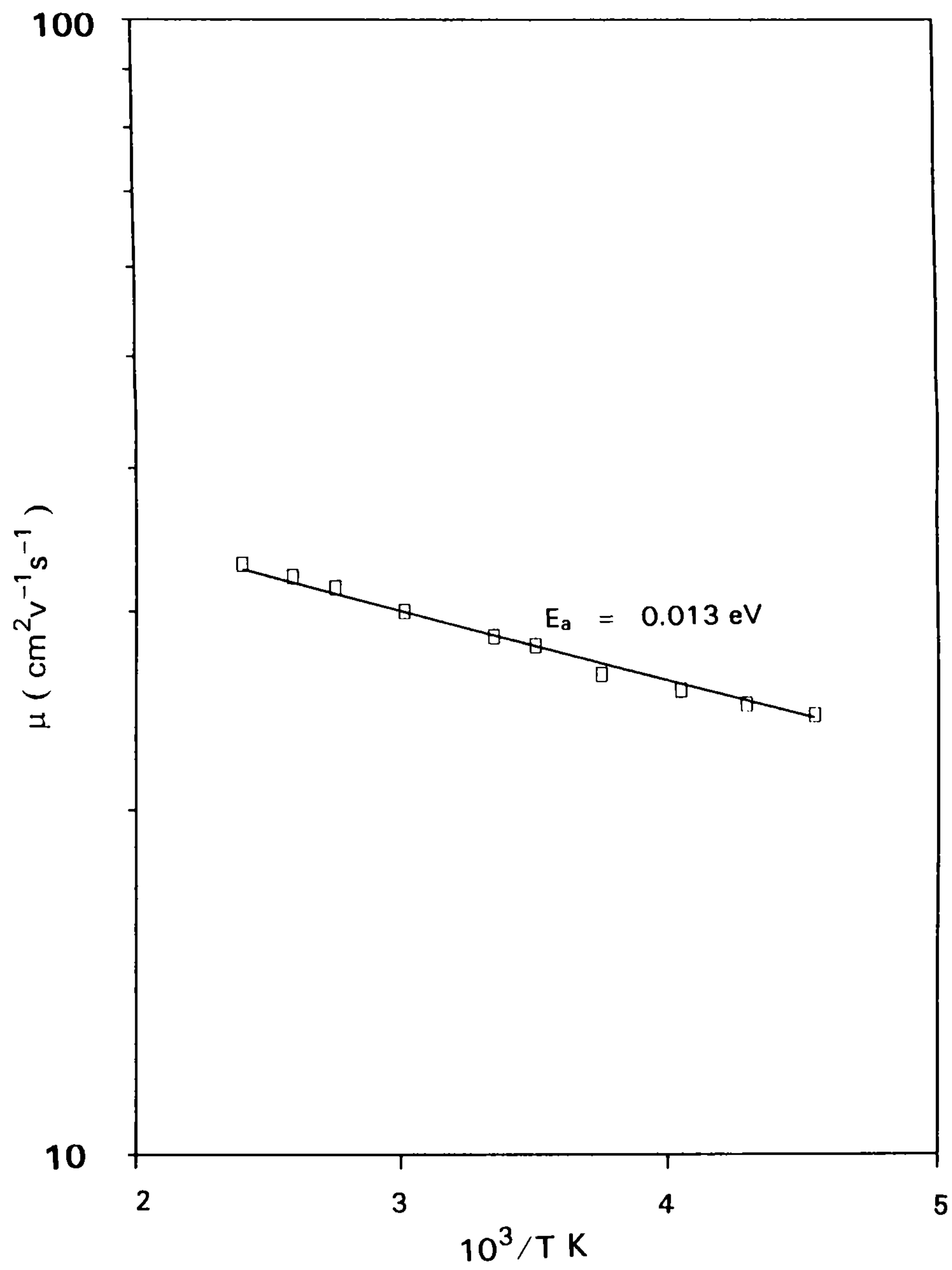

Fig. 5.3 Temperature dependence of mobility

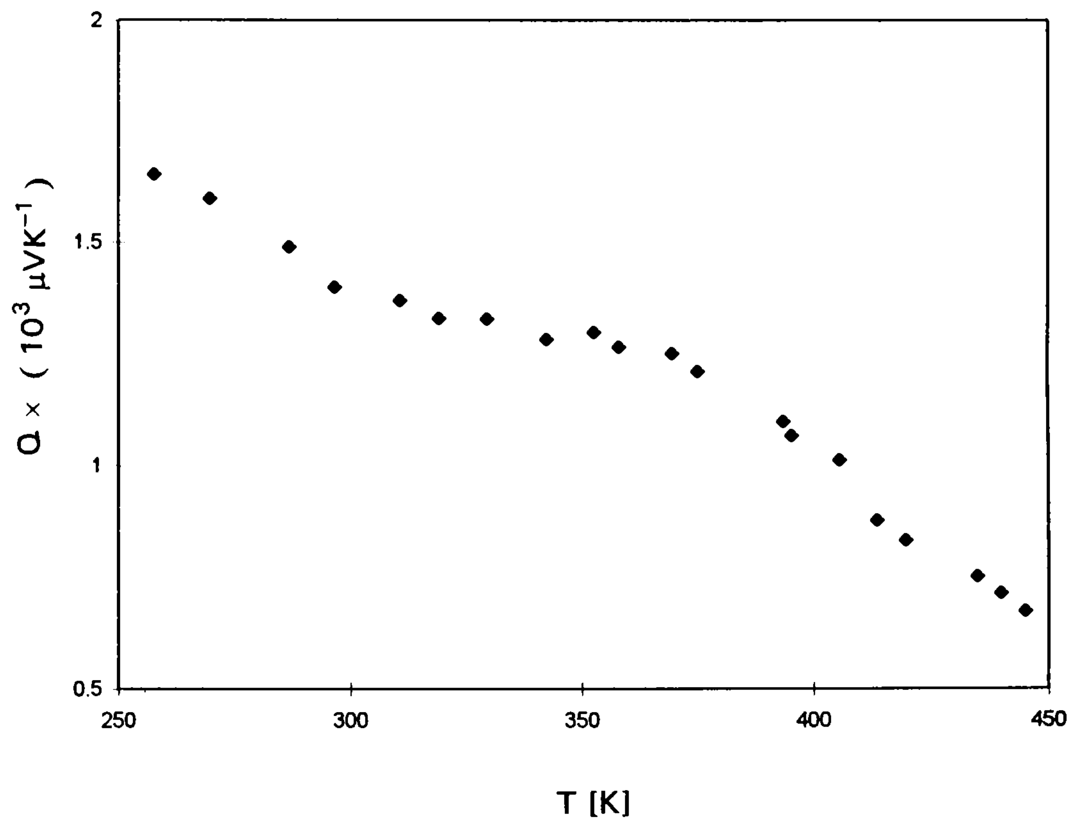

Fig. 5.4 Temperature dependence of thermoelectric power

variation of carrier concentration with temperature. The calculated room temperature value of thermoelectric power using the above relation, corresponding to the observed carrier density of 9.89×10^{15} cm^{-3} is 880 μ V/K. But room temperature thermoelectric power obtained in the present case is 1380 μV/K; which is around 1.6 times the single crystal value. A similar behaviour has been reported for polycrystalline films of PbSe [26,27] and PbS [28] which are very similar to SnSe films. Thermoelectric power as high as 2.3 times the single crystal value has been observed in evaporated PbSe films. Analogous to the case of these lead chalcogenide films, the increase in the present case can also be explained as due to energy selective carrier scattering by potential barriers associated with grain boundaries. When the heights of the potential barriers between the crystallites are close to the Fermi energy, the boundaries should scatter strongly the carriers with energies lower than the Fermi level while the boundaries scatter much less strongly the carriers with energies above the Fermi level. This should reduce the carrier flux and increase the thermoelectric power for the same parameters of the energy band structure.

5.3 VARIATION OF ELECTRICAL PROPERTIES WITH SUBSTRATE TEMPERATURE

SnSe films with thickness around 325 nm were used to study the variation of electrical properties with substrate temperature. The result of the measurements on typical SnSe films prepared at different substrate temperatures are reported here.

Figure 5.5 shows the variation of carrier density on inverse temperature for films prepared at different temperatures. It can be seen that, even though the carrier density of all samples increases with the film temperature irrespective of the substrate temperatures, it is less for the films prepared at higher substrate temperatures. In this method of preparation (reactive evaporation method described in chapter 4) the growing film surface of SnSe is always bombarded by selenium atoms/molecules at a much higher rate than the required, for the formation of the compound. As stated earlier, it is obvious that the p-type nature of these films is due to the presence of excess selenium vapour, which will not leave any unreacted tin inside the crystallites, during the deposition of the films. As the substrate temperature increases the concentration of these excess selenium will decrease and results the observed decrease in carrier concentration.

The variation of mobility with temperature of the films is shown in Fig. 5.6. It can be seen that the mobility is higher for the samples prepared at higher substrate temperatures. This may be ascribed to comparatively lower carrier scattering due to the decrease in carrier concentration resulted from the reduction of excess selenium atoms in samples prepared at higher substrate temperatures. The increase in mean free path of the charge carriers due to the possible higher order crystallinity with consequent enlarged grain size of the films prepared at higher substrate temperatures also accounts for the higher mobility observed.

The temperature dependence of conductivity of the films prepared at different substrate temperatures is shown in Fig. 5.7. In all the samples it is

observed that the conductivity increases with the temperature. It is already shown that the samples prepared at low substrate temperatures have higher carrier concentration while the carriers in high temperature samples have higher mobility. Therefore it is reasonable to conclude that the conductivity of the low temperature film is dominated by carrier density while that of the film prepared at higher temperature is mobility dominated.

In thermal equilibrium, the thermoelectric power of a semiconductor is given by [29, 30],

$$S = S_e + S_p = \frac{\Delta V}{\Delta T} \qquad (5.7)$$

where S is the measured thermoelectric power, S_e is the electron-diffusion component, S_p is the phonon-drag component, ΔT is the temperature difference and ΔV is the thermoelectric voltage associated with the existence of ΔT.

The value of S_e for an extrinsic semiconductor dominated by carriers of one type is given by [29, 31]

$$S_e = \pm \frac{k}{e}\left(A + \ln \frac{N_i}{n_i}\right) \qquad (5.8)$$

where the positive sign is for holes and the negative sign is for electrons, A is the scattering parameter, N_i is the effective density of states in the band and n_i is the density of free carriers.

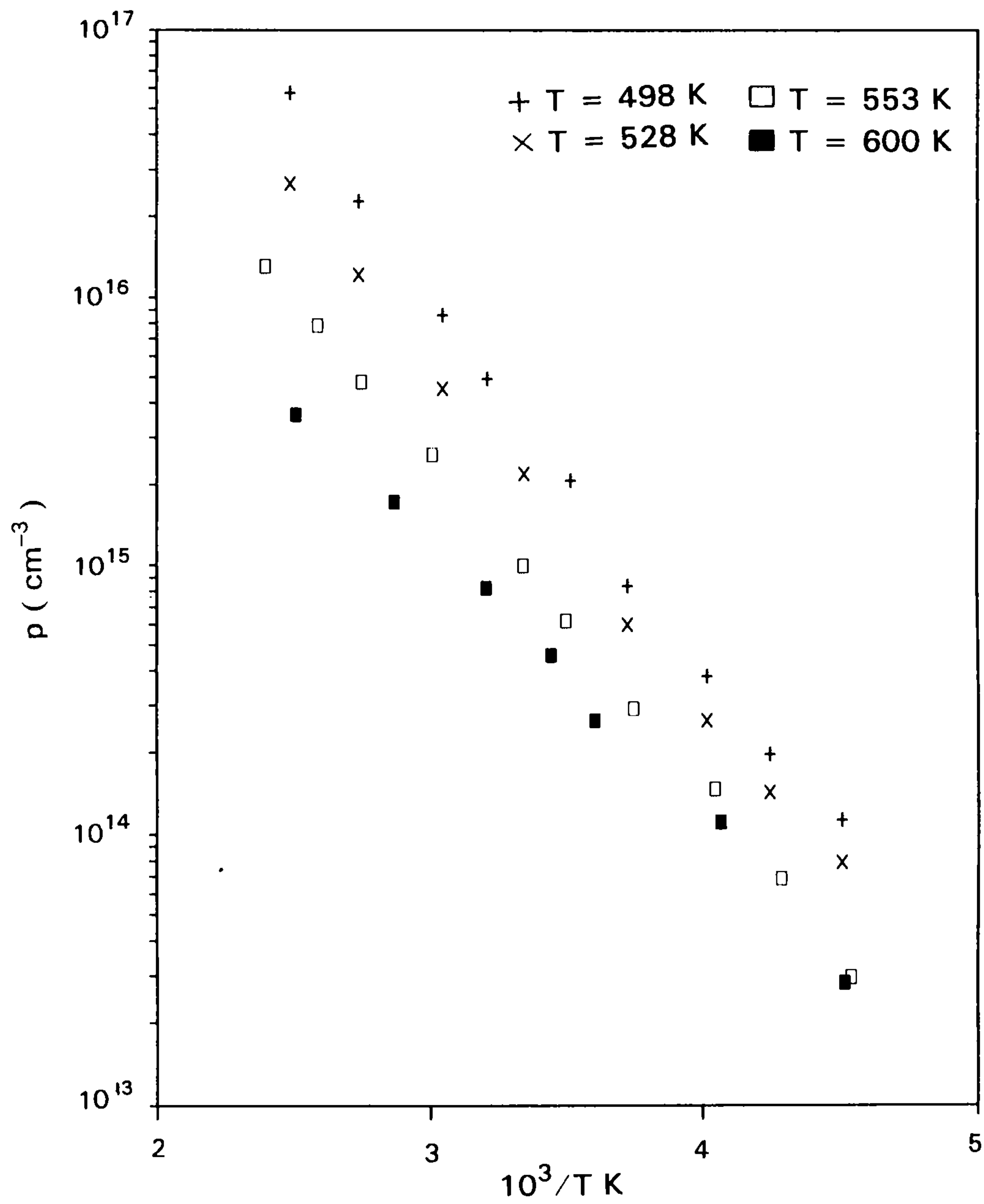

Fig. 5.5 **Variation of carrier concentration on inverse temperature (log p vs 1/T) for films prepared at different temperatures**

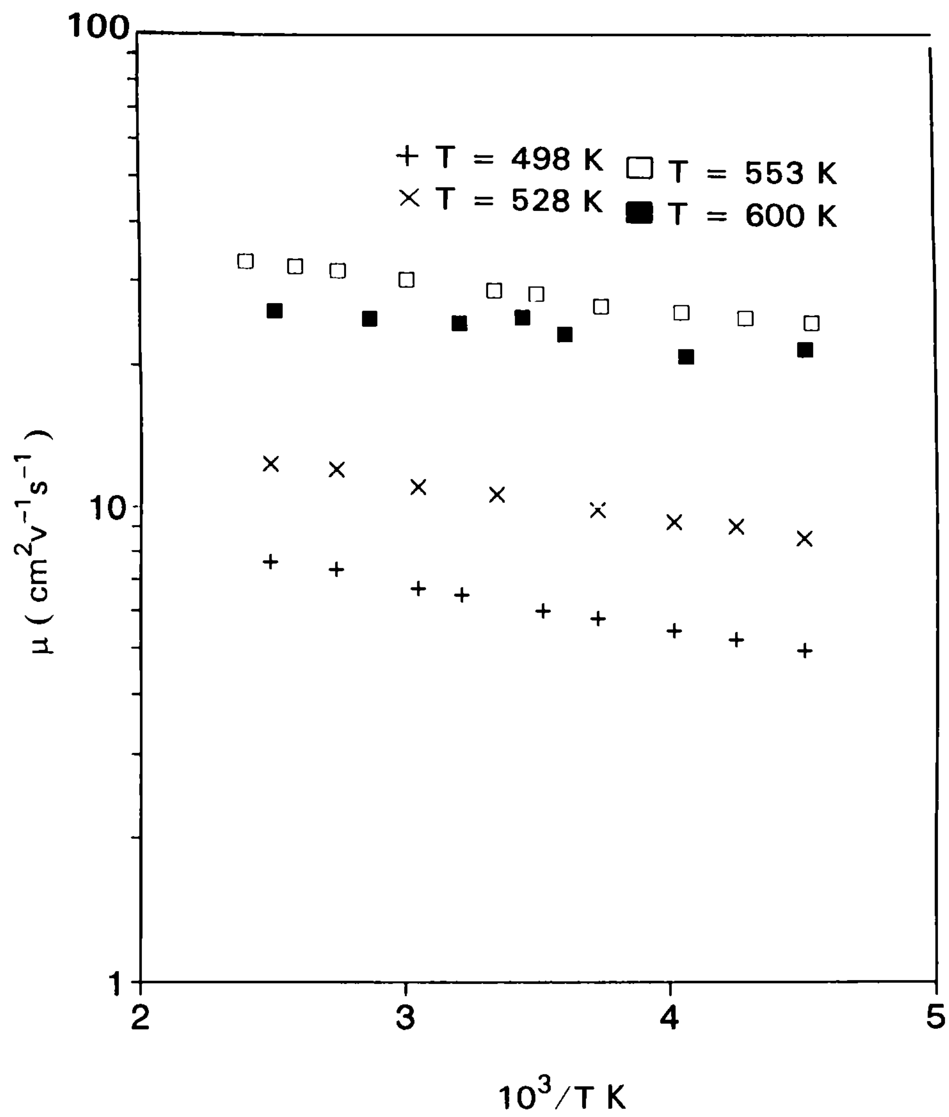

Fig. 5.6 **Temperature dependence of mobility of the films prepared at different temperatures**

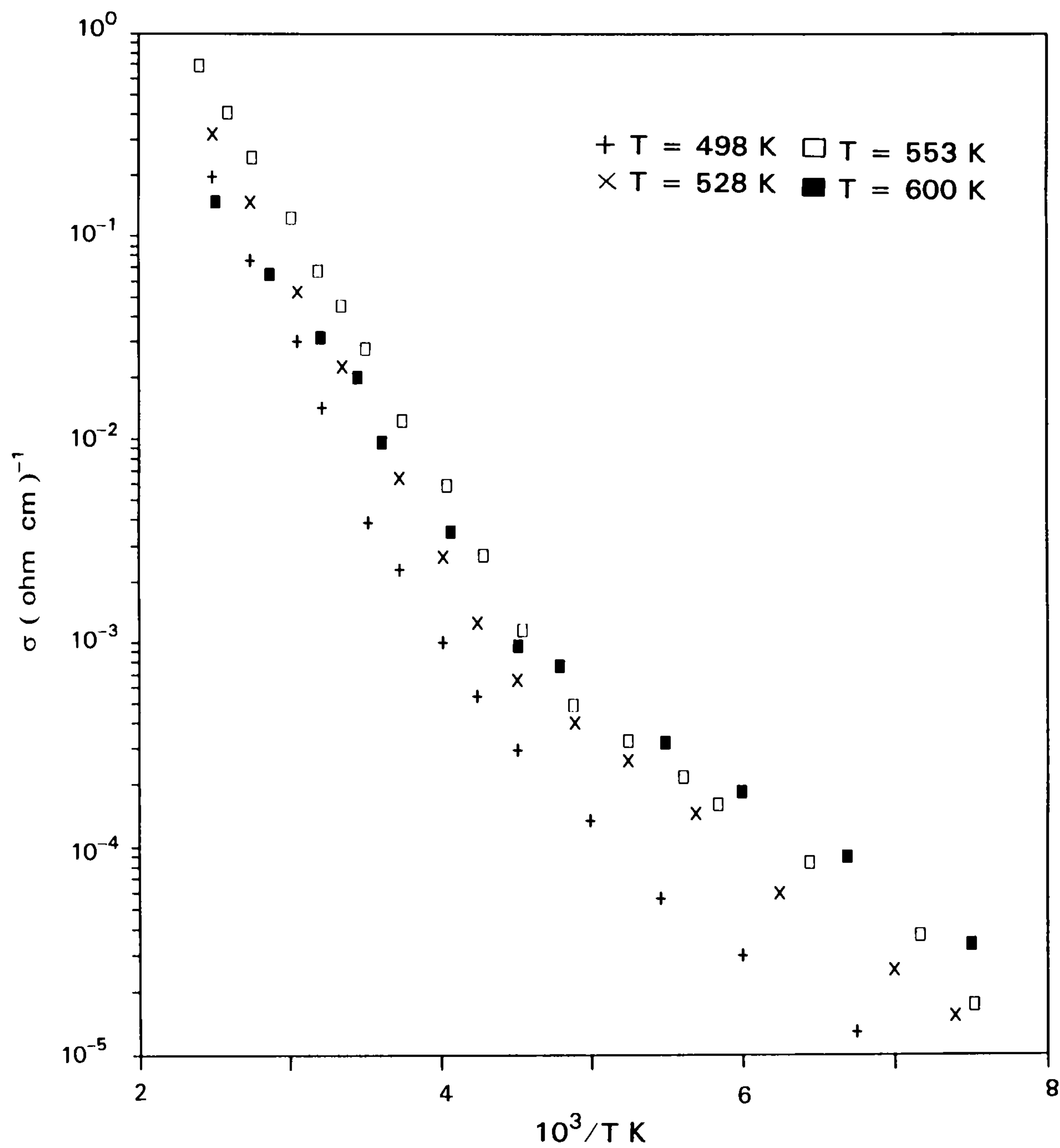

Fig. 5.7 **Variation of conductivity with temperature of the films prepared at different temperatures**

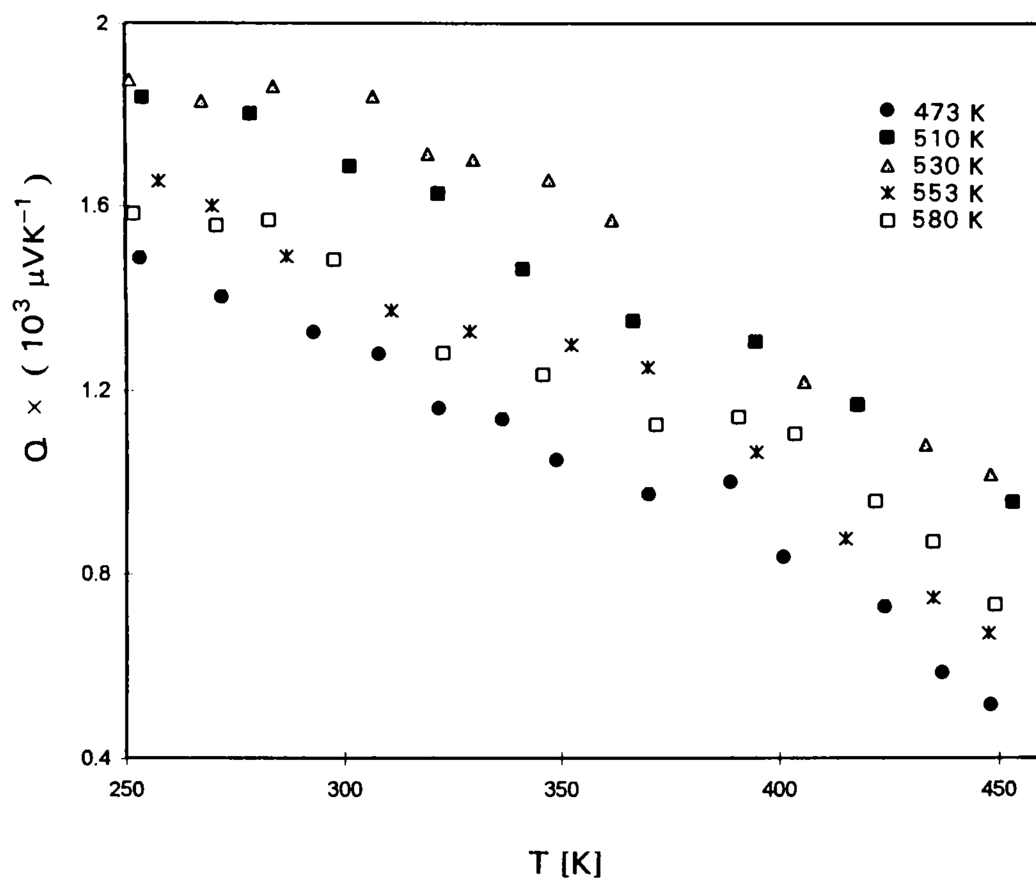

Fig. 5.8 **Variation of thermoelectric power with temperature of films prepared at different substrate temperatures**

From equation (5.8) it can be seen that an increase in carrier density results in a decrease in S_e where as increase in scattering parameter results in an increase in S_e.

The temperature dependence of thermoelectric power of the films prepared at different substrate temperatures is shown in Figure 5.8. The thermoelectric power is found to increase with preparation temperature up to 530 K and above that substrate temperature it is found to be lower. This may be due to the variation in electronic contribution satisfying the relation (5.8), resulting from the variation in carrier concentration and mobility of the film with the preparation temperature.

It is already seen that, the carrier concentration decreases with the increase in preparation temperature and so the observed increase in thermoelectric power of the film with the substrate temperature is due to the carrier density contribution in equation (5.8). But for the decrease in thermoelectric power of the films prepared at high temperatures, the scattering parameter in the equation is responsible. As mentioned earlier, the potential barriers between crystallites in a polycrystalline film have a pronounced effect in the various conduction mechanism. This will scatter strongly the carriers with lower energies and this should reduce the energy in a carrier flux and increase the thermoelectric power. That is, the scattering parameter should increase [26]. It may be noted that the barrier height in samples prepared at higher substrate temperatures are lower as evidenced from the variation of mobility with temperature for films prepared at different substrate temperatures, and so the scattering parameter A will be less in these samples. This should account for the decrease in thermoelectric power of films prepared at high substrate temperatures.

5.4 CONCLUSION

Hall effect measurements show that the prepared SnSe films have p-type conduction. The dependence of mobility and carrier concentration of these films with temperature is explained due to the grain boundary potential barrier mechanism associated with the polycrystallinity. The reduction in carrier concentration with the raise in substrate temperature is attributed to the decrease in excess selenium vapour inside the film. The observed high thermo-electric power of these films compared to the single crystal value is due to the energy selective carrier scattering by potential barriers associated with grain boundaries. Using a well known equation for electronic contribution of thermoelectric power, the variation in thermoelectric power of samples prepared at different substrate temperatures are explained.

REFERENCES

1. Asanabe S., *J. Phys. Sco. Japan* **14,** 281 (1959).

2. Maier.H and Daniel D.R., *J. Elect. Mater.* **6,** 693 (1977).

3. Yu J.G, Yue A.S. and Stafsudd O.M., *J. Cryst. Growth.* **54,** 248 (1981).

4. Shalvoy R.B, Fisher G.B and Shiles P.J., *Phys. Rev.* **B15,** 2021 (1977).

5. Chandrashekhar H.R, Humphery R.G, Zwick.U and Cardona,M. *Phys. Rev.* **B15,** 2177 (1977).

6. Mochida Y., *Sci. Light* **17,** 57 (1968).

7. Takahashi K, Arai T and Kudo K., *Sci. Light* **21,** 131 (1972).

8. Guseinova D.A, Krivaite G.Z. and Marnedov M.M., *Sov. Phys. Semicond.* **19,** 923 (1985).

9. Elkorashy A.M., *J. Phys. Chem. Solids* **47,** 497 (1986).

10. Elkorashy A.M., *J. Phys. Chem. solids.* **50,** 893 (1989).

11. Elkorashy A.M., *J. Phys. Chem. Solids* **51,** 289 (1990).

12. Bhatt V.P, Gireesan K and Pandya G.R., *J. Cryst. Growth* **96,** 649 (1989).

13. Julien C, Eddrief. M, Samaras. I, and Balkanski. M. *Mater. Sci & Eng.* **B15,** 70 (1992).

14. Garg A.K, Jain A.K, and Agnihotri O.P., *Ind. J. Pure & Appl. Phys.* **21,** 276 (1983).

15. Dang Tran Quan., *Phys. Stat. Sol (a)* **86,** 421 (1984).

16. Dang Tran Quan., *Thin Solid Films* **149,** 197 (1987).

17. Subba Rao. T, Chaudhuri A.K. *J. Phys. D: Appl. Phys.* **18**, L35 (1985).

18. Singh J.P and Bedi R.K, *Thin Solid Films* **199**, 9 (1991).

19. Singh J.P, and Bedi R.K. *J. Appl. Phys.* **68**, 2776 (1990).

20. Bhatt V.P, Gireesan K and Desai C.F, *Cryst. Res. Technol.* **24**, 187 (1989).

21. Ganesan N, and Sivaramakrishnan V., *Semicond. Sci. Technol.* **2**, 519 (1987).

22. R.L.Petritz, *Phy. Rev.* **104**, 1508 (1956).

23. H.Berger, *Phys Stat. Sol.* **1**, 739 (1961).

24. R.G.Mankarious., *Solid-state Electron.* 7, 702 (1964).

25. L.L.Kazmerski, F.R. White, M.S.Ayyagary, Y.J.Juang and R.P.Patterson., *J.Vac. Sci. Technol.* **14**, 65 (1977).

26. L.I. Bytenskii, T.S. Gudkin, E.K. Iordanishivili, S.A. Kaz'min, V.I. Kuidanaov, S.A. Nemov and Yu. I. Ravich., *Sov. Phys. Semicond.* **11**, 894 (1977).

27. T.S.Gudkin, I.A.Drabkin, V.I. Kaidanov and O.G. Sterlyadkina., *Sov. Phys. Semicond.* **8**, 453 (1975).

28. J. Geroge, T.I. Palson and K.S. Joseph., *Solid State Commun.* **58**, 605 (1986).

29. J.G. Harper, H.E. Mathews and R.H. Bube., *J. Appl. Phys.* **41**, 765 (1970).

30. C. Herring., *Phys. Rev.* **96**, 1163 (1954).

31. R.A. Smith., 'Semiconductors', 2nd Edn. (Cambridge University Press, 1978).

CHAPTER 6

REACTIVELY EVAPORATED THIN FILMS OF BISMUTH SELENIDE

6.1 INTRODUCTION

Semiconducting chalcogenide thin films have been extensively investigated due to their device applications in many fields like i.r. detectors, photoconductors thin film transistors etc. Bismuth selenide, an important member of the chalcogenides is a narrow gap semiconductor and has potential applications to thermoelectric power converters and Hall effect devices. The applications of this material has been extended to fabricate ideal Hall effect magnetometers [1], hyperfrequency power sensors, thermopiles and wide band radiation detectors [2]. It can also be used in the i.r. photography device as a photographic film [3]. The band gap of Bi_2Se_3 at room temperature is in the range of 0.2 to 0.35 eV [3-7]. Boechko & Isarev [8] have analysed the electrical properties of both n and p-type Bi_2Se_3 single crystals. The influence of various dopants on the transport properties of bulk Bi_2Se_3 were investigated by Dmitrieva et al. [9], Sher et al. [10] and Horak et al. [11]. The electronic properties of Bi_2Se_3 crystals have been reported by Hyde et al. [12] and others [13-15].

Even though a large number of investigations were carried out on the bulk form [4-20], not much work has been reported on the thin films of bismuth

selenide. Goswami and Koli [21] have reported the electrical properties of Bi_2Se_3 films prepared by evaporation from the bulk and the films prepared by the chemical method were characterised by Bhattacharya and Pramanik [3, 22]. Photoemission measurements were performed on amorphous Bi_2Se_3 films by Takahashi et al. [23]. To the best of our knowledge preparation of bismuth selenide thin films by reactive evaporation has not yet been reported.

In the work reported here Bi_2Se_3 thin films were prepared by co-evaporation of the constituent elements to avoid incongruent evaporation from a single source and the consequent lack of stoichiometry. The temperature dependences of the electrical conductivity, the Hall coefficient, the Hall mobility and the thermoelectric power of these films were studied in the temperature range 100-420 K.

6.2 EXPERIMENTAL

Thin films of bismuth selenide were prepared by evaporating high purity (99.999%) bismuth and selenium from two different sources, keeping the substrate at an elevated temperature in a conventional vacuum system at a pressure of about 10^{-6} torr. A quartz crucible placed in a conical basket of molybdenum wire was used as the selenium source and to evaporate bismuth a molybdenum boat was used. Chromal-alumel thermocouple placed in contact with the substrate was used for measuring its temperature. The detailed description of deposition technique is given in chapter 3.

It has been found that a stoichiometric interval exists for the reactive evaporation of bismuth selenide from its individual components with the following parameters:

Bismuth flux = $2 - 3 \times 10^{14}$ atoms $cm^{-2}s^{-1}$

Selenium flux = $5.7 \times 10^{14} - 1.2 \times 10^{15}$ atoms $cm^{-2}s^{-1}$

Substrate temperature = 433 - 488 K

The deposition rate of Bi_2Se_3 film was 0.3 - 0.4 nm per second. Highly reproducible films were obtained under these conditions; these films were opaque with a metallic lusture. All the films used in this study were prepared on glass substrate. Films deposited at substrate temperatures below 433 K were amorphous as indicated by the appearance of the X-ray diffraction pattern and non-uniform films with a dull appearance were obtained at temperatures above 500 K.

6.3 STRUCTURAL CHARACTERISATION

Microstructural characterisations were carried out by X-ray diffraction using films with thickness around 300 nm. Fig. 6.1 shows the X-ray diffraction spectrum of a typical Bi_2Se_3 film obtained using CuK_α radiation. The corresponding (hkl) planes are also indicated. The d-spacings and relative intensities given in the JCPDS Powder Diffraction File for Bi_2Se_3 [24] along with the results obtained in the present case is given in Table 6.1. All the diffraction lines are comparable well with the standard pattern. The variation

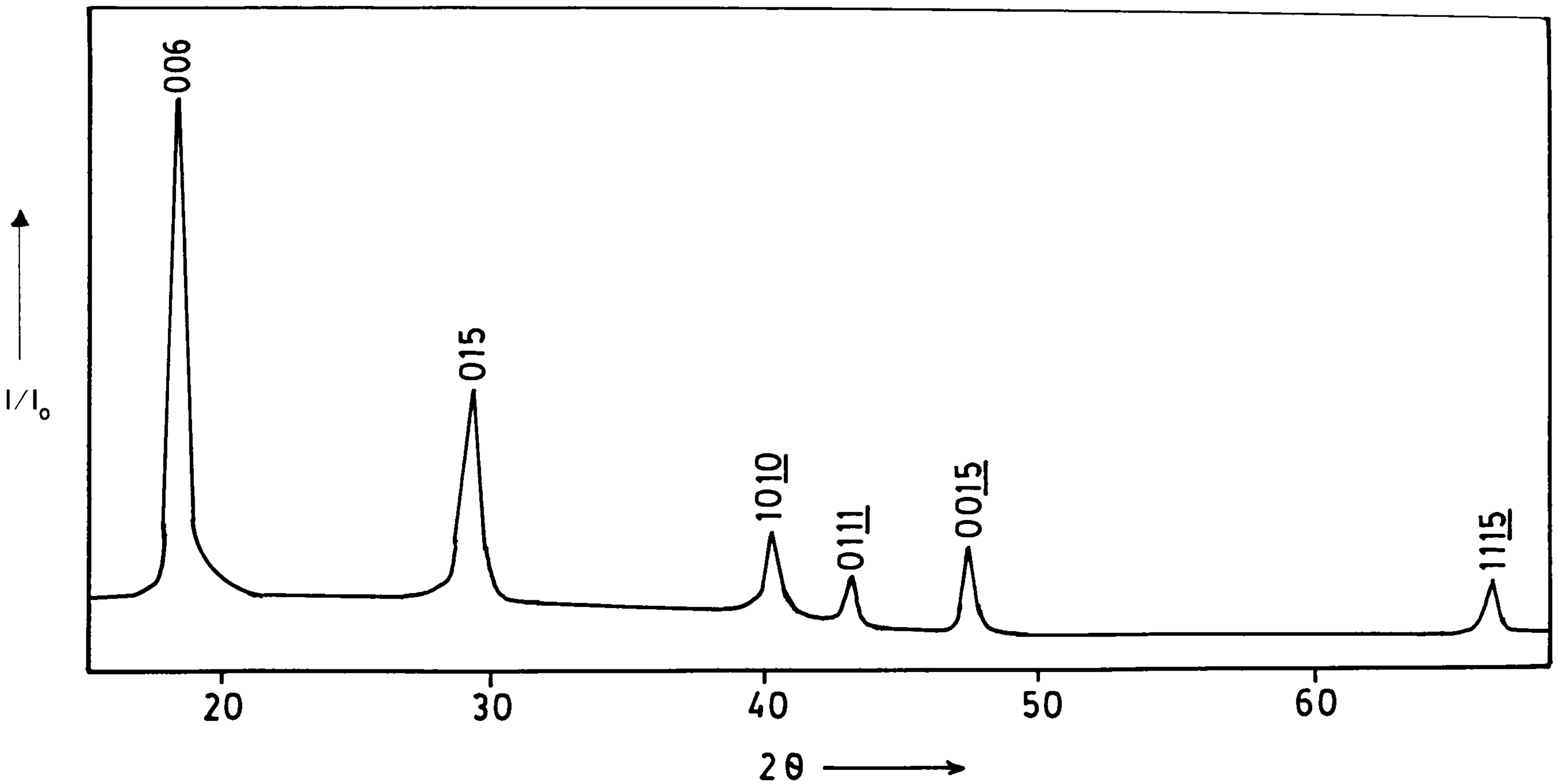

Fig. 6.1 X-ray diffraction pattern of the Bi_2Se_3 thin film

TABLE 6.1
X-ray diffraction data of reactively evaporated bismuth selenide film

hkl	Standard pattern		Prepared film	
	d Å	I/I_o	d Å	I/I_o
006	4.8	30	4.8	100
015	3.03	100	3.037	50
1010	2.23	60	2.237	24
0111	2.10	10	2.103	14
0015	1.907	30	1.917	21
1115	1.404	40	1.407	13

in relative intensities of the lines from the standard pattern can be explained by considering the fact that in a diffractometer with Bragg-Brentano geometry, at any incident angle, the film has an effective thickness of $t/\sin\theta$ and consequently the reflected intensity will be angle dependent. Since all the obtained peaks could be identified with the standard pattern it must be concluded that the prepared films were stoichiometric Bi_2Se_3 with polycrystalline nature.

6.4 ELECTRICAL PROPERTIES

The films prepared for electrical measurements were of thickness 150-200 nm. The thickness of the film was measured by Tolansky's multiple beam interferometric method [25]. A conventional four probe method [26] was used to measure the conductivity and the Hall coefficient. All these measurements were taken under a vacuum of better than 10^{-2} torr in an all metal cell (described in chapter 3), whose temperature could be varied from liquid nitrogen to 450 K. Ohmic contacts to the samples were made using silver paint. The ohmic nature of contacts was confirmed by the linear current-voltage characteristic throughout the temperature range studied (100-420 K). The conductivity of the film was measured by passing a known current through the film and measuring the voltage across the film. The electric current and voltage were measured using Keithley 195 system DMM. A stabilised magnetic field was applied across the sample and Hall voltage developed was measured using Keithley 181 nanovoltmeter. The length-to-width ratio of the samples used for the Hall measurements was greater than 4, so that the influence of the film geometry was negligible. Since Bi_2Se_3 is a material with high thermoelectric

power the measuring current will produce a temperature gradient which will cause a thermoelectric voltage across the conducting probes. This was eliminated by taking one reading after the current had established a steady state temperature distribution and then the current was immediately reversed and a second reading was taken. Thus, the temperature distribution for both the readings was maintained the same. From the average of these readings, the conductivity was calculated. All these measurements were repeated many times and were found to be reproducible.

Freshly prepared samples were used for the measurements. Over film thickness range investigated (150-200 nm), very few differences in the experimental results were observed from sample to sample. Hall measurements showed that these films were n-type with nearly constant carrier concentration throughout the temperature range studied.

6.4a Hall effect studies

The dependence of Hall coefficient (R_H) on temperature for a typical Bi_2Se_3 film 200 nm thick, is shown in Fig. 6.2. It is seen that the Hall coefficient is fairly constant in the temperature range up to 358 K. This is characteristic of an extrinsic degenerate semiconductor [27]. The investigations on this material in the bulk form by Hyde et al. [12] and Woollam et al. [13] revealed that both n-type and p-type samples of Bi_2Se_3 are highly degenerate. The carrier concentration has been calculated from the relation, $R_H = \left(\frac{3\pi}{8}\right)\left(\frac{1}{ne}\right)$ where n and e are the electron concentration and electronic charge respectively, and is

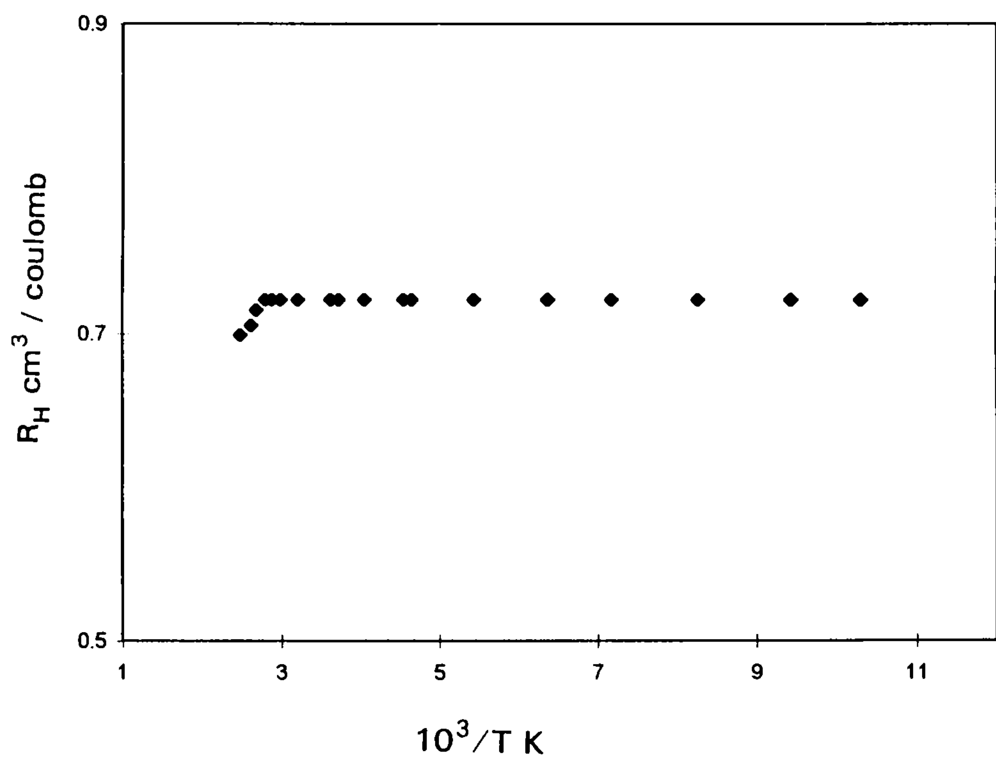

Fig. 6.2 Variation of Hall coefficient with reciprocal temperature

found to be 1.02×10^{19} cm^{-3} at this temperature range. A similar behaviour in the temperature dependence of R_H has been reported by Boechko et al [8] in Bi_2Se_3 single crystals. These authors have observed a very steep decrease in Hall coefficient and a sign reversal of it at some higher temperatures. They have also noticed that the temperature range up to which R_H remains constant and the temperature at which the sign reversal takes place depends upon the free carrier concentration of the samples. The lower the concentration of the carriers, the higher was the inversion temperature for the Hall coefficient. The inversion temperature was 475 K for a sample with carrier concentration 2×10^{19} cm^{-3}. But in the present study it has not been able to observe any appreciable change in R_H upto 420 K. This may be due to the lower carrier concentration of these samples.

Dimitrieva et al. [9] reported the carrier concentration of bulk Bi_2Se_3 as ranging from 1.2×10^{19} when there is an excess Bi to 8×10^{17} when there is an excess of Se. And for n-type single crystals of Bi_2Se_3 it lies between $1 - 4 \times 10^{19}$ cm^{-3} [8, 11, 12, 20].

6.4b Conductivity studies

Fig. 6.3 shows the variation of electrical conductivity ($\ln \sigma$) against reciprocal temperature. As the temperature is increased the conductivity decreases, becomes a minimum and then increases. The decrease in conductivity is caused by the increased defect scattering owing to the higher carrier concentration of these films. Boechko et al. [8] , Dmitrieva et al. [9] and

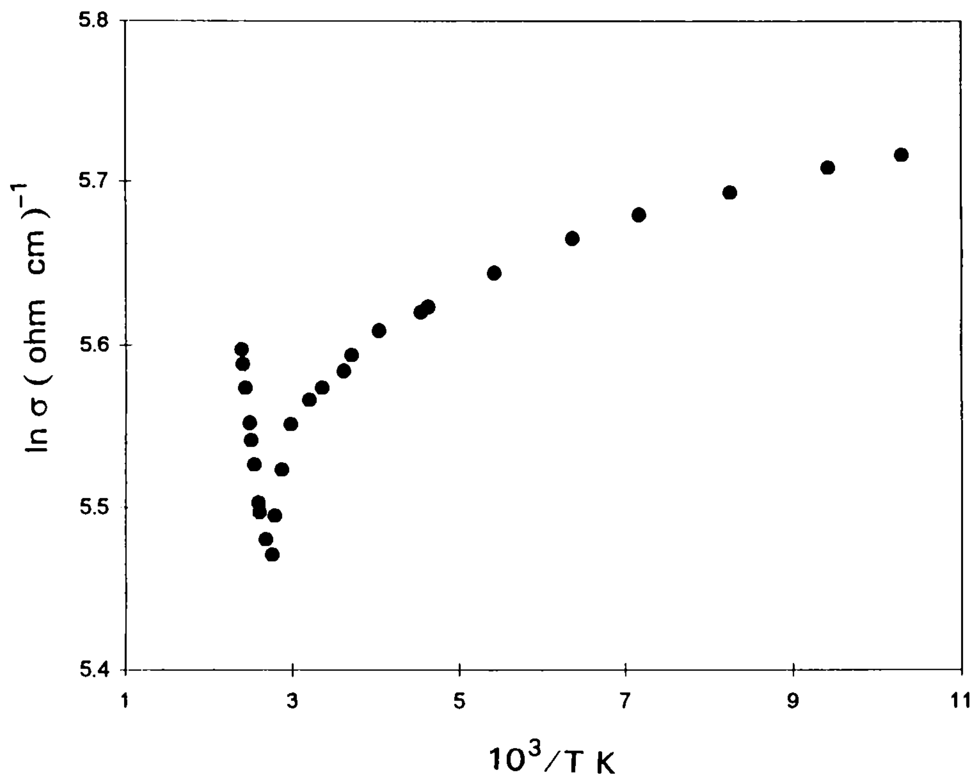

Fig. 6.3 **Variation of conductivity ($\ln \sigma$) with reciprocal temperature T ($\ln \sigma$ vs $10^3/T$)**

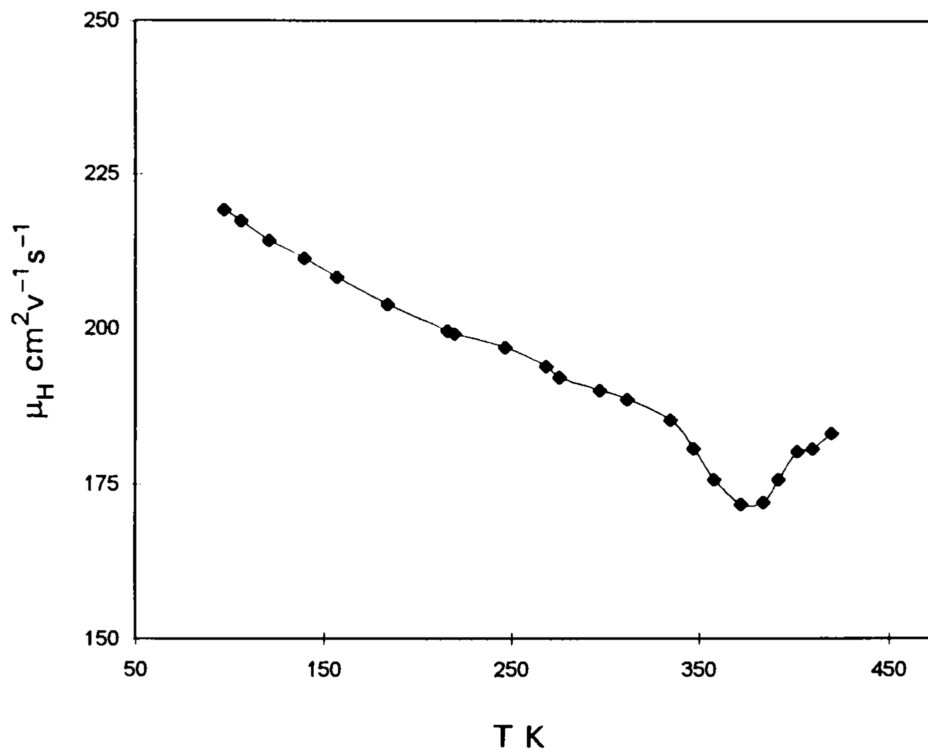

Fig. 6.4 **Variation of Hall mobility (μ_H) with absolute temperature (μ_H vs T)**

Sher et al. [10] had observed a similar temperature dependence of conductivity in n-type bulk Bi_2Se_3. Above 362 K, the conducvity is seen to increase with temperature. In this region the activation energy ΔE for conduction is found to be 0.08 ± 0.002 eV. This lower value of activation energy observed is attributed to the energy required for a transition between the defect level and the valence band or conduction band.

The variation of the mobility with temperature (μ_H vs T) is shown in Fig.6.4. It is seen that the mobility decreases with temperature, becomes a minimum and then increases as observed in conductivity. A polycrystalline material is composed of small crystallites joined together by grain boundaries. The resistance of such a material consists of the contributions from the grain-boundary region and the bulk of the crystallite. Inside each crystallite the atoms are arranged in a periodic manner so that it can be considered as a small single crystal. The grain-boundary is a complex structure, usually consisting of a few atomic layers of disordered atoms and this should exert a pronounced effect on the properties of the thin films.

Petritz [28] has considered the inhomogeneities in the structure of polycrystalline semiconductor films and proposed a model for accounting the electrical properties of it. He dealt with parameters as averages of many crystallites. The total resistivity in this case is

$$\rho = \rho_1 + \rho_2$$

where ρ_1 and ρ_2 are the resistivities in the crystallite and grain boundary respectively. It was also assumed that, for the usual case, $\rho_2 >> \rho_1$. Further, Berger [29, 30], Mankarious [31] and Kazmerski [32, 33] have showed that

$$E_\sigma = E_n + q\phi_b$$

where E_σ is the conductivity activation energy, E_n the carrier activation energy and ϕ_b a barrier potential relating to the concentration in the grain and boundary domains. Therefore for the case proposed by Petritz ($\rho_1 << \rho_2$), the mobility activation energy is identical to the conductivity activation energy, and R_H is constant [34].

6.4c Thermoelectric power measurements

Samples prepared on glass substrates with thickness ≈ 200 nm were used for the thermoelectric power measurements. Silver paint was used for the contacts to the specimen. The temperature of each end of the samples, and hence the average temperature and temperature difference were determined by thermocouples attached to both ends. The potential difference between both ends of the sample due to the temperature gradient was measured by a digital multimeter, while the sample was slowly warming up under vacuum. The maximum temperature difference between the ends of the sample was within 25 K. The details of the set up used for this measurement is described in chapter 3.

The variation of thermoelectric power (α) with temperature from 195 to 475 K is shown in Fig.6.5. Throughout this temperature range the

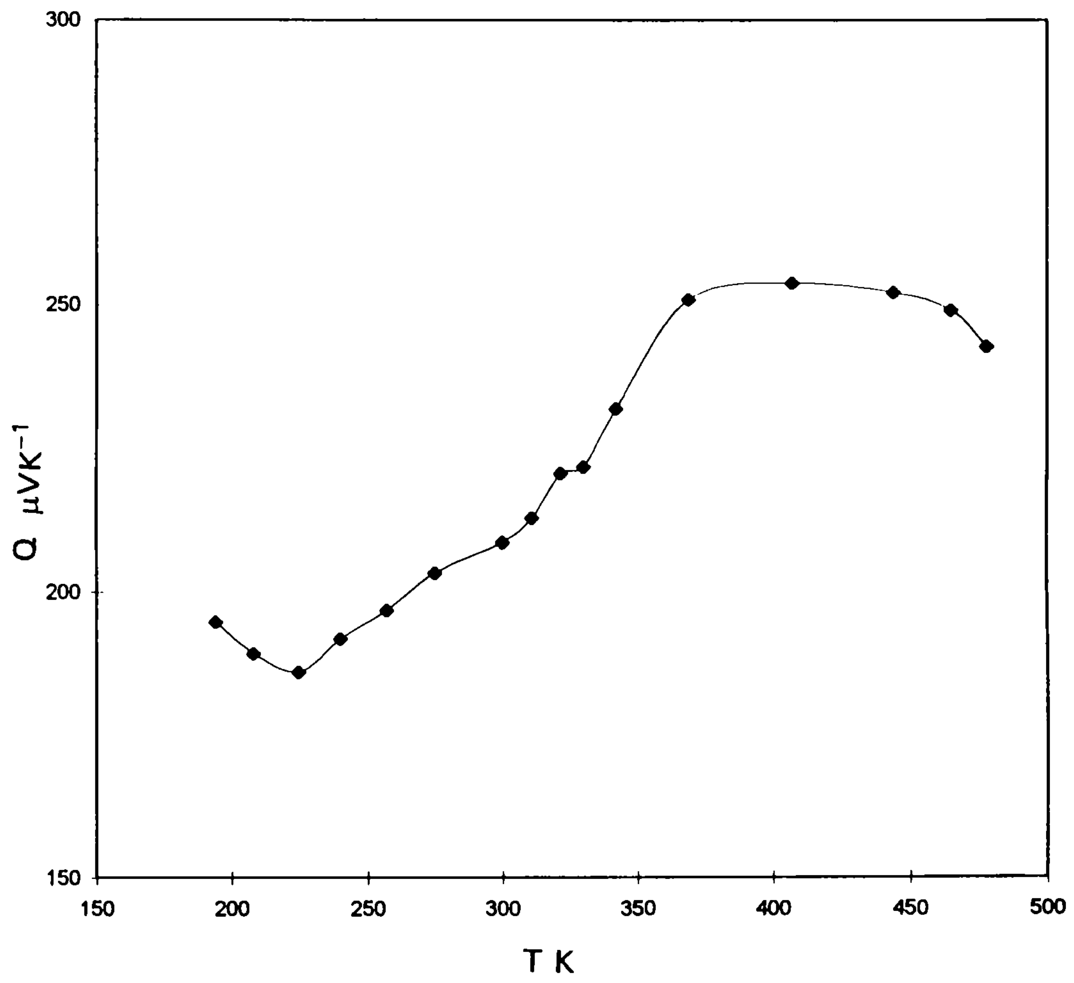

Fig. 6.5 **Variation of thermoelectric power with temperature (α vs T)**

thermoelectric power was negative, indicated the n-type conductivity of the sample. The thermoelectric power was observed to increase with increasing temperature due to the degenerate nature of this material and passed through a maximum of 255 μVK^{-1} at 405 K, beyond which it began to decline. The same behaviour has been observed in bulk bismuth selenide also [8-10]. The maximum value obtained in the present case is higher than that in the case of bulk and is attributed to the higher scattering of carriers in these samples. The thermoelectric power of doped Bi_2Se_3 samples has been observed [9] to increase with the decrease in concentration and mobility of carriers.

6.5 CONCLUSION

Polycrystalline stoichiometric Bi_2Se_3 thin films prepared by reactive evaporation were n-type. Throughout the temperature range studied the carrier concentration of it was nearly constant. An activation energy of 0.08 eV was obtained in the temperature range from 362 to 420 K. In this range the mobility was thermally activated and the mobility activation energy is identical to conductivity activation energy. These films showed an increase in thermo electric power with temperature, due to the degenerate nature of the material.

REFERENCES

1. J.A.Woollam, H.A.Beale & I.L.Spain, *Rev. Sci. Instrum.* **44**, 434 (1973).

2. A. Boyer, E.Cisse & E. Groubert., *Sensors 89, Technologies and Applications*, APIST and CIAME, Paris, PP. 242-247 (1989).

3. R.N.Bhattacharya and P.Pramanik, *J. Electrochem. Soc: Electrochemical Science and Technology*, **129**, 332 (1982).

4. J. Black, E.M.Conwell, L.Seigle & C.W.Spencer., *J. Phys. Chem. Solids* **2,** 240 (1957).

5. Drabble. J.R., Groves R.D., Wolfe. E., *Proc. Phys. Soc.* (London) **71** 430 (1958).

6. M.J.Smith, E.S.Kirk & C.W.Spencer., *J. Appl. Phys.* **32,** 1504 (1960).

7. N. kh: Abrikosov, V.F.Bankina & L.Poretskaya., 'Semiconducting, Chalcogenides and Alloys Based on Them', Nanka, Moscow (1975).

8. V.F.Boechko & V.I.Isarev., *Inorg. Mater.* (USA) **11,** 1288 **(1975).**

9. A.K.Dmitrieva, L.D.Dudkin, R.S.Erofeev, A.B.Ivanova & E.I.Shcherbina., *Inorg. Mater.* **14,** 326 (1978).

10. A.A.Sher, I.N. Odin & A.V.Novoselova., *Inorg. Mater.* **20,** 1109 (1984).

11. J.Horak, L.Koudelka, J.Klikorka & L.Siska., *Phys. Stat. Sol.* **111,** 575 (1982).

12. G.R.Hyde, H.A.Beale & I.L.Spain. *J.Phys. Chem. Solids.* **35,** 1719 (1974).

13. J.A.Woollam. H.A.Beale & I.L.Spain, *Phys. Lett. A* **41A,** 319 (1972).

14. H. Kohler., *Phys. Stat. Sol.* **58,** 91 (1973).

15. H.Kohler & C.R.Becker. *Phys. Stat. Sol.* **61,** 533 (1974).

16. H.Kohler & P.Fabricius., *Phys. Stat. Sol.* **71**, 487 (1975).

17. K. Hashimoto, *J. Phys. Soc. Japan* **16**, 1970(1961).

18. L.Tichy & J.Horak., *Phys. Rev.* **B19**, 1126 (1979).

19. E.V.Oleshko & V.N.Korolyshin., *Ukr. Fiz. Zh* **32**, 1499 (1987).

20. A. Vasco & M. Matyas., *Czech. J. Phys.* **B23**, 243 (1973).

21. A.Goswami & S.S.Koli., *Indian J. Pure. Appl. Phys.* **7**, 166 (1969).

22. P. Pramanik, R.N.Bhattacharya & A. Mondal., *J. Electrochem. Soc.* **127**, 1857 (1980).

23. T. Takahashi, T. Sagawa & H.Hamanaka., *J. Non-Cryst. Solids.* **65**, 261 (1984).

24. JCPDS card No. 12 - 732.

25. S.Tolansky, *'Multiple Beam Interferometry of Surface and Films'*. Oxford Univ. Press, London (1948).

26. E.H.Putley, *'The Hall effect and Related Phenomena'*, P. 24, Whitefriar's Press, London (1960).

27. N.B.Hannay, *Semiconductors*, P. 32, Chapman & Hall, London (1960).

28. R.L.Petritz, *Phys. Rev.* **104**, 1508 (1956).

29. H. Berger, *Phys. Status Solidi* **1**, 739 (1961).

30. H. Berger, W.Kahle & G. Jamiche, *Phys. Stat. Solidi.* **28**, K97 (1968).

31. R.G.Mankarious, *Solid-state Electron.* **7**, 702 (1964).

32. L.L.Kazmerski, F.R.White, M.S.Ayyagary, Y.J.Juang & R.P.Patterson, *J. Vac. Sci. Technol.* **14**, 65 (1977).

33. L.L.Kazmerski & Y.J.Juang, *J. Vac. Sci. Technol* **14**, 769 (1977).

34. L.L.Kazmerski, '*Polycrystalline and Amorphous Thin Films and Devices*', P. 89, Academic Press, London (1980).

CHAPTER 7

CRYSTAL GROWTH

7.1 INTRODUCTION

The advent of modern semiconductor based technology generated a demand for large, high-quality single crystals; not only of semiconductors but also of associated electronic materials. Because many properties of solids are best studied with single crystals, the increasing interest in the nature of solids also has required that crystals be grown under controlled conditions for a variety of investigations. The knowledge of the precise ways of growing perfect crystals is, thus, of prime importance. Due to the influence of numerous interdependent parameters, the process of crystal growth is rather complex. Several new techniques have been established to understand the kinetics of the process of crystal growth and a good number of informations have been gathered on theoretical basis.

In this chapter, the fundamentals of the theories and techniques of crystal growth are presented. A brief description of morphology and growth mechanism of crystals, as well as, a summary on the different types of defects in crystals are also included.

7.2 THEORIES OF CRYSTAL GROWTH

The first attempt to give an explanation for the process of crystal growth, on the basis of thermodynamics was made by Gibbs [1]. According to him, crystal growth processes are phase transformations, driven by chemical potential between the crystallizing and nutrient phases. The criterion for such a transformation from vapor to solid, forming crystals can be expressed as $\sum \sigma_i F_i$ is a minimum, where σ_i is the surface free energy per unit area of the ith face of area F_i.

The criterion of minimum free energy suggested by Gibbs was later developed by Curie [2] and Wulff [3]. The volume of the crystal can be written as

$$V = \frac{1}{3}\sum D_i F_i \tag{7.1}$$

where D_i is the perpendicular distance of the ith face of the crystal from a fixed point inside the crystal. For a very small change in volume,

$$dV = \sum F_i \, dD_i \tag{7.2}$$

where one set of faces is assumed to grow at the expense of another. From equation 7.1

$$dV = \frac{1}{3}\sum \left(F_i \, dD_i + D_i \, dF_i\right) \tag{7.3}$$

If the volume is kept at constant, dV = 0, and from equations 7.2 and 7.3, we get

$$\sum D_i \, dF_i = 0 \tag{7.4}$$

If the total free energy in the minimum energy criterion is a constant, then

$$\sum \sigma_i \, dF_i = 0 \tag{7.5}$$

From equations 7.4 and 7.5, we get $D_i \propto \sigma_i$. This theory implies that on a crystal, the velocities of growth of the different faces in the directions of the normals are proportional to the appropriate specific surface free energies.

Based on the assumption that the lattice planes having the largest reticular density are parallel to the slowest-growing crystal faces, Bravais [4] suggested that growth velocity of a face is inversely proportional to its atomic density. The Bravais theory was further developed by Donnay and Harker [5]. The combined Bravais-Donnay-Harker rule is a good generalization of the trend in form development for most crystals. After the theories of Gibbs and Curie, Soehncke [6] introduced the idea of surface energies by postulating that the faces which posses the greatest reticular densities are those with minimum surface energies, and hence have minimum velocities of growth.

Kossel [7], Stranski [8], and Volmer [9] independently developed atomic theories to explain the growth of ideal crystals. The KSV model is assumed that the energy due to the unsaturated atomic bonds at the crystal's surface is lowered when an atom attaches itself to the surface. The amount of energy released by such attachments is different in different parts of the crystal, being largest at a 'step' on the surface.

A molecule adsorbed on an atomically smooth crystal surface often migrate considerable distances before it becomes a part of the crystal. The

distance through which an adsorbed molecule migrate is given by Einstein's formula

$$X_s^2 = D_s T_s \tag{7.6}$$

Where D_s is the diffusion coefficient and T_s is mean life time on the surface. In the Kossel - Stranski model

$$X_s \approx a \exp(3\phi/2KT) \tag{7.7}$$

where ϕ is the nearest neighbour interaction.

The migrating molecules adhere to the kink sites on the steps. The mode of advance of the steps can be analysed on the basis of BCF theory [10]. A step advances by the process of incorporating more and more adsorbed molecules at kink sites at high supersaturation. The rate of advance of a straight step is given by the relation.

$$V = (\alpha - 1) X_s \upsilon \exp(-W/KT) \tag{7.8}$$

where α is the saturation ratio, υ is a frequency factor and W is the total evaporation energy.

On a perfect crystal surface steps are created by thermodynamic fluctuations. Once the step has covered the whole surface, further growth is possible only by the initiation of a new island monolayer, which requires additional energy. If it is assumed that only a single nucleus of monomolecular height is formed having a circular shape with radius r, then the excess free energy f of the system is given by

$$f(r) = -KT \ln \alpha \; \pi r^2/a^2 + \beta \, 2\pi r/a \tag{7.9}$$

where α is the supersaturation and β is the edge free energy per molecule.

The rate of nucleation is given by

$$I = Z N_o \exp(-F_o/KT) \quad (7.10)$$

where N_o is the number of lattice sites per unit area, Z is the number of molecules arriving per unit time towards the critical nucleus, and F_o is the maximum surface free energy.

According to the surface nucleation theory, the nucleation rate is a sensitive function of supersaturation and below a supersaturation of 25-50 percent, the probability of nuclei formation is negligible. However, real crystals can grow even when the value of supersaturation is much lower than that of the critical value obtained by the surface nucleation theory. This led to the conclusion that the growth of crystals at low supersaturation could only be explained by the fact that real crystals differ from ideal crystals.

Burton et al. [10] have developed the theory of growth of real crystals by taking into account the presence of dislocations. A mechanism of growth of real crystals has been proposed by Frank [11] who postulated that crystals grow by means of dislocations that produce steps in the crystals surface. When the atoms are adsorbed on the crystal surface, they prefer to attach themselves to this step. Growth proceeds, therefore, by a continuous growth of the same layer in the form of a continuous spiral. A ledge which forms a portion of the spiral and has a radius of curvature ρ, will advance with a velocity V_ρ given by,

$$V_\rho = V_\infty (1 - \rho_c/\rho) \quad (7.11)$$

where V_∞ is the rate of advance of a straight step and ρ_c is the critical radius of curvature.

Let θ (r) represents the rotating spiral in polar co-ordinates (r, θ). The radius of curvature at a point r will be,

$$\rho = (1 + r^2 \theta'^2)^{3/2} / (2\theta' + r^2 \theta'^3 + r\,\theta'') \qquad (7.12)$$

where θ' and θ'' are the derivatives of θ (r). The normal velocity at the point r is,

$$V(r) = \omega\, r\, (1 + r^2 \theta'^2)^{-1/2} \qquad (7.13)$$

where ω is the angular velocity. The spacing between the successive arms of the spiral will be constant and is given by,

$$dr = 4\, \pi\, \rho_c \qquad (7.14)$$

Frank's [11] views have been extended by others who have gathered a large amounts of observational evidence to support them.

7.3 TECHNIQUES OF CRYSTAL GROWTH

Depending on the phase transitions involved in the process of crystal growth, the growth methods can be classified in to three; viz: melt growth, vapour growth, and solution growth.

7.3.1 Growth from melt

For the growth of single crystals from melt, the transition from an equilibrium state in which the substance is completely molten to a state where

the substance is completely solid, is to be controlled effectively. In principle, the crystals of all materials can be obtained from melt, provided they melt congruently, they do not decompose before melting and they do not undergo a phase transformation between the melting point and room temperature.

The crystallization of a melt is a first order change from liquid to solid involving the liberation of latent heat. On the basis of the free-energy change between the two phases, the driving force of a melt growth process can be expressed as

$$\Delta G_{SL} = \Delta H_{SL} - T\,\Delta S_{SL} \tag{7.15}$$

Where ΔH_{SL} and ΔS_{SL} represent the changes of enthalpy and entropy at the temperature T.

At equilibrium,

$$\Delta S_{SL} = \frac{\Delta H_{SL}}{T_M} \tag{7.16}$$

where T_M is the equilibrium melting point for a near equilibrium process, in which the melt is undercooled at a temperature T, below the melting temperature T_M,

$$\Delta G_{SL} = \Delta H_{SL} \frac{T_M - T}{T_M} = \Delta H_{SL} \left(\frac{\Delta T}{T_M}\right) \tag{7.17}$$

$\frac{\Delta T}{T_M}$ is the relative undercooling and it gives the effective driving force of the crystallization process. It can also be expressed in terms of supersaturation σ.

$$P_M = A \exp \frac{-\Delta H_{SV}}{KT_M} = A' \exp \frac{-\Delta H_{LV}}{KT_M} \tag{7.18}$$

where P_M represents the saturated vapor pressures. If the melt is undercooled at $T < T_M$, the vapor pressure at T for the solid and liquid phases will be

$$P_S = A \exp \frac{-\Delta H_{SV}}{KT}$$

$$P_L = A' \exp \frac{-\Delta H_{LV}}{KT} \tag{7.19}$$

Putting, $\Delta H_{SL} = \Delta H_{SV} - \Delta H_{LV}$ and from equation (7.18),

$$\sigma = \frac{P_L}{P_s} - 1 = \exp \left[\Delta H_{SL}\left(\frac{1}{KT} - \frac{1}{KT_M}\right)\right] - 1 \tag{7.20}$$

where $P_L / P_S = \alpha$ is the saturation ratio.

The free energy change between the two phases is expressed as,

$$\Delta G_{SL} = -KT \ln \alpha = -\Delta H_{SL}\left(\frac{T_M - T}{T_M}\right) \tag{7.21}$$

Assuming the atom motion at the solid-liquid interface as an activated process, the rate at which atoms join the crystal can be written as [12],

$$R_F = R_F^o \exp(-\Delta G/KT) \tag{7.22}$$

where ΔG is the activation energy for liquid diffusion of growth unit.

Similarly the rate at which atoms leave the crystal is,

$$R_M = R_M^o \exp\left[-(\Delta G + \Delta H_{SL}) / KT\right] \tag{7.23}$$

where $(\Delta G + \Delta H_{SL})$ represents the activation energy for melting.

At equilibrium,

$$R_M^o / R_F^o = \exp\left(\frac{\Delta H_{SL}}{KT_M}\right) \qquad (7.24)$$

The net growth rate is given by

$$V = R_F - R_M$$

$$= R_M^o \exp\left(\frac{-\Delta G}{KT}\right) \exp\left(\frac{-\Delta H_{SL}}{KT_M}\right) \left[1 - \exp\left(\frac{-\Delta H_{SL}\,\Delta T}{KT_M T}\right)\right] \qquad (7.25)$$

In this formulation it is assumed that all the sites at the crystal liquid interface are equivalent and are active growth sites. But in the real cases, only a fraction of sites will be available for growth unit attachment, which can be accounted for by multiplying equation (7.25) by suitable factors. For screw dislocation mechanism , the factor will be,

$$f = \alpha_1 \frac{\Delta H_{SL}}{\gamma_L} \frac{\Delta T}{T_M} \qquad (7.26)$$

where γ_L is ledge free energy, and α_1 is geometric constant. From equations 7.25 and 7.26, we get $V \alpha (\Delta T)^2$ for small under cooling. For surface nucleation growth,

$$f = \alpha_2 \exp\ (-T^* / \Delta T) \qquad (7.27)$$

$$\text{where } T^* = \frac{\alpha_2 \gamma_L^2\ T_M}{KT\ \Delta H_{SL}} \qquad (7.28)$$

From equations (7.25) and (7.28) one gets an expression predicting small growth rates until $\Delta T \sim T^*$, and v increases very rapidly with increasing undercooling.

The growth from melt thus essentially involves the control of temperatures and the various methods described below achieves this by a variety of techniques.

7.3.1a Czochralski method

One of the most important bulk crystal growth techniques is the crystal-pulling or Czochralski method, in which a rotating seed crystal is dipped into the melt. Rotation reduces radial temperature gradients, and slow withdrawal of the rotating seed results in growth of a cylinder of single crystal material. Large single crystals with high crystallline perfection can be obtained by this method at high speeds. Crystal diameter and length depend upon the details of the temperature and pulling rate, and the dimensions of the melt container.

7.3.1b Bridgman method

In this method the material is melted in a vertical cylindrical vessel which tapers conically to a point at the bottom. The vessel then is lowered slowly into a cold zone. Crystallization begins in the tip and continues usually by growth from the first formed nucleus.

7.3.1c Horizontal Normal Freezing

In this method, the charge is contained in a closed container which can be mounted horizontally. A boat can also be used as container. If a seed is not used, the entire charge is melted; solidification is initiated and the solid-melt

interface is advanced horizontally by moving the container through a furnace with appropriate thermal gradients or by moving the furnace past the container. The interface can also be advanced by controlled power reduction. For obtaining specific orientation, a seed is commonly used at one end of the container.

7.3.1d Zone Melting

Single crystals of ultrahigh purity have been grown by zone melting, in which a narrow molten region is passed through a relatively large ingot of single or polycrystlline material.

7.3.1e Float-Zoning

It is essentially zone melting in a vertical configuration without a container. The zone is sustained by surface tension force. Thus this method is suitable for materials with high surface tension and low density. The unique advantage of float-zoning is the elimination of the melt container which reduces contamination.

7.3.2. Growth from the Vapour Phase

Growth from the vapour phase is the most versatile technique for growing crystals with high purity and crystalline perfection. The method is widely used for growing bulk crystals, epitaxial films, thin coating, filamentary and platelet crystals. The thickness and the doping of the layers can be closely controlled and the process can be recycled. The various transport mechanisms involved in the vapour phase growth process has been treated by Faktor and Garrett [13].

Any substance, which has appreciable vapour pressure, may be grown as single crystals by condensation on a comparatively cold surface. During growth, molecules or atoms get incorporated into the kinks on a step after the adsorption and diffusion. According to the process which promotes the crystallization from the vapour phase, the growth methods can be distinguished into two:

7.3.2a Physical Vapour Deposition (PVD)

Single crystals can be grown by sublimation where the substance is converted directly from the solid to vapour and back again to solid. In this method, an evacuated sealed ampoule containing the starting material is placed in the temperature gradient. One end of the ampoule at which the charge material is placed; known as the source zone, is maintained at a higher temperature. A concentration gradient is established in the ampoule, due to the temperature dependence of the equilibrium vapour pressure. Under the effect of this gradient, the substance is transported to the colder region, known as the crystallization/growth zone, where the vapour gets supersaturated and condensed. This method is also called closed-ampoule method and the details are described in literature [13, 14]. To obtain flawless crystals the growth rate is to be controlled by working under low supersaturations. The temperature gradient may be conveniently controlled to produce optimum supersaturations.

7.3.2b Chemical Vapour Deposition (CVD)

In this method a chemical reaction is used to produce a solid deposit from the gaseous reactants. This reaction serves not only to supply material for crystallization but also has an active influence on the crystallization process. The material to be grown as single crystals is made to react with a transporting agent to convert the same into a volatile material and deposition is made by inducing the reverse chemical reaction. The process is mainly used in systems which has low vapour pressures by themselves and can undergo a reversible chemical reaction.

7.3.3 Growth from Solution

In this process, a saturated solution is prepared in a suitable solvent and crystallization is initiated by the slow evaporation of the solvent. Material which melt incongruently, decompose before melting or undergo a phase transformation between the melting point and room temperature are grown from solutions. Solution growth is generally simple and inexpensive.

7.3.4 Growth from Gels

Growing crystals from gel is successful in the case of materials which cannot be grown from melt, vapour and solution, due to the decomposition before melting, low vapour pressure or low solubility. In the gel method the growth takes place at low temperatures and hence crystals will have lower concentration of non-equilibrium defects than those grown at elevated temperatures.

7.4. MORPHOLOGY OF CRYSTALS

The macroscopic form and structure exhibited by a crystal is its morphology. During its growth, a crystal often develops and maintains a definite polyhedral form which may reflect the characteristic symmetry of the molecular pattern of the crystal. The growth velocity of a crystal face is inversely proportional to its atomic density. Since the densest lattice planes have the largest interplanar spacings the so-called law of Bravais states that the most prominent faces of a crystal are those with the largest lattice spacings.

The molecular binding sites on the surface of a crystal can be of several kinds. A molecule must be more strongly bound at a ledge formed by an incomplete plane than on a perfectly developed plane of molecules at the crystal surface. Thus there exist a periodic bond chain (PBC) [15] between the crystallising units. Layer growth is possible only when there is strong bonds between periodic bond chains. Each layer is repeated at a distance of d_{hkl}. Such faces with strong bonds are called Flat faces (F-faces). In the absence of a PBC, since the nucleation probability is the same everywhere, the layer growth mechanism is impossible. In such a case the surface will be stepped and is called S-face. In addition due to total absence of PBC's, kinked faces also exist and are called K-faces. The different nature of bonding that exist in the various faces of a crystal thus promotes or prevents growth to give the crystal, the observed morphology.

In general, crystals exhibit various external habits and they are:

7.4a Whiskers

Whiskers are hair like crystals which have negligible dimensions compared to their length. Whiskers can be grown by the solid-solid transformation [16], from solution [17], and by electromigration [18]. Whiskers exhibit high mechanical strength. In addition to exceptional strength, whiskers often have unique electrical, magnetic or surface properties. This behaviour can be interpreted to mean that the crystal structure of whiskers is perfect.

The morphology of the whiskers have been found to depend upon the material, growth method and temperature of growth. Several theoretical models have been proposed to explain the growth of whiskers under a variety of conditions. The various observations of dislocation loops, spiral and helices in whiskers support the dislocation model suggested by Frank [19] and Eshelby [20]. In several materials the growth of dislocation free whiskers were also observed. The investigations on these whiskers led Wagner and Ellis [21] to the formulation of the Vapour - Liquid - Solid (VLS) mechanism. However, no general correlations between whisker properties and whisker structure have been established.

7.4b Platelets

Vapour growth whiskers are often accompanied by plate like or two dimensional crystals. A genetic relation between these two crystalline forms have been noted by various investigators. In the case of platelets growth is inhibited in one direction where as in whiskers, it is inhibited in two directions. The platelet formation is caused by the crystal structure of materials. Various

compounds, such as the members of III - VI (GaS, GaSe etc), IV - VI (SnS_2, $ZrSe_2$ etc.) and V - VI (Bi_2Te_3, Bi_2Se_3, Sb_2Te_3, etc.) families, exhibit layer structures. The bonding between the layers is weak, being of Van der Waal's type, whereas strong covalent bonds exist within the layers. Accordingly, these compounds tend to crystallize in platelet form. The platelet growth have been found to depend upon the crystallization conditions, such as temperature, supersaturation, impurities etc.

7.4c Dendrites

The dendritic morphology of crystals is a highly branched structure with the different branches oriented in crystallographic directions. The observation of this morphology, during the crystallization of a large number of materials from all the three states of matter, showed that the dendritic growth is a widespread phenomenon. The dendritic growth usually start with the development of a fibre tip growing into the melt or solution soon develops instabilities which subsequently grow out as primary branches. The process repeats often systematically, producing secondary and ternary branches, all of which are oriented crystallographically.

7.4d Spherulites

The spherulitic morphology consists of spherically symmetric crystalline aggregates and are exhibited by minerals, polymers and other materials. This macroscopic spherical symmetry is in violation with the uniform packing of microscopic units. The spherulites thus radiate, from a nucleus with the substructure of needles, with small angle branching, to fill the area created by

the outwardly increasing volume. The experimental findings on the spherulitic crystallisation show that this mode of growth is restricted to melts having high viscosities.

7.5. DEFECTS IN CRYSTALS

Natural crystals always contain defects, often in abundance, due to the uncontrolled conditions under which they formed. Even though, considerable effort have been made to control their type, concentration, and distribution, crystals prepared in the laboratory will also always contain defects. Crystal defects are responsible for many of the important properties of materials. Hence, much of solid-state physics and chemistry and materials science involves the study and engineering of defects so that solids will have desired properties.

Defects in a real crystal may be divided into chemical impurities and structural defects. The various crystal defects is as follows:

1. Electronic - excess electrons and holes.
2. Point defects - vacancies and self interstitials.
3. Line imperfections - dislocations
4. Surface imperfections

   a. Stacking faults

   b. Twin boundaries

   c. Grain boundaries

d. Free surfaces

e. Interstitial and vacancy loops

f. Domain wall boundaries

5. Volume defects: voids, inclusions, second phase particles etc.

Chemical impurity is an important class of crystal defect and substitutional impurity is the simplest one. In metals, the impurities usually lead to an increase in resistivity. Impurities in semiconductors are responsible for the important electrical properties which lead to their widespread use. The energy levels associated with impurities and other defects in non-metals may lead to optical absorption in interesting regions of the spectrum. The phenomenon of light emission or luminescence is often impurity - related.

Even in a chemically pure crystal, structural defects will occur. Defects belonging to the point defects category are thermodynamically stable defects, because their occurrence in crystals lowers the crystal free energy as a result of an increase in the defect configurational entropy. Crystal dislocations, which increase the overall free energy of crystals, are metastable defects.

A common planar structural defect is the stacking fault and is produced by the extension of perfect dislocations in close packed structures.

When a perfect crystal block is sheared and the slip process stopped partially within the crystal, the boundary between the slipped and the un-slipped portion is a dislocation. Dislocation generally have some edge and screw character. An edge dislocation is a line defect which may be thought of

as the result of adding or subtracting a half-plane of atoms (Fig.7.1). A screw dislocation is a line defect which can be thought of as the result of cutting part way through the crystal and displacing it parallel to the edge of the cut (Fig.7.2). The lattice displacement associated with a dislocation is called the 'Burgers vector'. Since dislocations cannot terminate inside a crystal, they either intersect the surface or an internal surface (grain boundary) or form a closed loop within the crystal.

Dislocations are incorporated into growing crystals by various modes. Thermal stresses, constitutional stress, mechanical stress, vacancy supersaturation, probability accidents, multiplication and annihilation mechanisms, dislocation interactions leading to the formation of dislocation networks, and mechanical handling of good crystals, are the factors that affect the dislocation density in growing crystals. The details of the theoretical and experimental study of dislocations has been dealt with by various authors [22-26]

A wide range of techniques have been used to study the distribution, arrangement and density of dislocations and to determine their properties. They are: surface methods, decoration methods, transmission electron microscopy, field ion microscopy and X-ray diffraction technique. Of the various methods, etching is the simplest method for the detection and characterization of crystal defects such as grain boundaries, slip lines, dislocations, stacking faults and vacancies.

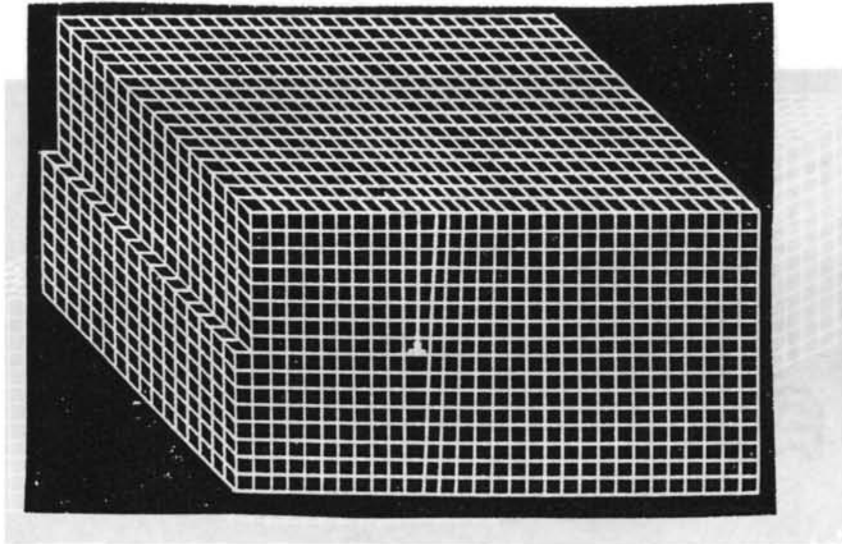

Fig. 7.1 An edge dislocation

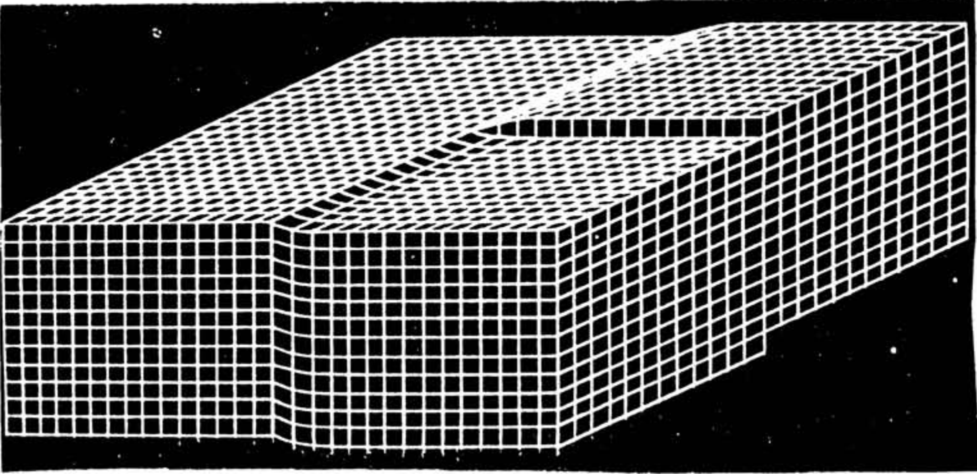

Fig. 7.2 A screw dislocation

REFERENCES

1. J.W.Gibbs., *Collected works*, (Longman's Green & Co., London, 1878), P. 325.

2. P. Curie., *Bull. Soc. Franc. Miner.*, **8**, 145 (1885).

3. G. Wulff., *Z.Kristallogr.* **34**, 449 (1901).

4. A. Bravais and A. Etudes., *Crystallographiques*, (Gauthier Villars, paris, 1866).

5. J.D.Donnay and D. Harker., *Amer. Min.* **22**, 446 (1937).

6. L. Soehncke., *Entwicklung einer theories d. Krystalla strucktur*, (Leipzig, 1879).

7. W. Kossel., *Nachr, Ges. Wiss., Gottingen*. P. 135 (1927).

8. I.N. Stranski., *Z. Phys. Chem.* **136**, 259 (1928).

9. M. Volmer., *Kinetic der phasenbildung* (Steinkopffr Dresden and Leipzing, 1939).

10. W.K.Burton, N. Carbrera, and F.C.Frank., *Phil. Trans. Roy. Soc.*, **A243**, 299 (1951).

11. F.C.Frank., *Disc. Faraday Soc.* **5**, 48 (1949).

12. K.A. Jackson and B. Chalmers., *Can. J. Phys.* **34**, 473 (1956).

13. M.M. Faktor and I. Garrett; *Growth of crystals from the vapour* (Champman & Hall, London, 1974).

14. C.H.L. Goodman., *Crystal Growth, Theory and Techniques*, Vol. 1 (Plenum Press, London, 1974).

15. P. Hartman., *Crystal Growth: An introduction*, (North Holland, 1973) P. 367.

16. K. Nakahigashi and Y. Shimomura., *J. Cryt. Growth.* **28**, 367 (1975).

17. N. Zelingher, J. Fliastein and A. Zangvil, *J. Cryst. Growth.* **42**, 253 (1977).

18. Y. Smooha and Y. Komem, *J. Cryst. Growth.* **38**, 149 (1977).

19. F.C.Frank., *Philos. Mag.* **44**, 854 (1953).

20. J.D. Eshelby., *Phys. Rev.* **91**, 755 (1953).

21. R.S. Wagner and W.C. Ellis., *Trans. met. Soc. AIME*, **233**, 1053 (1965).

22. W.T. Read, *Dislocations in Crystals.* (Wiely, New York, 1953).

23. J. Friedel, *Dislocations.* (Pergamon Press, London, 1964).

24. I. Kovacs and L. Zsoldes., *Dislocations and Plastic Deformations* (Pergamon Press, New York, 1973)

25. F.R.N. Nabarro., *Dislocations in Solids.* (North Holland Pub. Co., New York, 1979).

26. D. Hull and D.J. Bacon., *Introduction to Dislocations.* (Pergamon Press, New York, 1984).

CHAPTER 8

EXPERIMENTAL TECHNIQUES

The horizontal zone levelling (HZL) method and the physical vapour deposition (PVD) technique were used to grow Bi_2Se_3 crystals, for the present investigations. Dislocation studies have conducted by chemical etching technique. A brief account of the various experimental techniques employed in these investigations is given in this chapter.

8.1 GROWTH TECHNIQUES

8.1a Reaction ampoules

Quartz tubes with different diameters have used to fabricate the reaction ampoules for the growth. One end of the ampoule was closed and for easy vacuum sealing, the other end was uniformly constricted to a narrow bore, sufficient enough to introduce the starting material. Inorder to increase the degree of mixing of the vapours, two round dimples were also made on the walls of the ampoules used for the growth by physical vapour transport method. All the ampoules, used in this work, were thoroughly cleaned, treated in HNO_3, washed with liquid Teepol detergent and repeatedly rinsed in double distilled water. Finally, the ampoules were ultrasonically agitated in acetone and then dried.

A specially designed adapter system, which can be fixed to the base plate of the oil diffusion pumped vacuum unit was used to evacuate and seal the ampoules with reactants. The adapter has provisions to connect the ampoule and to fix a penning gauge head for the pressure measurement. The ampoules were connected to the vacuum system and sealed off at ~ 10^{-5} torr. To avoid any chance for the sublimation of the charge during fusing, usually the lower end of the ampoules was kept in a freezing mixture.

8.1b Preparation of homogeneous charge

For preparing the starting material of Bi_2Se_3, high purity (99.999%) bismuth and selenium in appropriate proportion were vacuum sealed in pre-cleaned quartz ampoules of length 10 cm and 12 mm. To prepare a homogeneous charge, the ampoule was heated in a uniform temperature by means of a 'muffle furnace', which can attain a maximum temperature of 1000°C. The temperature of the furnace can kept constant within ±5°C by a built-in temperature controlling assembly. An arrangement to rotate and rock the ampoule for proper mixing of the reactants is also attached to the furnace. To avoid the chance for cracking the ampoule, it was very slowly heated to the required temperature and allowed to complete the reaction.

8.1c Growth of crystals from vapour

For the physical vapour deposition of Bi_2Se_3, crystals, a two-zone horizontal linear gradient furnace, the temperatures of which can kept constant to an accuracy of ±1°C by two independent temperature controllers, was used.

Both zones of the furnace can attain a maximum temperature of 1000°C. In closed-tube- vapour-transport technique, transporting of the reactants from the hot zone to the cold zone is taking place at a low pressure in the ampoule. The sealed reaction ampoule was placed in the furnace and before starting the growth, a reverse temperature gradient was applied such that the source region was at a lower temperature than the condensation zone. After two to three hours in a reverse temperature gradient, any traces of starting material in the growth zone are removed. For the growth process, the source zone was maintained at a higher temperature and the growth zone at a lower temperature. The ampoules were removed from the furnace after the growth and the crystals were taken out carefully for further studies by etching the ampoules in HF.

8.1d Growth of crystals from melt

Crystals of Bi_2Se_3, from its melt were grown by horizontal zone levelling (HZL) method. For this, the ampoules containing the charge material were heated in linear temperature gradient by means of a horizontal furnace. The temperature of the middle of the furnace can be raised upto a maximum of 1000°C. The temperature profile along the axis of the furnace was carefully determined using chromel-alumel thermocouple. For the growth, the reaction ampoule was placed in the furnace such that the charge end is at the middle of the furnace, where the temperature is heighest. The ampoule was slowly heated to melt the entire charge; solidification was initiated and the solid-melt interface was made to advance horizontally by controlled power reduction. Good stoichiometric crystals were obtained and were cleaved to get optically plane surface for their characterisation.

8.2 OPTICAL MICROSCOPY

One of the most suitable methods for observing crystals surfaces is optical microscopy. Growth patterns on crystal surfaces can give valuable informations about the growth mechanisms of crystals.

Union Versamet - 2 model metallurgical microscope was employed for the microtopographical studies. Because the crystals studied in the present case was opaque, their surfaces were examined in the reflection mode of the microscope. The microphotograph of the crystal surfaces were taken by the built-in photographic mechanisms of the microscope. Large size photo films as well as 35 mm role films can be used in the built-in photo mechanism. The photographic lenses are attached on a rotating turret and the magnification of each lens can be seen through a display window. For the measurement of very small length, a micrometer eyepiece is also provided with the unit. The specimen to be studied is placed on a movable stage above the objective lens, which can be moved in circular and cross-wire directions.

8.3 ETCHING STUDIES

Chemical etching technique was employed to conduct the dislocation studies during the present investigations. It was performed by immersing the crystals in a suitable etchant and the etched surfaces were examined under a optical microscope.

According to Gilman et al. [1], when a perfect crystal face is exposed to a solvent, dissolution probably begins by the nucleation of 'unit pits' of one

molecules depth. On a real crystal dislocations may be preferential sites for nucleation of unit pits, and repeated nucleation at a dislocation leads to the formation of an etch pit. Different theories of dissolution have been formulated to explain the etching phenomenon. Nucleation of etch pits at dislocations has been attributed to the elastic strain associated with the dislocations which causes a decrease in the activation energy for nucleation [2]. The screw dislocations have shear stress fields which vanishes at the surface except at the core, where as strain energy associated with an edge dislocation is retained at the surface and extends to a considerable distance beyond the core.

The morphology of dislocation etch pits depends on the nature of dislocation and on the angle at which the dislocation line intersects the surface. The dislocation perpendicular to the surface will produce symmetrical pits while any deviation from it produces asymmetry [3]. If the dislocations are parallel or almost parallel to the surface, etch grooves or pits elongated in the direction of dislocation will result [4]. If the dislocation moves from its pit position during etching, as in the case of shallow dislocation half-loops, or as a result of applied stress, then the bottom of the pit becomes flat and upon continued non-preferential etching, the pit is eliminated. The formation of visible dislocation etch pits is influenced by the etching rates along the dislocation line, parallel to the surface and perpendicular to surface. Depending upon the relative values of the etching rate, the morphology of pits will change. The etch pit morphology depends strongly on the crystal structure also [5].

Impurities also have a prominent role in controlling the etching behaviour. The impurities incorporated with the dislocation as well as those

present in the etchants will affect the etch pit formation. In the dissolution process, the presence of impurities in the etchant presumably reduces the flow of steps across the surface in a manner exactly analogous to the reverse of growth process, where it has been observed that certain poisons in the solution still impede the rate of crystal growth. The impurity will probably be adsorbed at the steps and more particularly at the kinks in them, and therefore it will tend to protect them from chemical attack. The overall rate of dissolution of the crystal is thereby decreased and higher under saturations can be maintained. Under such conditions, the tendency to from etch pits is increased.

In addition to dislocations, point defect clusters, precipitates, as well as surface damages can also be produce etch pits on crystal surfaces. The pits other than that of dislocations, usually disappear continuously on prolonged etching or on repeated polishing and etching, as they are due to shallow defects. On the other hand the etch patterns due to dislocations persist on prolonged etching or on alternate polishing and etching, because dislocation lines do not terminate within a crystal. For crystals which can have a cleavage, a one-to-one correspondence between the etch pits on the opposite cleavage halves will obtain, if pits are formed at dislocation sites. An experimental verification of such a one-to-one correspondence on the opposite halves of a cleavage is generally considered as an adequate proof to establish the reliability of a particular etchant for revealing dislocations on a crystallographic plane.

REFERENCES

1. J.J. Gilman, W.G. Johnston and W.G.Sears., *J. Appl. Phys.* **29**. 747 (1958).

2. N. Cabrera, In *'The surface chemistry of metals and semiconductors'*, ed. H.C.Gatos (John Wo;ey, 1960).

3. S. Amelinckx., *'Direct observation of dislocations'*, Vol. 6, Eds. F. Seitz and D. Trunbull (Academic Press, New York, 1964).

4. W.C. Dash., *J. Appl. Phys.* **29**, 705 (1958).

5. A. Koma, E.Takimoto and S. Tanaka., *Phys. Stat. Solidi.* **40**, 239 (1970).

CHAPTER 9

DISLOCATION STUDIES IN MELT-GROWN Bi_2Se_3 CRYSTALS

9.1 INTRODUCTION

The semiconducting V_2VI_3 compounds Bi_2Se_3, Bi_2Te_3 and Sb_2Te_3 crystallize in a layer-type structure belonging to the space group D^5_{3d} (R $\bar{3}$ m). The basic unit cell of these crystals is rhombohedral and the atoms are arranged in two-dimensional hexagonal net works perpendicular to the *c* axis, and the sequence of layers is as follows:

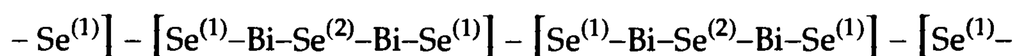

$$- Se^{(1)}] - [Se^{(1)}-Bi-Se^{(2)}-Bi-Se^{(1)}] - [Se^{(1)}-Bi-Se^{(2)}-Bi-Se^{(1)}] - [Se^{(1)}-$$

Crystals of these materials are distinctly eleavable along the basal planes (0001). The binding between Bi and Se layer is generally considered to be predominantly covalent. The easy cleavage of these materials perpendicular to the *c* axis is believed to be due to weak forces (Van der Waal's forces) between the $Se^{(1)}$ layers. In other words, the structure of these compounds consists of packages and sandwiches of five layers $[Se^{(1)} - Bi - Se^{(2)} - Bi - Se^{(1)}]$ with covalent bonds within the sandwiches and weak bonds between them.

Because of their potential applications to i.r. detectors and thermoelectric generators, the electronic properties of the narrow gap semiconductors Bi_2Se_3 ($Eg \approx 0.2$ eV) and Bi_2Te_3 ($Eg \approx 0.15$ eV) have attracted much attention. The electrical conductivity and mobility [1 - 5], the optical [6 - 10], and galvanomagnetic [10 - 12] properties as well as thermoelectrical properties [3, 4, 13] of pure and doped crystals of Bi_2Se_3 have been extensively investigated.

In fact, it is well known that the electronic properties of the semi-conducting crystal chips are strongly influenced by the defects and impurities incorporated to them during their growth. Unlike point defects, dislocations get introduced into the crystals during their preparation and subsequent handling also. Since the nature and distribution of these dislocations have sensitive effect on many physical properties of the crystals, its knowledge is important for the improved reliability and performance of electronic devices. Dislocation studies on the cleavage planes of crystals of Bi_2Te_3 and other members of the V - VI family have been conducted by various groups [18, 26-28]. Even though a large number of investigations were carried out on the various properties of Bi_2Se_3 crystals, by different groups, dislocation studies on these crystals have not been closely conducted. Of the various methods used to study the distribution, arrangement and density of dislocations, etching is a simple, yet powerful technique. Kolakowski [14] has observed triangular etch pits on the cleaved surfaces of Bi_2Se_3 crystals, with different etching solutions. But any one of these can not be used as a reliable etchant for dislocation studies as one cannot with certainty say which of the pits are due to dislocations. It is

therefore of interest to study the development of etch pits on the (0001) cleavage planes of Bi_2Se_3 crystals by chemical etching method.

Reported below, the etching characteristics of the Bi_2Se_3 crystals grown from its melt by horizontal zone levelling (HZL) technique. An etchant was found which is capable of revealing dislocations on the cleavages of Bi_2Se_3 crystals. The reliability of the etchant has been established by: (1) successive etching, (2) etching of matched cleavage faces, and (3) intersecting lineage lines.

9.2. EXPERIMENTAL

The elements Bi and Se used in the preparation of the compound were of 99.999% purity and were obtained from the Nuclear Fuel Complex, Hyderabad, India. The compound Bi_2Se_3 was prepared by melting together Bi and Se in 2 : 3 atomic ratio in a sealed quartz ampoule of length 10 cm and diameter 12 mm, evacuated to a pressure of 10^{-5} torr. This charge was slowly heated and maintained at a temperature of 800°C for 24 hours. The ampoule was rotated and rocked periodically to ensure complete mixing and reaction. The charge was then slowly cooled to room temperature. Samples from different parts of this ingot were used for taking X-ray powder diffractograms to confirm the formation of stoichiometric compound.

For growing crystals of Bi_2Se_3, a horizontal gradient furnace was used. The high vacuum sealed ampoule containing the homogeneous charge was placed in the furnace and the growth was carried out by keeping the ampoule

at a temperature of 800°C at the hotter end and 720°C at the cooler end for about 72 hours. The ampoule was then slowly cooled to room temperature. X- ray diffraction studies were carried out with CuK_α radiation. It has been found that good stoichiometric crystals of Bi_2Se_3 are obtained under the present growth conditions.

The samples were carefully cleaved at liquid-nitrogen temperature to study the dislocations in these crystals by chemical etching technique. All the work reported here was done on the *c* plane of Bi_2Se_3 crystals, at room temperature. The composition of an etchant is empirical; but its basic requirement is an oxidising agent and a complexing agent. Several etchants were tried to find out a suitable one to delineate the dislocations in Bi_2Se_3 crystals.

The etched crystal surfaces were then cleaned with double distilled water, dried and examined under reflection mode using Carl Zeiss Jena and Union Versamet - 2 metallographic microscopes.

9.3. XRD STUDIES

Fig. 9.1 shows the X-ray diffractogram of a typical bismuth selenide crystal grown by HZL technique. The corresponding (hkl) planes are also indicated. The d- spacing and relative intensities of the standard pattern given in the JCPDS Powder Diffraction File for Bi_2Se_3 [15] along with the data obtained in the present case are given in Table 9.1. All the diffraction lines and their relative intensities are comparable well with the standard pattern.

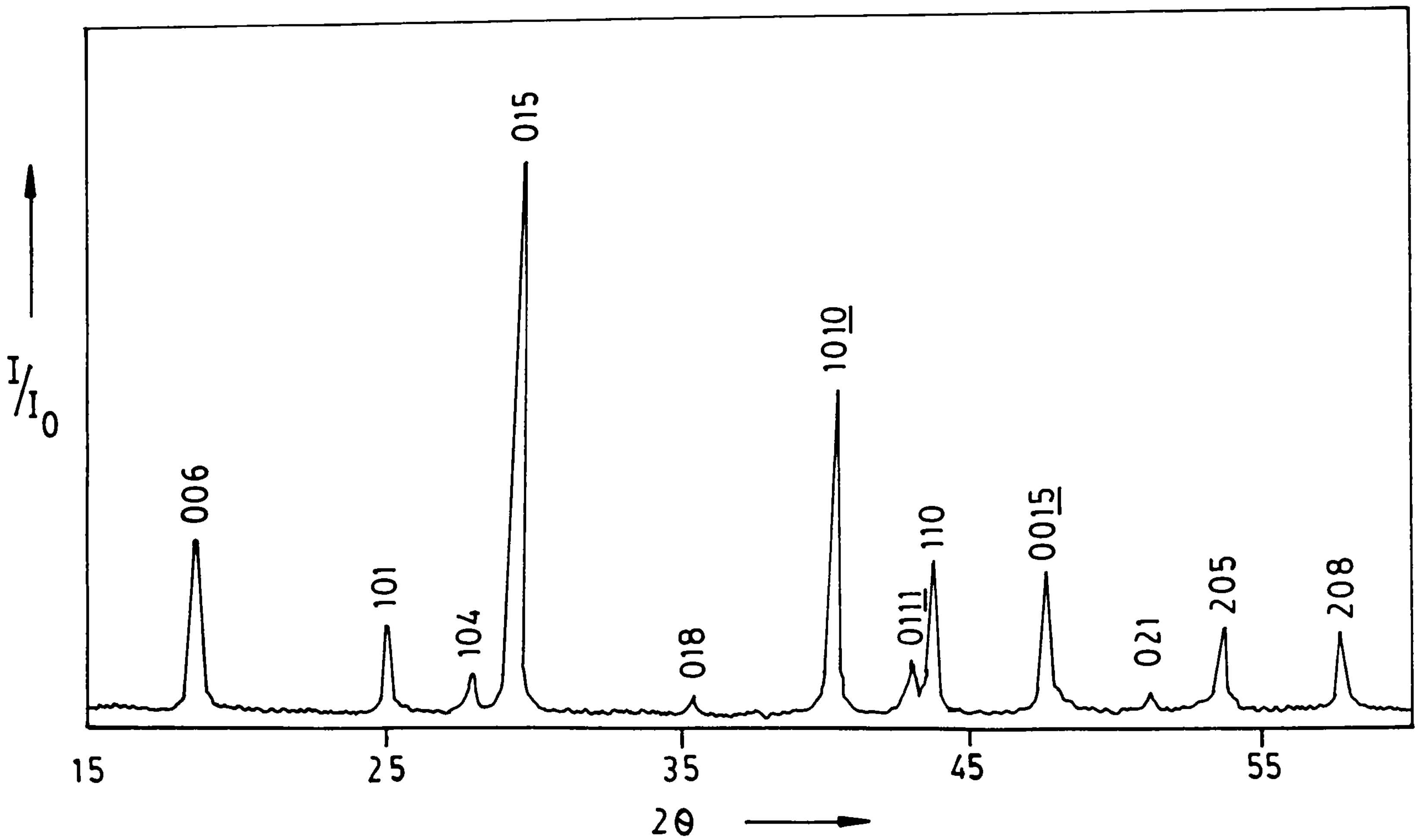

Fig. 9.1 X-ray diffraction profile of Bi_2Se_3 crystal

TABLE 9.1
X-ray diffraction data of melt-grown $Bi_2 Se_3$ crystals

hkl	Standard Pattern		Grown Crystal	
	d Å	I/Io	d Å	I/Io
006	4.80	30	4.802	34
101	3.56	20	3.557	18
104	3.21	10	3.201	9
015	3.03	100	3.028	100
018	2.54	5	2.534	6
1010	2.23	60	2.228	58
0111	2.10	10	2.101	12
110	2.07	30	2.07	30
0015	1.907	30	1.909	28
021	1.787	5	1.789	6
205	1.710	20	1.705	17
208	1.600	20	1.596	16

9.4. DISLOCATION STUDIES

The samples were carefully cleaved with a knife for these studies. The cleavage surfaces of crystals are never atomically smooth. The propagation of cleavage cracks in solids has been the subject of a number of investigations [17, 18, 29]. They present a system of steps very nearly parallel to the cleavage direction. These steps converge to form higher steps or rivers. The opposite halves of matched cleavage faces of these crystals are shown in Fig. 9.2(a&b).

It was found that a solution of iodine, bromine and methanol could produce triangular etch-pits on the cleavage planes of Bi_2Se_3 crystals. A solution of 100 mg iodine in 10 ml methanol with 0.2 ml bromine is able to produce etch pits. The effect of varying the composition of etchant was studied and the concentration was not found to be critical. However, a solution of 250 mg I_2 + 0.2 ml Br_2 + 10 ml CH_3OH was found to be good, to produce well-defined pits on a clear back ground. The etching time usually was anywhere from 10 sec to 2 minutes. The size of the pits has been found to increase when the iodine content is increased, keeping the other components in the same concentration. But surface roughening due to corrosion occurred at its higher concentration. Figs. 9.3(a-c) are the photomicrographs of three samples etched for 20 sec. in solutions of 10 ml CH_3OH and 0.2 ml Br_2 with 200 mg, 400 mg and 500 mg iodine respectively.

Well-defined triangular pits as shown in Fig. 9.4(a-g) were observed. Most of them are point-bottomed, some are flat-bottomed and some others are terraced. Deep flat-bottomed and shallow flat-bottomed pits are also observed quite often. Individual large isolated pits as well as crowded pits are formed.

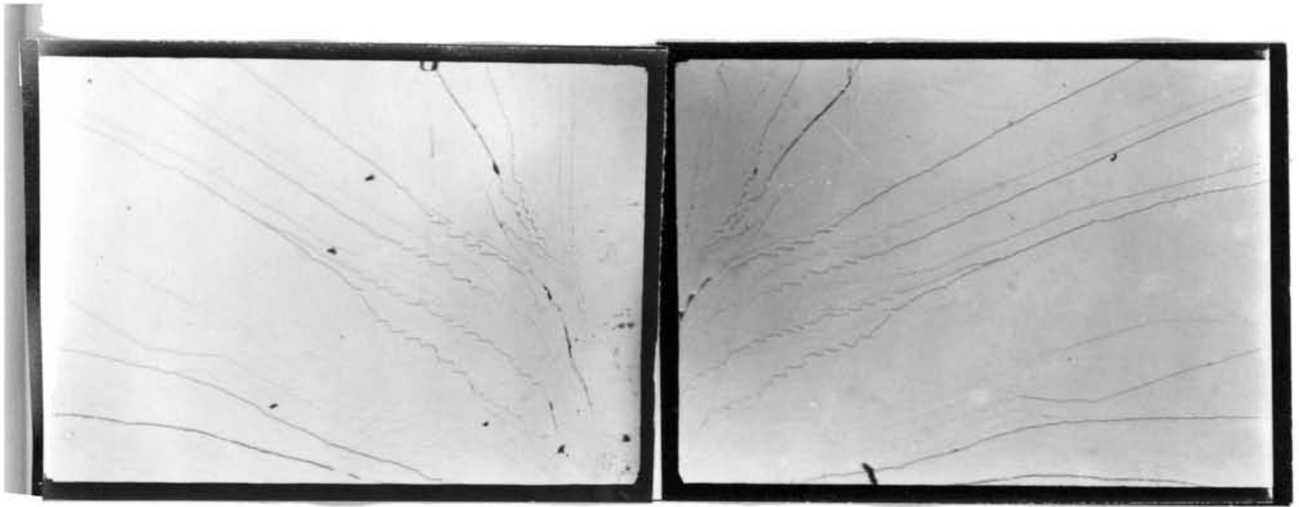

Fig. 9.2a × 50

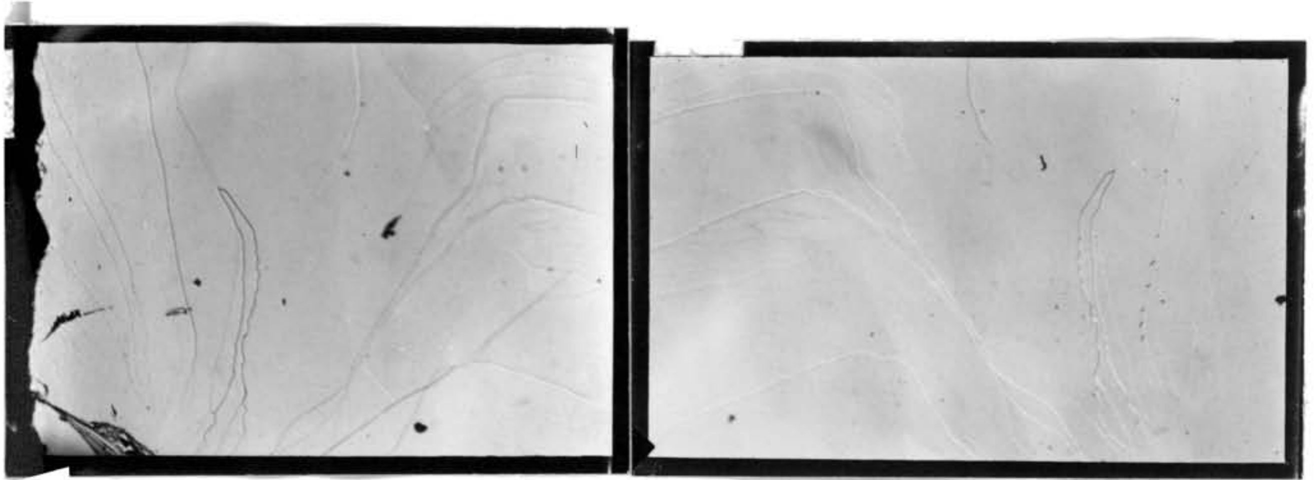

Fig. 9.2b × 50

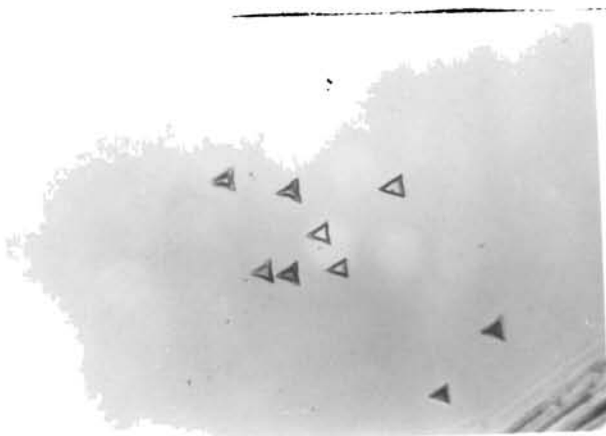

Fig. 9.3a × 330

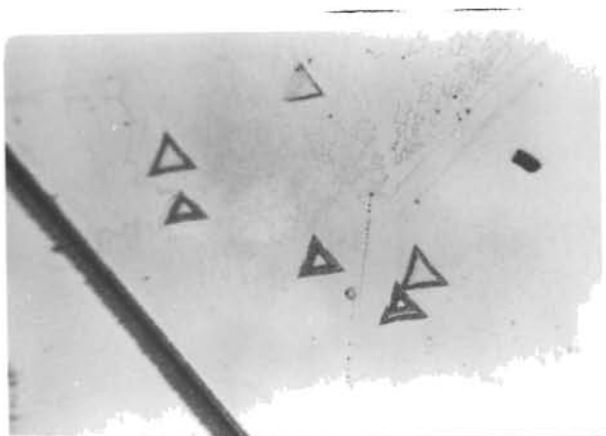

Fig. 9.3b × 330

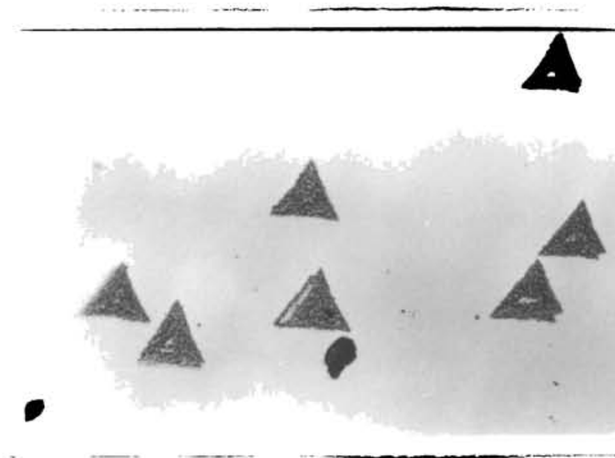

Fig. 9.3c × 330

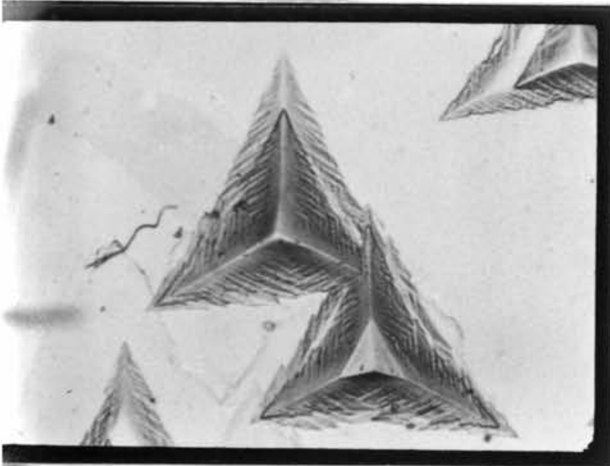

Fig. 9.4a × 400

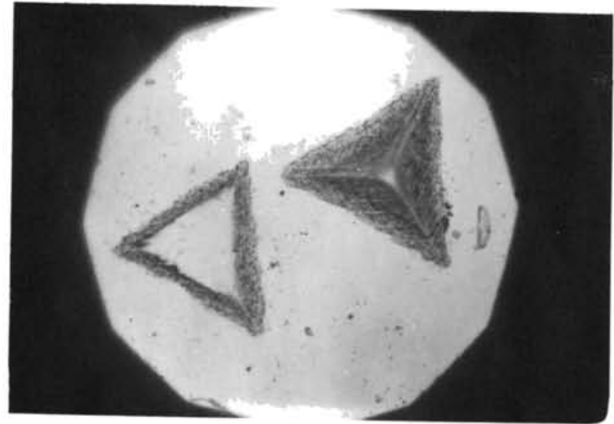

Fig. 9.4b × 660

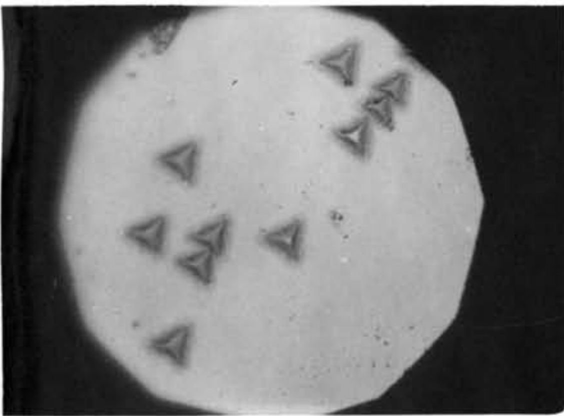

Fig. 9.4c × 330

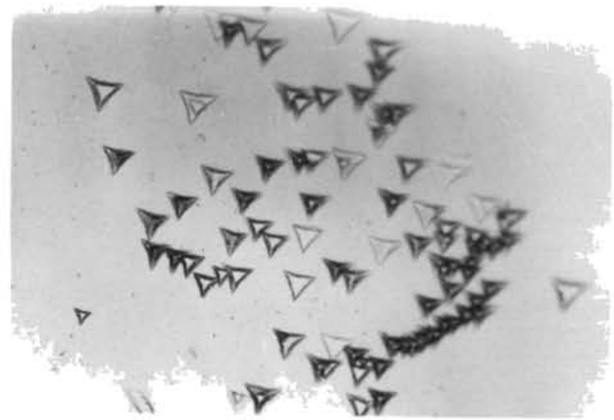

Fig. 9.4d × 165

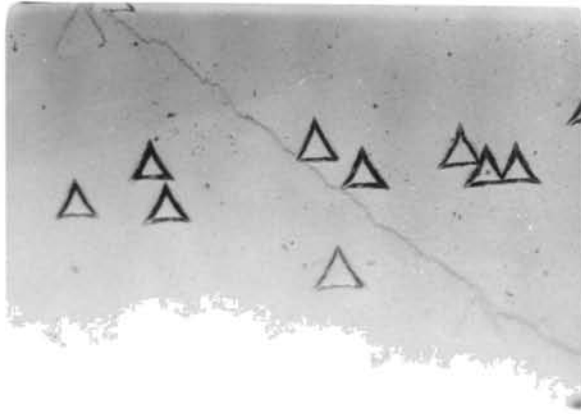

Fig. 9.4e × 330

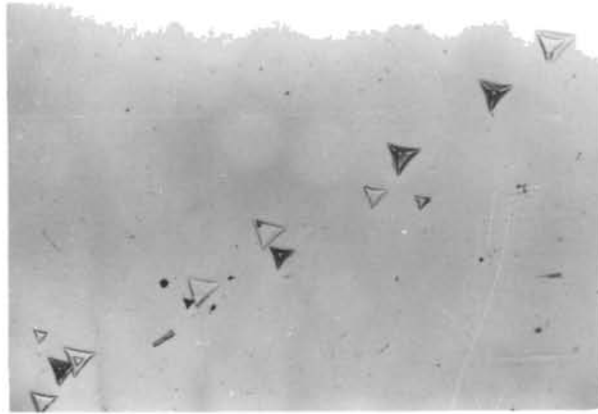

Fig. 9.4f × 165

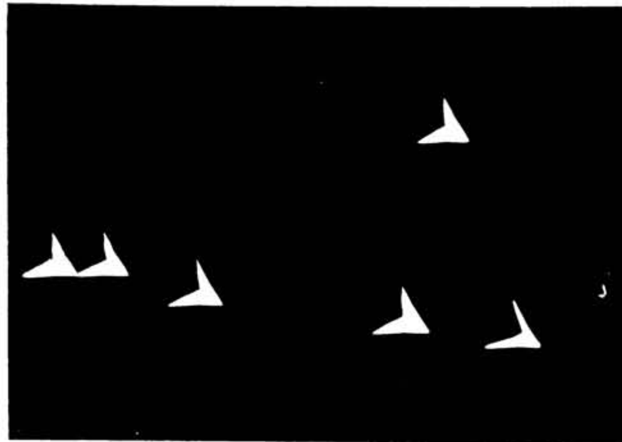

Fig. 9.4g × 330

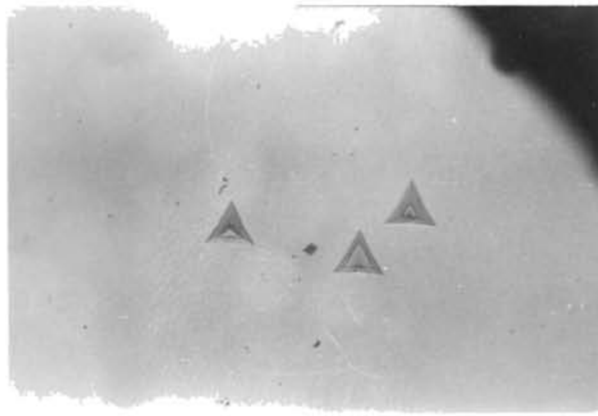

Fig. 9.5a × 330

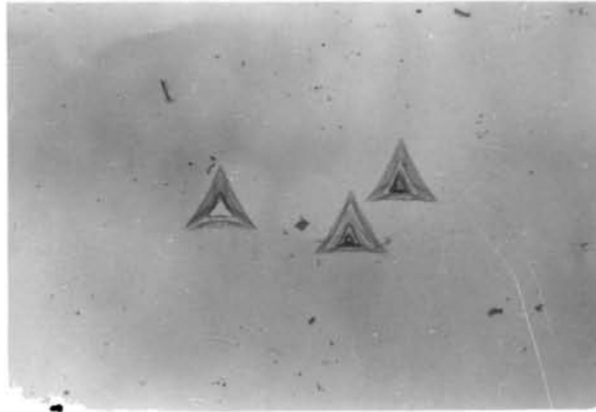

Fig. 9.5b × 330

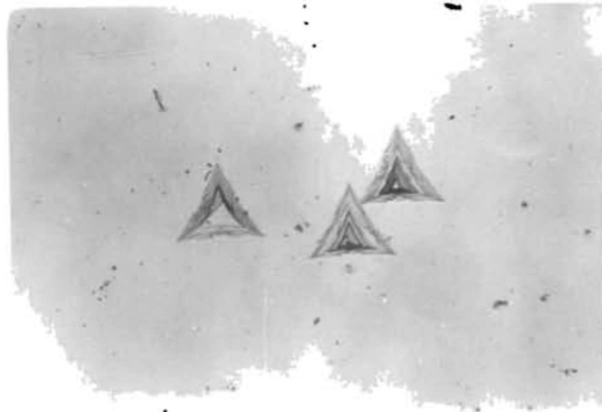

Fig. 9.5c × 330

Some of the triangular pits have their point bottoms at their centroid, while some others have eccentric point bottoms. The size of the majority of the pits are nearly the same, however, pits of different sizes are often observed on the same surface [Fig. 9.4(f,g)]. The sides of these pits are always found to be parallel to the binary axes.

On prolonged etching these pits become larger in size and generally preserve their shapes. The number and positions of the pits have also remained the same. Fig. 9.5(a-c) show the respective size of the pits obtained for three successive etching, each of 10 sec. duration in a solution of 250 mg I_2 + 0.2 ml Br_2 + 10 ml CH_3OH. The fact that an etchant produces well-defined triangular pits which retain their shapes while growing larger on further etching strongly suggests that these pits are the sites of emergence of the dislocations on the surface. The difference in pit size at different sites on the same surface [Fig. 9.4(f,g)] may be attributed to the different strengths of dislocations and the inclination of dislocation lines with the surface.

In general,it is assumed that the attack of the etchant should be greater along the dislocation lines and hence, the tips of the point bottomed pits should always follow the dislocation lines. The eccentricity in the point bottoms observed in the asymmetric pits can thus be explained by postulating the existence of dislocations, the lines of which are inclined to the *c* axis. The symmetric pits show that the dislocations at these sites are parallel to the *c* axis. The mechanism responsible for the flat-bottom pits involves the formation of a pit at the emergence on the *c* plane of a dislocation which changed its course near the surface and followed some arbitrary direction in the *c* plane. The fast etching rate along the dislocation responsible for the pyramidal pit is now absent and the pits become flat-bottomed [18].

The impurity segregation at dislocations may attribute to the terracing of etch pits in semiconductors [20]. The dissolution rate of etch pit at a dislocation will be high until an impurity precipitate is encountered [Fig. 9.6]. And then, because of the poor solubility, if the impurity slows down the dissolution, the dissolution rate along the dislocation line will reduce. The step formed during this period will advance away from the dislocation line. The dissolution rate along the dislocation line will increase only after the removal of the precipitate by its own dissolution or by dissolution around it. An etch pit with a number of terraces as observed in Fig. 9.7 can be formed by the repetition of this process.

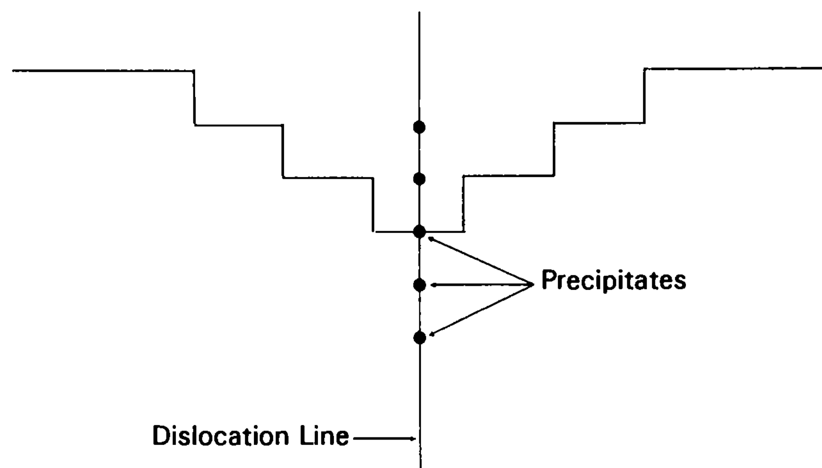

Fig. 9.6. Formation of terraced etch pits by impurity precipitates concentrated along a dislocation line [Sangwal (20)].

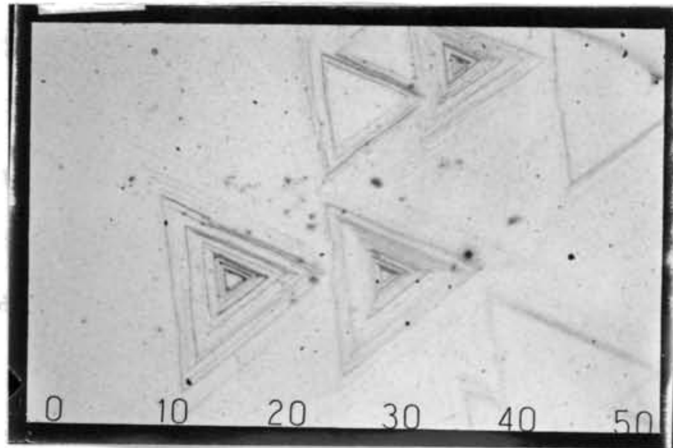

Fig. 9.7 × 150

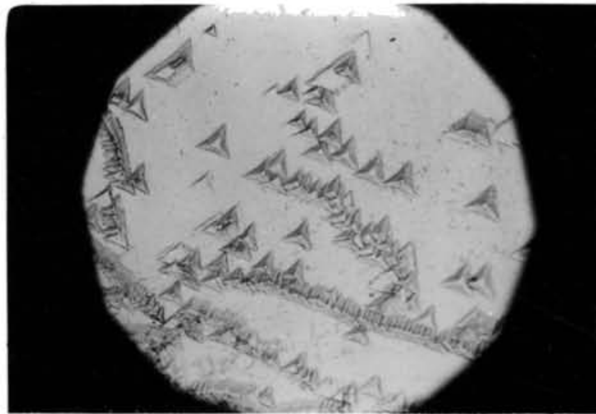

Fig. 9.8 × 330

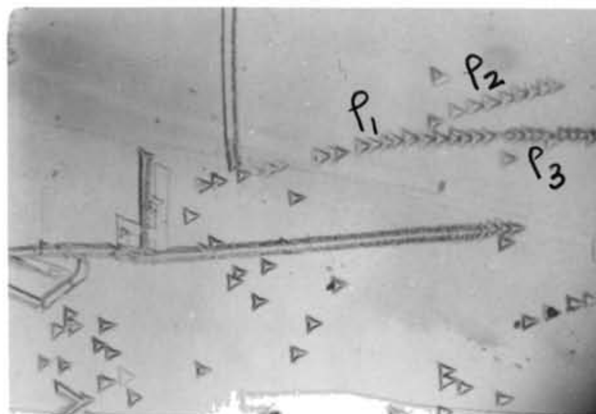

Fig. 9.9 × 330

Deep flat-bottomed pits are also often observed [Fig. 9.8]. The density of these pits varies from sample to sample and from one area of the sample to another. This may also be explained as the basis of pit formation by impurity precipitates. These pits stop growing and become flat bottomed after the precipitates have been etched out [19].

In addition to the randomly distributed etch pits developed on the cleavages, rows of closely spaced pits and sometimes branching of the rows was observed as shown in Fig. 9.9. These rows resemble the low-angle boundaries observed in Bi_2Te_3 by Sagar & Faust [20]. For three intersecting tilt boundaries [Fig. 9.9] there exists a relation between the dislocation densities ρ_i.

$$\sum \rho_i / (\cos\phi_i + \sin\phi_i) = 0$$

where ϕ_i is the angle between the direction of the boundaries and the direction of a symmetrical tilt boundary. For small values ϕ_i, one has

$$\rho_1 + \rho_2 = \rho_3$$

Thus if the pits are at dislocation sites, the sum of the densities in two branches should be equal to the density in the third [21]. The pit densities in the example shown in Fig. 9.9 obey this relationship very closely. Thus we can conclude that these rows of pits mark tilt boundaries, and that each etch pit marks the site of an edge dislocation. This is a supporting evidence about the reliability of the etchant for revealing dislocations on the cleaved surface of Bi_2Se_3.

Unresolvable pits and bands were also observed on the cleaved surfaces of Bi_2Se_3 [Fig. 9.10]. The most important source for such bands may be the etched remains of lines of dislocation networks lying in the *c* plane [18].

A one-to-one correspondence between the etch pits on the opposite halves of a cleavage is generally considered as a proof of the reliability of an etchant for revealing dislocations. Figs. 9.1(a-d) shows the etch pit patterns produced on matched cleavage faces of Bi_2Se_3 crystals. It can be seen that the orientation of the pits on the two opposite cleavage faces does not posses the mirror image character. They are inverted with respect to each other. This type of etch pit inversion on matched cleavages has been observed in CaF_2 by Patel & Desai [23], and in Bi_2Te_3 by Sagar & Faust [18].

In the case of the (100) face of NaCl - type crystals, for example, the arrangement of ions on the matched halves is identical. But in the case of fluorite-type crystals, the arrangement of the ions on the other face is identical after a lateral shift of a <100> array of atoms by one-half interplanar spacing. Consequently, the etch pits on matched cleavages of this type crystals do not show a mirror symmetry but are oriented by 60° [22]. The crystallographic situation being identical, analogous to CaF_2 and Bi_2Te_3, the inversion in etch pit orientation on the matched halves of Bi_2Se_3, observed in the present case, can be explained.

The one-to-one correspondence was observed for all the different types of etch pits (such as point bottomed, flat bottomed, terraced etc.) shows in

Fig. 9.10 × 330

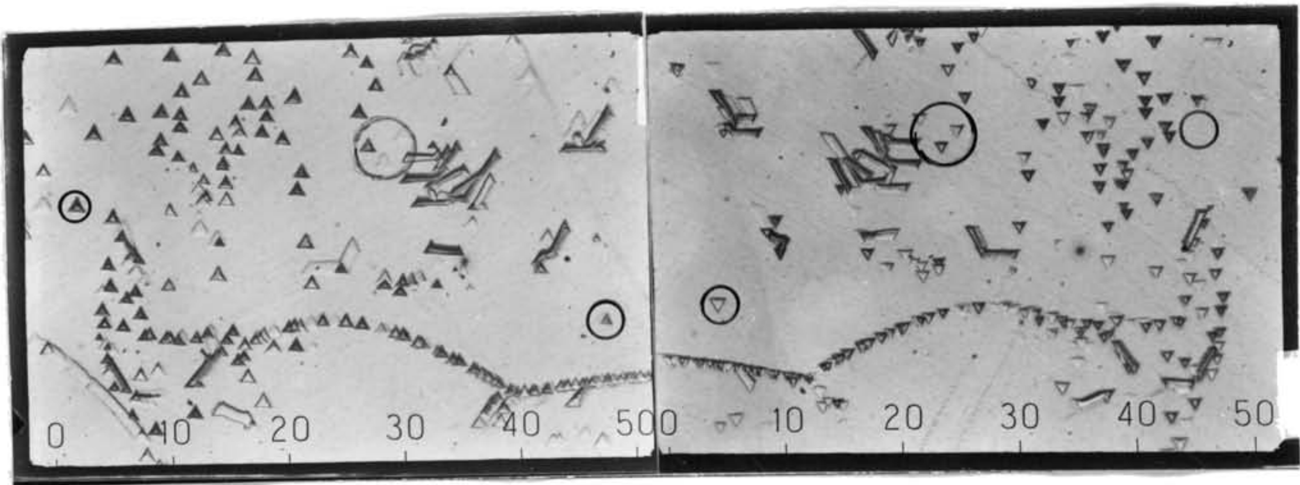

Fig. 9.11a × 150

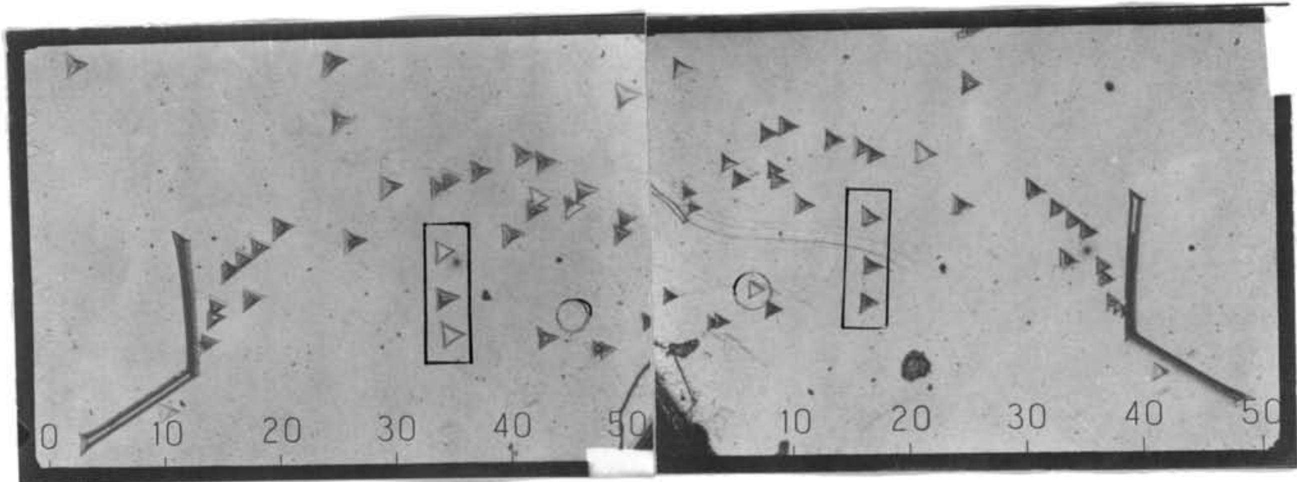

Fig. 9.11b × 150

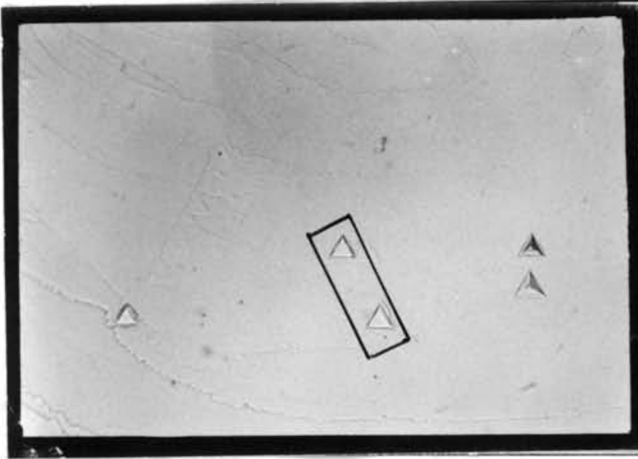
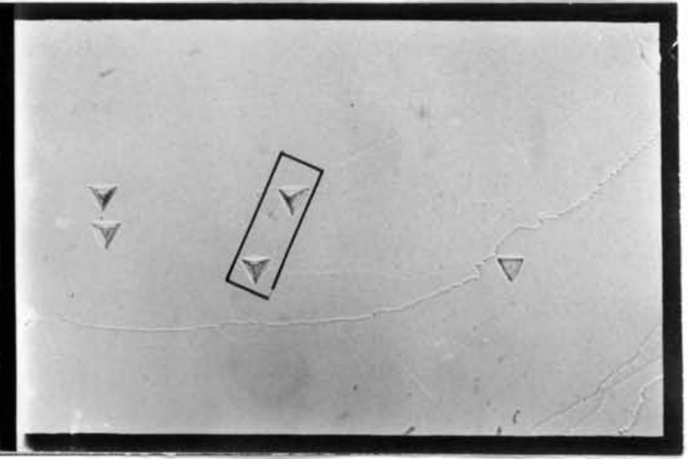

Fig. 9.11c × 150

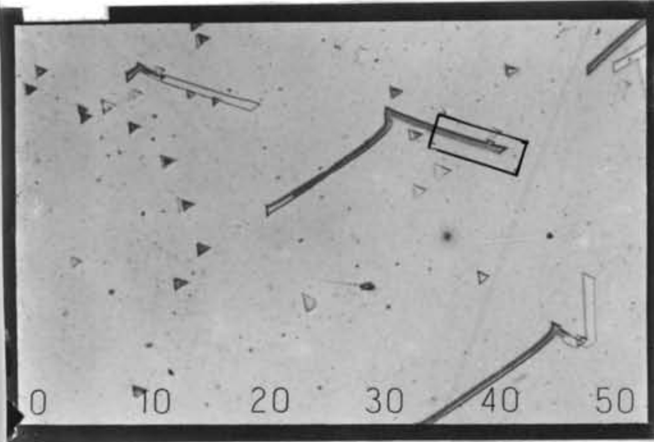

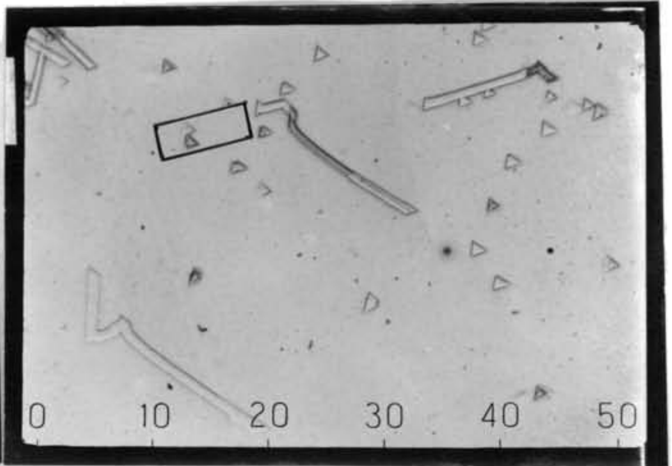

Fig. 9.11d × 100

Figs. 9.11(a-d), thus establishing that these different types of pits produced on the cleavage plane of Bi_2Se_3 crystals do mark the sites of dislocations.

Small deviations from a perfect match; such as missing of pits, existence of flat - bottomed pits corresponding to point - bottomed one etc., between the two opposite halves of a cleavage may normally be take place, due to the spatial dislocation net works present inside the crystal. The spots marked in the Figs. 9.11(a-d) represent some of the discrepancies observed in the present case. This can be explained as due to the branching and bending of dislocations [19, 24, 25].

9.5 CONCLUSION

A study of dislocations in Bi_2Se_3 crystals grown by horizontal zone levelling technique was conducted by chemical etching. An etchant was found which is very reliable and is easy to use for revealing dislocations on cleaved surfaces of Bi_2Se_3. It consists of a solution of iodine and bromine in methanol. This has been produced well-defined and contrasting triangular pits at the point of emergence of the dislocations. The reliability of the etchant has been verified by different methods.

FIGURE CAPTIONS

Fig. 9.2(a,b). Opposite halves of matched cleavage faces of Bi_2Se_3 crystals

Fig. 9.3(a-c). Etch pits formed on the (0001) face of Bi_2Se_3 crystals by solutions of 10 ml CH_3OH + 0.2 ml Br_2 with (a) 200 mg I_2 (b) 400 mg I_2 and (c) 500 mg I_2

Fig. 4(a-g). Etch patterns formed on the (0001) face of Bi_2Se_3 crystals

a. point-bottomed and deep flat-bottomed (etched for 5 minutes), b. point-bottomed and flat-bottomed pits, c. deep flat-bottomed pits, d. crowded pits e. isolated flat-bottomed pits, f. different size pits on the same surface, g. pits with eccentric point-bottom

Fig. 9.5(a-c). Variation of the dimensions of etch pits produced by 250 mg I_2 + 0.2 ml Br_2 + 10 ml CH_3OH

(a) for 10 sec. (b) for 20 sec. (c) for 30 sec.

Fig. 9.7. Terraced etch pits with higher magnification

Fig. 9.8. Deep flat-bottomed etch pits

Fig. 9.9. Trisection boundaries on (0001) face of Bi_2Se_3 produced by 200 mg I_2 + 0.2 ml Br_2 + 10 ml CH_3OH

Fig. 9.10. Unresolvable pits and bands formed on the cleavage surfaces of Bi_2Se_3

Fig. 9.11(a-d). Etch pit patterns produced on matched cleavage faces of Bi_2Se_3 by 250 mg I_2 + 0.2 ml Br_2 + 10 ml CH_3OH

REFERENCES

1. J. Black, E.M. Conwell, L. Seigle & C.W. Spencer., *J. Phys. Chem. solids* **2,** 240 (1957).
2. H. Gobrecht, K.E. Boeters & G. Pantzer., *Z. Physik* **177,** 68 (1964)
3. V.F. Boechko & V.I. Isarev., *Inorg. Mater.* **11,** 1288 (1975).
4. A.K.Dmitrieva, L.D.Dudkin., R.S. Erofeev, A.B. Ivanova & E.I. Shcherbina., *Inorg. Mater.* **14,** 326 (1978).
5. J. Horak, L. Koudelka, J. Klikorka & L. Siska., *Phys. Stat. Sol.* **111,** 575 (1982).
6. H. Gobrecht, S. Seeck & T. Klose., *Z. Physik.* **190,** 427 (1966).
7. A. Vasko, M. Matyas, L. Tichy & J. Horak., *Czech. J. Phys.* **B23,** 243 (1973).
8. H. Kohler & C.R. Becker., *Phys. Stat. Sol.* **61,** 533 (1974).
9. H. Kohler & P.Fabricius., *Phys. Stat. Sol.* **71,** 487 (1975).
10. G.R.Hyde, H.A. Beale & I.L. Spain., *J. Phys. Chem. Solids.* **35,** 1719 (1974).
11. K. Hashimoto., *J. Phys. Soc. Japan.* **16,** 1970 (1961).
12. J.A. Woollam, H. Beale & I.L. Spain., *Phy. Lett.* **41A,** 319 (1972).
13. A.A.Sher., I.N. Odin & A.V. Novoselova., *Inorg. Mater.* **20,** 1109 (1984).
14. B. Kolakowski., *Act. Phys. Polon.* **20,** 103 (1961).
15. JCPDS Card no. 12-732
16. J.Y. Lee & K.N.Subramanian., *J. Mater. Sci.* **18,** 1765 (1983).
17. M.J. Kaufman & A.J. Forty., *J. Mater. Sci.* **21,** 3167 (1986).

18. A. Sagar & J.W. Faust., *J. Appl. Phys.* **38,** 482 (1967).

19. A. Sagar & J.w.Faust., *J. Appl. Phys.* **38,** 2240 (1967).

20. K. Sangwal., In: 'Etching of Crystals, Theory, Experiment and Application'. (North - Holland, Amsterdam) (1987) P. 295.

21. Ibid. P. 361.

22. Ibid Ch. 9

23. A.R.Patel & C.C.Desai., *Z. Kristallogr.* **121,** 55 (1965)

24. S.Amelinckx., *Philos. Mag.* **1,** 269 91956).

25. A.R. Patel & S.M. Patel., *Z. Kristallogr.* **126,** 214 (1968).

26. A.G.Kunjomana & E. Mathai., *J. Mater. Sci.* **26,** 6171 (1991).

27. I. Teramoto & S. Takayanagi., *J. Appl. Phys.* **32,** 119 (1961).

28. B. Lampert & K. Reichelt., *J. Cryst. Growth.* **51,** 203 (1981).

29. A.G. Kunjomana., *Ph. D. Thesis,* Cochin University of Science & Technology (1992).

CHAPTER 10

GROWTH AND MORPHOLOGY OF VAPOUR-GROWN Bi_2Se_3 CRYSTALS

10.1 INTRODUCTION

The narrow band gap semiconductor Bi_2Se_3 , which possesses the layer structure is of interest for its desirable thermoelectric and Hall-effect applications. As stated in chapters 6 & 9, extensive investigations [1-12] have been made to study the optical, electrophysical, and galvanomagnetic properties of this compound. For all these studies Bi_2Se_3 crystals grown from its melt have been used. Crystals of V_2–VI_3 group compounds (Bi_2Se_3, Bi_2Te_3, Sb_2Se_3, Sb_2Te_3 etc.) have been rather easier to grow from the melt than from their vapour. Due to the high vapour pressure of chalcogens, it is more difficult to obtain the stoichiometric crystals of these compounds. Arivuoli et al. [13] have studied the microhardness of the vapour-grown crystals of V_2–VI_3 family compounds. The morphological studies of the vapour-grown crystals of Bi_2Te_3 and Sb_2Te_3 have been conducted by Kunjomana [14] and Ivan Sommer [15], respectively. But the study of the growth morphology of Bi_2Se_3, a prominent member among this group has not been reported.

In this chapter, the growth of Bi_2Se_3 crystals by physical vapour deposition technique and their morphology is presented. According to Ghosh et al [16], in sublimation method, platelets do grow only in a gas ambient and it is also reported [17] that the growth of well defined crystals at high temperature is favoured by the ambient gas (argon, hydrogen, air etc.), by lowering the evaporation rate. But in the present investigation well defined platelets of Bi_2Se_3 have been grown by vacuum sublimation. One of the most striking features of crystals with layered structures is the existence of screw dislocations with Burgers vector perpendicular to the plane of the layers giving rise to growth spirals. Such growth spirals have been observed on the as-grown faces of Bi_2Se_3 crystals for the first time.

10.2 EXPERIMENTAL

Bismuth selenide was synthesized from high purity (99.999%) elements; Bi and Se. Appropriate amount of the elements with little excess selenium were sealed at low pressure ($\sim 10^{-5}$ torr) into a quartz ampoule with length 10 cm and diameter 12 mm. The ampoule was then slowly heated to 800^0C in a muffle furnace and maintained at this temperature for 24 hours, to complete the reaction. The ampoule was rotated and rocked mechanically to ensure the proper mixing of the constituents.

Pre-cleaned quartz ampoules with typical dimensions of 190 mm in length and 10 to 18 mm in diameter were loaded with about 10 gm, of the synthesized charge to grow Bi_2Se_3 crystals by PVD method. The whole system was evacuated and sealed off at about10^{-5} torr. The reaction ampoule was then heated in a temperature gradient by means of a two-zone horizontal

furnace, the temperatures of which were kept at constant with in ±1°C, using temperature controllers. Inorder to remove any trace of the starting material at the growth zone of the ampoule, a reverse temperature gradient was applied before starting the growth. For this, the source region was kept at a lower temperature than the condensation for more than three hours.

In closed-tube-vapour-transport technique, it is observed that the transport rate mainly depends on the cross-section of the reaction ampoule [18], and to obtain best results the length-to-diameter ratio of the ampoule should be greater than 7 [19]. In the present case, best results were obtained with the 15 mm diameter reaction ampoules.

The effect of the temperatures of the two zones for the successful growth of the crystals was also studied. When the temperatures of the source zone and growth zone were 760°C and 655°C respectively, metallic coloured thin platelets with maximum surface area 0.5 cm^2 were obtained after a growth period of 72 hours. Identification of the grown crystals was made by X-ray diffraction studies with CuK_α radiation. The as-grown surfaces of the crystals were observed under reflection mode of the metallographic microscope. Chemical etching characteristics of these crystals were also studied.

10.3 X-RAY DIFFRACTION STUDIES

A typical, X-ray diffraction pattern using CuK_α radiation, obtained for vapour-grown crystals is shown in Fig. 10.1. The d-values and the relative intensities of the peaks are given in Table 10.1. All the values obtained in the present case are well matched with the standard pattern for Bi_2Se_3 [20].

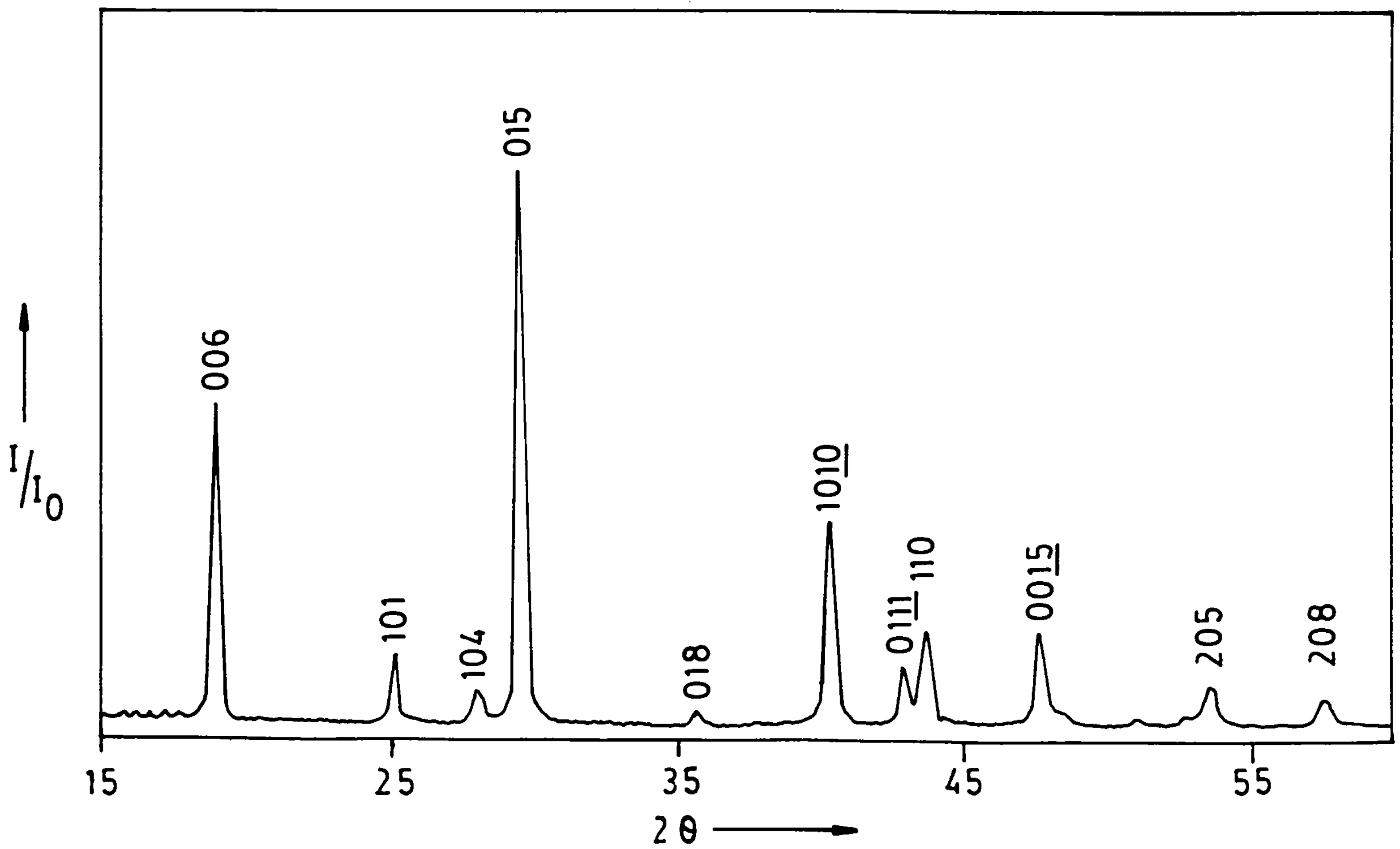

Fig. 10.1 X-ray diffraction profile of Bi_2Se_3 crystal

TABLE 10.1
X-ray diffraction data of vapour-grown $Bi_2 Se_3$ crystals

hkl	Standard Pattern		Grown Crystal	
	d Å	I/Io	d Å	I/Io
006	4.80	30	4.77	57
101	3.56	20	3.55	12
104	3.21	10	3.195	6
015	3.03	100	3.033	100
018	2.54	5	2.527	3
1010	2.23	60	2.231	37
0111	2.10	10	2.102	11
110	2.07	30	2.065	17
0015	1.907	30	1.905	17
205	1.710	20	1.708	7
208	1.600	20	1.599	5

10.4 MORPHOLOGY AND GROWTH MECHANISM

The predominant shape of the crystals grown in closed system by physical vapour deposition technique was plate-like. Very few ribbon-like crystals were also found. A good few of these vapour-grown Bi_2Se_3 crystals have been examined under the reflection mode of the microscope. Well developed areas of the crystals have been found as ideally smooth. However, a variety of interesting growth patterns were observed on the as-grown surfaces of the crystals.

Fig 10.2a shows the typical growth steps observed on the as-grown faces of the crystals, which is characteristic to the layer structure of Bi_2Se_3. Such growth steps have been observed on the surfaces of vapour-grown crystals of Bi_2Te_3 [21], and Sb_2Te_3 [15], which also have a similar layer-type structure as that of Bi_2Se_3. Fig. 10.2b, shows the magnified "feather pattern" observed at the tip of the plate having smoothed surface (upper part of Fig. 10. 2a).

Fig. 10.3 shows an interesting "fountain view" of layers appearing at the tip of another platelet. A ribbon shaped crystal pattern is shown in Fig.10.4(a,b). Unlike on the platelets, holes and longitudinal cavities, as seen, are present on the ribbon-like crystals. This may be due to the difference in growth mechanisms responsible for the growth of platelets and ribbon-like crystals. Fig. 10.5 shows a kinked net work with well smoothed surfaces.

There are different growth mechanisms responsible for the growth of crystals. The theory of crystal growth in presence of screw dislocation

mechanism have been developed by Burton, Cabrera and Frank [22]. According to them, when a single screw dislocation emerges on the face of the crystal, a molecular ledge will run from the point of emergence on the crystal surface, to the boundary of the face. If the supersaturation of the vapour in contact with the crystal is higher than that of a critical value, the crystal will start to grow and the ledge will wind itself into a helicoid. Such a spiral originating from an isolating single dislocation will have a regular shape, if it is not perturbed by spiral layers from other sources and the growth conditions are steady [22-24]. Ideal spirals originating from isolated screw dislocations are not commonly observed on crystal faces.

Fig. 10.6(a,b) shows a circular spiral pattern observed on the as-grown face of the Bi_2Se_3 crystal. The two spiral having the same sign are originating from the single screw dislocation with a change of curvature as they escape from the central core. On the basis of the theoretical predictions of Frank [25], and Cabrera & Levine [23], and from the experimental evidence obtained from haematite crystals, Sunagawa et al. [26] reported that if the step height of the spiral is very high, the spiral steps escapes with a change of curvature from the central core depending on the stress field. The eccentricity of the growth spirals may be due to supersaturation gradient over the surface of the crystals during the growth process. At the higher supersaturation side, the spiral step advance more rapidly and form wider step separation, while at the lower supersaturation side the step separation becomes narrower and the spiral as a whole take the eccentric shape.

The intersection and further development of growth spirals originating from screw dislocation at separate points is shown in Fig. 10.7.

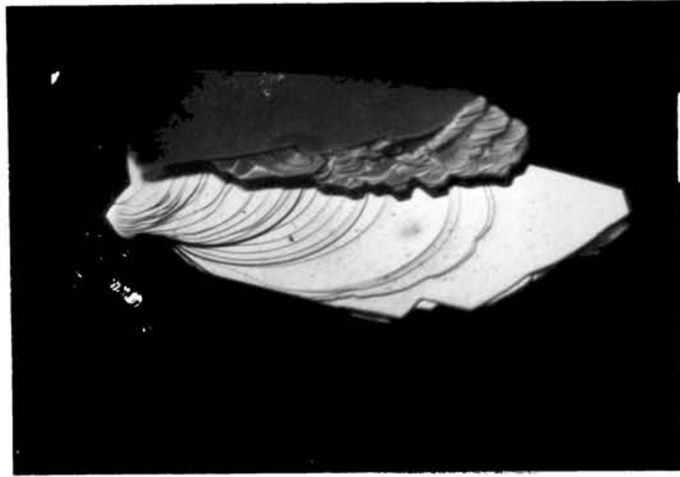

Fig. 10.2a × 62.5

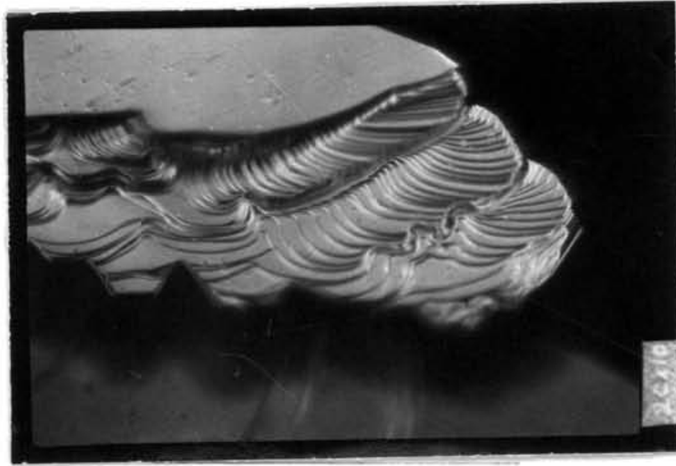

Fig. 10.2b × 200

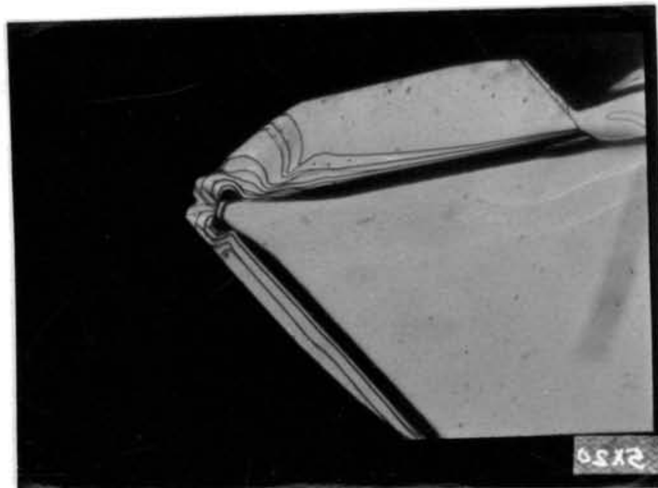

Fig. 10.3 × 100

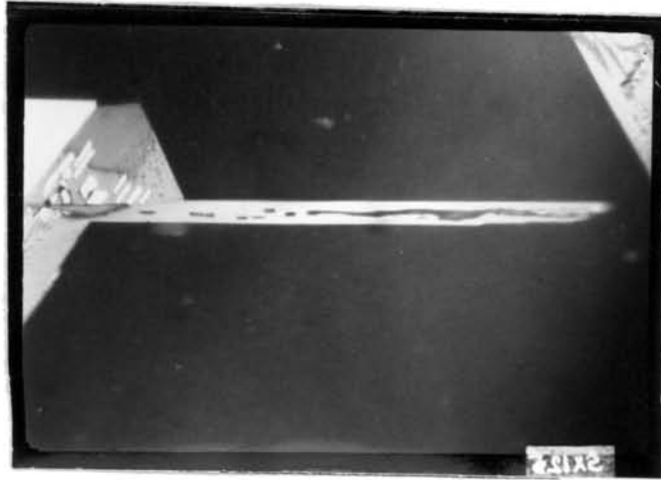

Fig. 10.4a × 62.5

Fig. 10.4b × 50

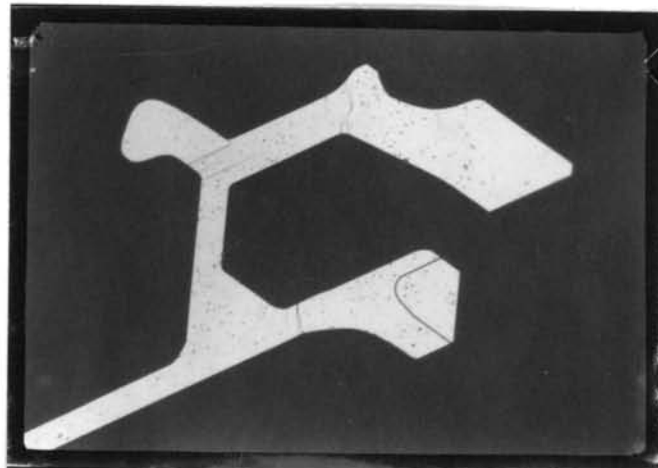

Fig. 10.5 × 50

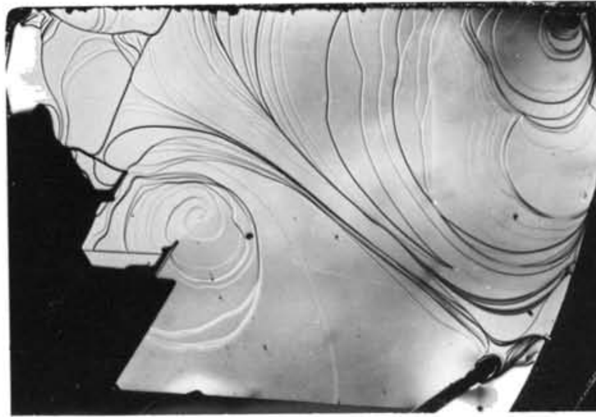

Fig. 10.6a × 82.5

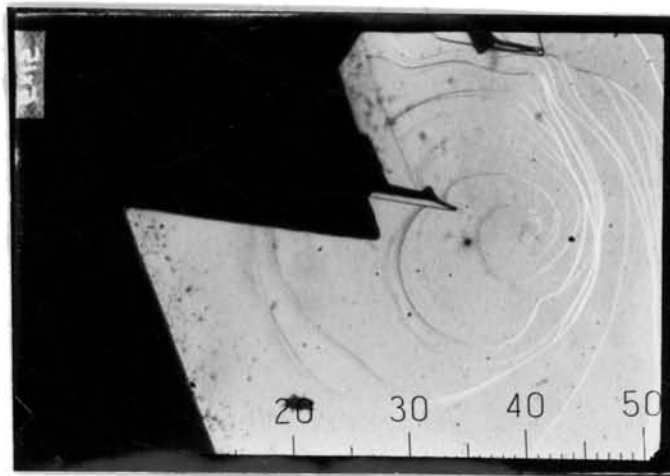

Fig. 10.6b × 75

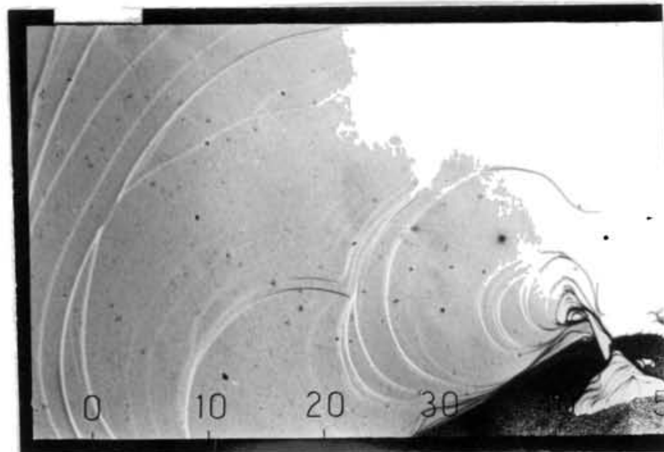

Fig. 10.7 × 75

The presence of growth spirals on the surfaces of Bi_2Se_3 crystals grown by physical vapour transport method establishes that these crystals are grown from the vapour phase by the screw dislocation mechanism. As mentioned earlier, during the growth process in closed-tube-vapour-transport a supersaturation gradient exists over the surfaces of the growing crystal and this can account for the distinct features observed in vapour-grown crystals [27]. At high supersaturation, the growth mechanism by screw dislocations becomes less important and causes the growth of ribbon-shaped crystals. Cardetta et al. [18] have observed the growth of the ribbon and needle shaped crystals of GaSe from vapour with its platelets, which have also been accounted for the supersaturation gradient exist in the closed-tube sublimation.

10.5 CHEMICAL ETCHING STUDIES

Chemical etching on the as-grown faces of the crystals were carried out to study the etching characteristics of the vapour-grown Bi_2Se_3 crystals. A solution of iodine, bromine and methanol, which is found to be a reliable etchant for revealing the dislocations in Bi_2Se_3 crystals (described in chapter 9) have been used to etch the vapour grown crystals.

Fig. 10.8 shows the etched pattern of the surface of a platelet in a solution of 200 mg I_2 + 10 ml CH_3OH + 0.2 ml Br_2 for 30 sec. As seen, very few shallow triangular pits were found to develop on the as-grown faces of Bi_2Se_3 crystals. Repeated etching suggests that these triangular pits are at the sites of emergence of the dislocations on the surface. A close observation on the circular patterns developed on the crystals surface revealed that these patterns are constituted

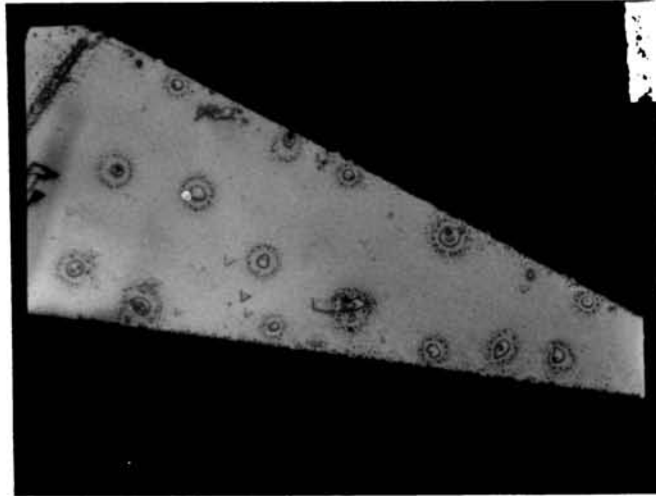

Fig. 10.8 × 400

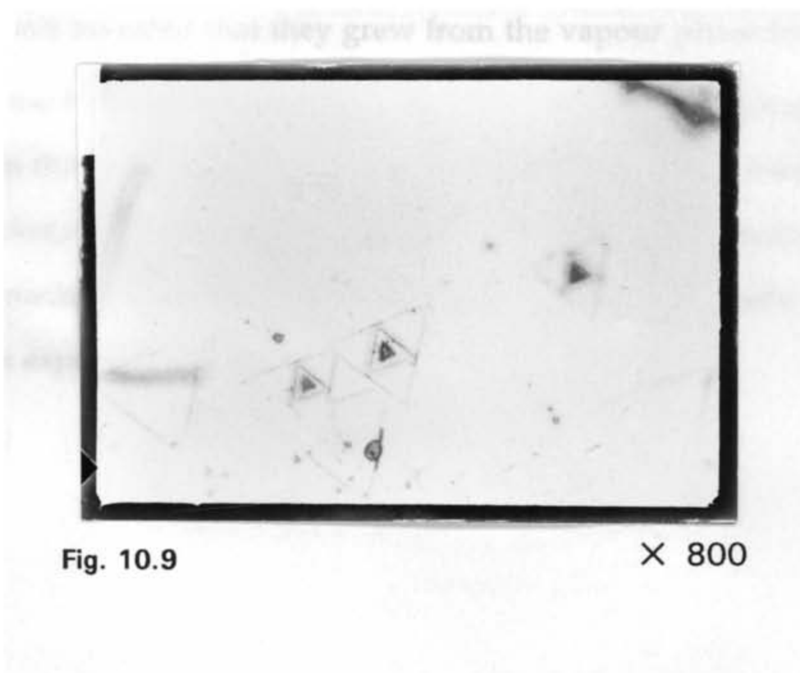

Fig. 10.9 × 800

by tiny circles. These closed circular features are at the sites of the vacancy condensation. Similar features have been observed on the surfaces of vapour-grwon Bi_2Te_3 crystals also [21]. An interesting pit shape that is occasionally observed on the surface of a platelet is shown in Fig. 10.9.

Comparing to melt-grown crystals described in chapter 9, it can be seen that the dislocation density in this case is much less and is as expected in vapour-grown crystals.

10.6 CONCLUSION

The presence of circular growth spirals observed on the basal plane of Bi_2Se_3 crystals revealed that they grew from the vapour phase by the screw dislocation mechanism. The change of the curvature of the spiral step as it escapes from the centre core is due to the increase in strain at the dislocation centre. The distinctive growth features are due to the supersaturation gradient over the growing crystals. Dislocation density in vapour-grown crystals is much less as expected.

FIGURE CAPTIONS

Fig. 10.2a.	Step-like growth features on the as-grown faces of Bi_2Se_3 crystals
Fig. 10.2b.	A 'feather pattern' appeared at the upper part of the plate-let in Fig 10.2a with higher magnification
Fig. 10.3.	A 'fountain view' of layers formed at the tip of a plate-let
Fig. 10.4a.	A ribbon-like vapour grown crystal of Bi_2Se_3
Fig. 10.4b.	A group of ribbon-like crystals
Fig. 10.5.	A kinked Bi_2Se_3 crystal
Fig. 10.6a.	Circular spirals on the as-grown faces of Bi_2Se_3 crystals
Fig. 10.6b.	The spiral pattern in Fig. 10.a with higher magnification
Fig. 10.7.	The intersection of growth spirals originated from separate screw dislocations
Fig. 10.8.	Etch patterns formed on the as-grown face of Bi_2Se_3 crystal after etching in 200 mg I_2 + 10 ml CH_3OH + 0.2 ml Br_2 for 30 sec.
Fig. 10.9.	Triangular etch pits formed on the surface of the vapour-grown Bi_2Se_3 crystal

REFERENCES

1. Gobrecht, S.Seeck and T.Klose., *Z.Physik.* **190**, 427 (1966).

2. A. Vasko, M. Matyás, L. Tichy and J. Horak., *Czech. J. Phys.* **B23**, 243 (1973).

3. H. Kohler and C.R.Becker., *Phys. Stat. Sol.* **61**, 533 (1974).

4. H.Kohler and P.Fabricius., *Phys. Stat. Sol.* **71**, 487 (1975).

5. G.R.Hyde, H.A. Beale and I.L. Spain, *J. Phys. Chem. Solids.* **35**, 1719 (1974).

6. J. Black, E.M. Conwell, L. Seigle and C.W.Spencer., *J. Phys. Chem. Solids.* **2**, 240 (1957).

7. G. Gobrecht, K.E. Boeters and G.Pantzer., *Z. Physik.* **177**, 68 (1964).

8. V.F. Boechko and V.I. Isarev., *Inorg. Mater.* **11**, 1288 (1975).

9. A.K.Dmitrieva, L.D.Dudkin, R.S. Erofeev, A.B. Ivanova and E.I. Shcherbina., *Inorg. Mater.* **14**, 326 (1978).

10. J. Horak, L. Koudelka, J.Klikorka and L.Siska., *Phys. Stat. Sol.* **111**, 575 (1982).

11. K. Hashimoto., *J. Phys. Soc. Japan.* **16**, 1970 (1961).

12. J.A.Woollam, H. Beale and I.L. Spain., *Phys. Lett.* **41A**, 319 (1972).

13. D.Arivuoli, F.D.Gnanam and P.Ramasamy., *J. Mater. Sci. Let.* **7**, 711 (1988).

14. A.G.Kunjomana and E.Mathai., *Cryst. Res. Technol.* **27**, 329 (1992)

15. Ivan Sommer., *J. Cryst. Growth,* **12**, 259 (1972).

16. B.Ghosh and G.P.Kothiyal., *Prog. Cryst. Growth Charact.* **6**, 393 (1983).

17. B.A.Smith, N. Cowlam and A.M.Shamah., *Phil. Mag.* **B39**, 111 (1979).

18. V.L.Cardetta, A.M.Mancini, C.Manfredotti and A.Rizzo., *J. Cryst. Grwoth* **17**, 155 (1972).

19. J.G. Yue, A.S. Yue and O.M. Stafsudd. Jr., *J. Cryst. Growth.* **54**, 248 (1981).

20. JCPDS Card No. 12 - 732.

21. A.G. Kunjomana., *Ph.D. Thesis*, Cochin University of Sci. & Tech., Kochi. (1992).

22. W.K. Burton, N. Cabrera and F.C. Frank., *Phil. Trans. Roy. Soc. London.* **A243**, 299 (1951).

23. N. Cabrera and M.M. Levine., *Phil. Mag.* **1**, 450 (1956).

24. H. Muller - Krumbhaar, T.W. Burkhardt and D.Kroll., *J. Cryst. Grwoth* **38**, 13 (1977).

25. F.C.Frank., *Acta. Cryst.* **4**, 497 (1951).

26. I. Sunagawa and P.Bennema., *J. Cryst. Growth,* **53**, 490 (1981).

27. J. George and C.K. Valsalakumari., *Cryst. Res. Technol.* **21**, 273 (1986).